Faculty of Biological and Environmental Sciences
Department of Biosciences
University of Helsinki
Finland

Structural studies of membrane –bound pyrophosphatases

Juho Kellosalo

ACADEMIC DISSERTATION

To be presented for public examination with the permission of the Faculty of Biological and Environmental Sciences of the University of Helsinki in lecture room PIII, Porthania,
on 17th of October 2013, at 12 noon.

Supervised by:
Professor Adrian Goldman
Faculty of Biological and Environmental Sciences, Divison of Biochemistry, Department of Biosciences
University of Helsinki, Finland and,
Department of Biomedical Sciences
University of Leeds, UK

Members of the thesis advisory commitee:
Professor Mårten Wikström
Insititute of Biotechnology, Structural Biology and Biophysics
University of Helsinki, Finland
And
Docent Pirkko Heikinheimo
Department of Biochemistry,
University of Turku, Finland

Reviewed by:
Professor Peter Henderson
Astbury Centre for Structural Molecular Biology,
University of Leeds, UK
And
Professor Poul Nissen
Department of Molecular Biology and Genetics,
University of Aarhus, Denmark

Opponent:
Sir, Professor John Walker
Mitchondrial Biology Unit
Medical Research Council, UK

Custos:
Professor Kari Keinänen
Faculty of Biological and Environmental Sciences, Divison of Biochemistry, Department of Biosciences
University of Helsinki, Finland

ISBN 978-952-10-9305-0 (paperback)
ISBN 978-952-10-9306-7 (PDF)
ISSN 1799-7372
Helsinki University Printing House, electronic version published at: http://ethesis.helsinki.fi
Helsinki 2013

“Kaiken viisauden alku on tosiasioiden tunnustaminen”
-J.K. Paasikivi

Contents

List of original publications

This thesis is based on the following publications:

I **Kellosalo J**, Kajander T, Palmgren MG, Lopéz-Marqués RL, Goldman A. (2011). Heterologous expression and purification of membrane-bound pyrophosphatases. *Protein Expression and Purification,* 79, 25-34.

II **Kellosalo J**, Kajander T, Honkanen R, Goldman A. (2013). Crystallization and preliminary X-ray analysis of membrane-bound pyrophosphatases. *Molecular Membrane Biology,* 30, 64-74.

III **Kellosalo J***, Kajander T*, Kogan K, Pokharel K, Goldman A. (2012). The structure and catalytic cycle of a sodium pumping pyrophosphatase. *Science,* 337, 473-476. * = equal contribution.

The publications are referred to in the text by their roman numerals. The articles have been reprinted with permission of the copyright holders. Unpublished data will also be presented.

Abstract

Membrane-bound pyrophosphatases (M-PPases) catalyze a reaction where the free energy released from pyrophoshate (PPi) hydrolysis is converted into a sodium and/or proton gradient by pumping these ions across the membrane (Luoto et al., 2013). They are found in plants, protozoans and prokaryotes and are important for survival in abiotic stress conditions such as cold, hypoxia, salt stress and low-light intensity (Garcia-Contreras et al., 2004; Lopéz-Marqués et al., 2004; Serrano et al., 2007). In plants, M-PPases are the main hydrolysers of cytoplasmic pyrophosphate, which source in plants, and in other organisms, are the various anabolic reactions such as DNA, RNA and protein synthesis in which PPi is released as a by-product of ATP hydrolysis (Baykov et al., 1999). This hydrolytic activity is important for plant maturation (Ferjani et al., 2011), as build up of pyrophosphate inhibits the gluconeogenesis and cellulose synthesis and the above mentioned anabolic reactions (Baykov et al., 1999). Based on their function, M-PPases can be divided into four groups: K^+-dependent Na^+-pumps, K^+-dependent H^+-pumps, K^+-dependent Na^+, H^+-pumps and K^+-independent H^+-pumps (Luoto et al., 2013). The K^+-dependent pumps require potassium for full activity, but have reduced activity without it (Maeshima, 2000).

M-PPases are dimeric (Serrano et al., 2007) and have 14 to 17 transmembrane helices (Mimura et al., 2004). Most of the conserved residues necessary for M-PPase activity occur in the cytoplasmic part of the protein (Maeshima, 2000; McIntosh and Vaidya, 2002; Serrano et al., 2007). These residues take part in binding Mg_2PPi, the physiological substrate of M-PPases, and Mg^{2+}, a necessary cofactor for catalysis.

The aim of this study was to solve the structure of a membrane-bound pyrophosphatase. To find a suitable target protein for X-ray crystallography, eight M-PPases were expressed in *Saccharomyces cerevisiae*. Three expressed at levels of 0.5 mg/l or higher: the K^+-dependent Na^+-pump of *Thermotoga maritima* (TmPPase) and the K^+-independent H^+-pumps of *Pyrobaculum aerophilum* (PaPPase) and *Thiobacillus denitrificans* (TdPPase). TmPPase and PaPPase were purified by the ”hot-solve”-protocol (Kellosalo et al., 2011; López-Marqués et al., 2005) and I showed that both proteins were purified in their native oligomeric, dimeric, form (Kellosalo et al., 2011).

Both TmPPase and PaPPase were crystallised, and the activity and crystallisability of both of these proteins were tested in a range of different detergents (Kellosalo et al., 2011; Kellosalo et al., 2013). TmPPase crystals diffracting to 2.6 Å could be grown (Kellosalo et al., 2012; Kellosalo et al., 2013) in the presence of a novel octyl neopentyl glycol detergent (OGNPG, Chae et al., 2013), and these crystals allowed the protein structure to be solved.

Phasing the TmPPase structure was done by multiple isomorphous replacement with anomalous scattering (MIRAS) using Na_2WO_4 and tri-metyl lead acetate (TMLA) derivatised crystals and molecular replacement with Rosetta (Cowtan, 2001). This work

yielded a 2.6 Å structure of TmPPase in the metal-bound, resting state (TmPPase:Mg:Ca). Molecular replacement using this structure as a model was used to solve a 4 Å structure of TmPPase in the product bound conformation (TmPPae:Mg_4:K:Pi_2).

The solved, high-resolution TmPPase structure is very similar (r.m.s.d 1.57 Å for 517/618 aligned Cas) to that of *Vigna radiata* proton pumping M-PPase, which was also solved in 2012 (VrPPase:PNP, Lin et al., 2012). Both structures show a dimeric protein where the monomer consists of 16 α-helix containing subunits. The membrane spanning helices extend up to 27 Å into the cytoplasm and six of them (helices 5, 6, 11, 12, 15 and 16) enclose the active site cavity. Below the active site is a series of small cavities surrounded by helices 5, 6, 12 and 16 that leads to the periplasm/lumen and seems to form the exit channel for ion transfer. The cytoplasmic active site cavity is lined by conserved residues and has a three part structure consisting of a hydrolytic centre where the substrate binds, a ”coupling funnel” that couples pyrophosphate hydrolysis to ion-pumping, and a ”gate” that connects the cytoplasmic and periplamic/vacuolar cavities.

Comparison of the TmPPae:Mg_4:K:Pi_2 and TmPPase:Mg:Ca structures with VrPPase:PNP allowed me to analyse the catalytic cycle of M-PPases. The three M-PPase structures show that binding of the substrate induces both the ordering and movement of the loop between helices 5 and 6, which in turn closes the active site, and the movement of helix 12 towards the periplasmic part of the protein. Also, in the VrPPase:PNP structure, a conserved arginine is close to the cluster of conserved residues forming the gate. Based on these observations, I proposed a model of the catalytic cycle of M-PPases in which binding of the substrate leads to the formation of a transitory intermediate in which movement of helix 12 and the conserved arginine leads to opening of the gate and exit channel and to ion pumping.

The molecular structures of TmPPase have also shed light on the evolution of M-PPases: superposition of a structural motif containing four α-helices shows that M-PPases arose through gene triplication.

Abbreviations and acronyms

αUDM	n-Dodecyl-α-D-maltoside
αDM	n-Decyl-α-D-maltoside
aa	Amino acid
AFM	Atomic force microscopy
AMDP	Aminomethylene diphosphonate
ATP	Adenosine triphosphate
AtPPase	*Arabidopsis thaliana* membrane-bound pyrophosphatase
BPB	Bromophenacyl bromide
BvPPase	*Beta vulgaris* membrane-bound pyrophosphatase
C12E8	Octaethylene glycol monododecyl ether
C12E9	Nonaethylene glycol monododecyl ether
C-HEGA-10	Cyclohexylbutanoyl-N-Hydroxyethylglucamide
CHAPSO	3-[(3-Cholamidopropyl)-Dimethylammonio]-2-Hydroxy-1-Propane Sulphonate
CD	Circular dichroism
CmPPase	*Cucurbita moschata* membrane-bound pyrophosphatase
CsPPase	*Cucurbita sp.* membrane-bound pyrophosphatase
CtPPase	*Clostridium tetani* membrane-bound pyrophosphatase
CyFos-6	6-Cyclohexyl-1-Hexylphosphocholine
CYM-6	6-Cyclohexyl-1-hexyl-b-D-maltoside
CYM-5	5-Cyclohexyl-1-pentyl-b-D-maltoside
CYM-4	4-Cyclohexyl-1-butyl-b-D-maltoside
DCCD	*N,N'*-Dicyclohexylcarbodiimide
DDM	n-Dodecyl-β-D-maltoside
DEPC	Diethylpyrocarbonate
DM	n-Decyl-β-D-maltoside
DMNPG	Decyl maltose neopentylglycol
DNA	Deoxiribonucleic acid
D-thio-M	n-Decyl-β-D-thiomaltopyranoside
EDAC	1-Ethyl-3-(3-dimethylaminopropyl)carbodiimide.
FITC	Fluorescein isothiocyanate
FosC-12	n-Dodecylphosphocholine
FRET	Förster resonance energy transfer
GPCR	G-protein coupled receptor
H^+-PPase	Proton pumping membrane-bound pyrophosphatase
HEGA-10	Decanoyl-N-hydroxyethylglucamide
IDP	Imidodiphosphonate
K^+-dep H^+-PPase	Potassium dependent proton pumping membrane-bound pyrophosphatase
K^+-indep H^+-PPase	Potassium independent proton pumping membrane-bound pyrophosphatase
LDAO	Lauryldimethylamine-oxide

LCP	Lipidic cubic phase
M-PPase	Membrane-bound pyrophosphatase
MaPPase	*Methanosarcina acetivorans* membrane-bound pyrophosphatase
MIRAS	Multiple isomorphous replacement with anomalous scattering
MEGA-9	Nonanoyl-N-Methylglucamide
MmPPase	*Methanosarcina mazei* membrane-bound pyrophosphatase
MtPPase	*Moorella thermoacetica* membrane-bound pyrophosphatase
Na^+-PPase	Sodium pumping membrane-bound pyrophosphatase
Na^+, H^+-PPase	Sodium and proton pumping membrane-bound pyrophosphatase
NEM	*N*-ethylmaleimide
NG	Nonyl-β-glucoside
NPM	*N*-(1-pyrenyl)maleimide
OG	Octyl-β-glucoside
OGNPG	Octyl glycol neopentylglycol
OM	n-Octyl-β-D-maltoside
PGO	Phenylglyoxal
PAGE	Polyacrylamide gel electrophoresis
PaPPase	*Pyrobaculum aerophilum* membrane-bound pyrophosphatase
PcPPase	*Pyrus communis* membrane-bound pyrophosphatase
PEG	Polyethyleneglycol
Pi	Phosphate
PM	Plasma membrane
PPi	Pyrophosphate
PPase	Pyrophosphatase
RNA	Ribonucleic acid
r.m.s.d.	Root mean square deviation
RrPPase	*Rhodospirillum rubrum* membrane-bound pyrophosphatase
ScPPase	*Streptomyces coelicolor* membrane-bound pyrophosphatase
SDS-PAGE	Sodium dodecyl sulphate polyacrylamide gel electrophoresis
SEC-MALLS	Size exclusion coupled multi-angle laser light scattering
Se-Met	Seleno methionine
sPPase	Soluble pyrophosphatase
StPPase	*Symbiobacterium thermophilum* membrane-bound pyrophosphatase
TcPPase	*Trypanosoma cruzi* membrane-bound pyrophosphatase
TdPPase	*Thiobacillus denitrificans* membrane-bound pyrophosphatase
TgPPase	*Toxoplasma gondii* membrane-bound pyrophosphatase
TmPPase	*Thermotoga maritima* membrane-bound pyrophosphatase
TM	Transmembrane
TMH	Transmembrane helix
TMLA	Trimethyllead acetate
TNM	Tetranitromethane

UPR	Unfolded protein response
VrPPase	*Vigna radiata* membrane-bound pyrophosphatase
wt	Wild type
Å	Ångström (10^{-10} m)

Abbreviations of amino acids

A	Ala	Alanine
C	Cys	Cysteine
D	Asp	Aspartic acid
E	Glu	Glutamic acid
F	Phe	Phenylalanine
G	Gly	Glycine
H	His	Histidine
I	Ile	Isoleucine
K	Lys	Lysine
L	Leu	Leucine
M	Met	Methionine
N	Asn	Asparagine
P	Pro	Proline
Q	Qln	Glutamine
R	Arg	Arginine
S	Ser	Serine
T	Thr	Threonine
V	Val	Valine
W	Trp	Tryptophan
Y	Tyr	Tyrosine

Introduction

Membrane-bound pyrophosphatases were discovered in the 1970's when the presence of pyrophosphate was found to induce pumping of protons through the purple membranes of *Rhodospirullum rubrum* (Moyle et al., 1972). Later, pyrophosphate hydrolysis coupled proton pumping was discovered in plants (Karlsson, 1975), other bacteria (Schöke and Schink, 1998), archae (Drozdowicz et al., 1999) and protozoans (Scott et al., 1998). It was also shown that this activity came from a protein with just a single polypeptide chain (Nyren et al., 1991b; Kim et al., 1994), and that the protein is a dimer in its native state (Maeshima, 2000).

As the activity of some of the M-PPases increases in the presence of K^+ (Karlsson, 1975), the M-PPases can be classified into two different functional groups: K^+-dependent and K^+-independent enzymes. The K^+-dependent enzymes can be further classified on the basis of their pumping specificity into pyrophosphatases that pump either Na^+, H^+ or both Na^+ and H^+ (Luoto et al., 2013).

The activity of M-PPases is upregulated in plants and in bacteria in abiotic stress conditions such as anoxia, mineral defiency, cold, drought, salt stress and low light exposure (Garcia-Contreras et al., 2004; Lopéz-Marqués et al., 2004; Serrano et al., 2007). Under these conditions, cells are energy deficient and the upregulation is thought to take place because M-PPases can use PPi as an alternative energy source for the creation of a membrane potential. This relieves stress by allowing the maintenance of membrane integrity and intracellular transport (Stitt, 1998; Greenway and Gibbs, 2003). Over-expression of M-PPases has been shown to make plants more resistant to many of the above mentioned stress conditions (Serrano et al., 2007) and also to protect them from exposure to heavy metals (Khoudi et al., 2012).

The activity of M-PPases is also upregulated in young plant tissues (Maeshima, 2000). This is because, in plants, M-PPases are needed for the removal of cytoplasmic pyrophosphate, the build up of which would otherwise interfere with plant maturation by inhibiting various anabolic procesess, including gluconeogenesis and cellulose, nucleic acid and protein synthesis (Ferjani et al., 2011).

M-PPase inihibitors and knock-out of M-PPase expression by RNA-interference have been shown to inhibit the growth of protozooan parasites (Lemercier et al., 2002; McIntosh and Vaidya, 2002). Also, changes in the trafficking of M-PPases have been shown to abolish the virulence of *Leishmania major* in mice (Besteiro et al., 2008).

M-PPases have 14-17 transmembrane helices (Mimura et al., 2004) with most of the conserved residues situated in the cytosolic portion of the protein. The physiological substrate of M-PPases is Mg_2PPi and they require Mg^{2+} as a necessary co-factor for catalysis (Baykov et al., 1993a). Different studies have revealed the necessity of cytoplasmic conserved aspartates, lysines and glutamates for enzyme activity (Maeshima,

2000; McIntosh and Vaidya, 2002; Serrano et al., 2007). Studies have also revealed that certain residues have an effect on the coupling of pyrophosphate hydrolysis and ion-pumping (Zancani et al., 2007; Schultz and Baltscheffsky, 2003; Hirono et al., 2007a; Hirono et al., 2007b); the most significant effect is seen upon the mutation of a semi-conserved glutamate as this creates an uncoupled enzyme that shows pyrophosphate hydrolysis, but not ion-pumping activity (Luoto et al., 2011).

The recently solved structure of a proton-pumping pyrophosphtase of *Vigna radiata* with a competitive inhibitor bound (VrPPase:PNP, Lin et al., 2012)) and the structure of *Thermatoga maritima* Na^+-pumping pyrophosphatase discussed in this work have shed light on the structure and function of M-PPases. The two structures, taken together, complement each other and have allowed me to propose a structure-based catalytic cycle of M-PPases.

1 Literature review

1.1 M-PPases in the three domains of life

M-PPases are found in plants, algae, protozoans, bacteria and archae. M-PPases have also been detected by M-PPase specific antibodies in two insect species, *Periplaneta americana* (Motta et al., 2009) and *Rhodnius prolixus* (Motta et al., 2004). However, as these insects are known to be carriers of protozoan parasites and no genes coding for M-PPases have yet been found in insects, it is likely that M-PPases are only coded by the genomes of the parasite protists (Malinen, 2009). If the, at the moment doubtful, presence of M-PPases in insects is ignored, the M-PPases are absent in both Animalia and Fungi and were probably lost in the clade leading to these kingdoms when the Opisthokonta and Amoebozoa were separated.

All plant species studied so far are known to have M-PPases (Gaxiola et al., 2007). In algae only species from the group glaucophytes lack M-PPases (Malinen, 2009). The distribution is more sporadic in protozoans and prokaryotes and only certain groups of these organisms contain M-PPases (Malinen, 2009). In prokaryotes, the distribution can also be sporadic inside a certain group: for example, the firmicutes *Clostridium tetani* and *Clostridium thermocellum* have M-PPases while *Clostridium perfringes* and *Clostridium acetobutylicum* lack them (Malinen, 2009).

On the basis of their pumping and co-factor specificity, M-PPases can be divided into four different functional classes: K^+-independent H^+-pumping pyrophosphatases (K^+-indep H^+-PPases), K^+-dependent H^+-pumping pyrophosphatases (K^+-dep H^+-PPases), K^+-dependent Na^+-pumping pyrophosphatases (Na^+-PPases) and K^+-dependent Na^+ and H^+-pumping pyrophosphatases (Na^+, H^+-PPases) (Luoto et al., 2013). The K^+-dependency was discovered when it was realized that the enzyme activity could be increased by the addition of K^+ (Karlsson, 1975). Both K^+-independent and K^+-dependent H^+-PPases occur in all of the above-mentioned sub-kingdoms and kingdoms, but only prokaryotes have Na^+-PPases and Na^+, H^+-PPases.

As the utilisation of PPi as an energy carrier has been hypothesized to have taken place in the early evolution of life, before the adoption of ATP (Lipmann, 1965), M-PPases might have been the very first enzymes coupling hydrolysis or formation of the phosphoanhydride bond to changes in electrical potential energy (Baltscheffsky et al., 1999; Hedlund et al., 2006; Holm and Baltscheffsky, 2011). As more complex, less leaky, membrane structures are required for the retention of protons than for the retention of sodium ions and as it is unlikely that the complex Na^+-binding site of the different Na^+-pumping A/F/V-ATPases would have evolved multiple times independently, Mulkidjian and coworkers (2008a,b) proposed that the use of Na^+ could have preceded the use of H^+ in the creation of membrane potential. Following this thought, the first M-PPases would

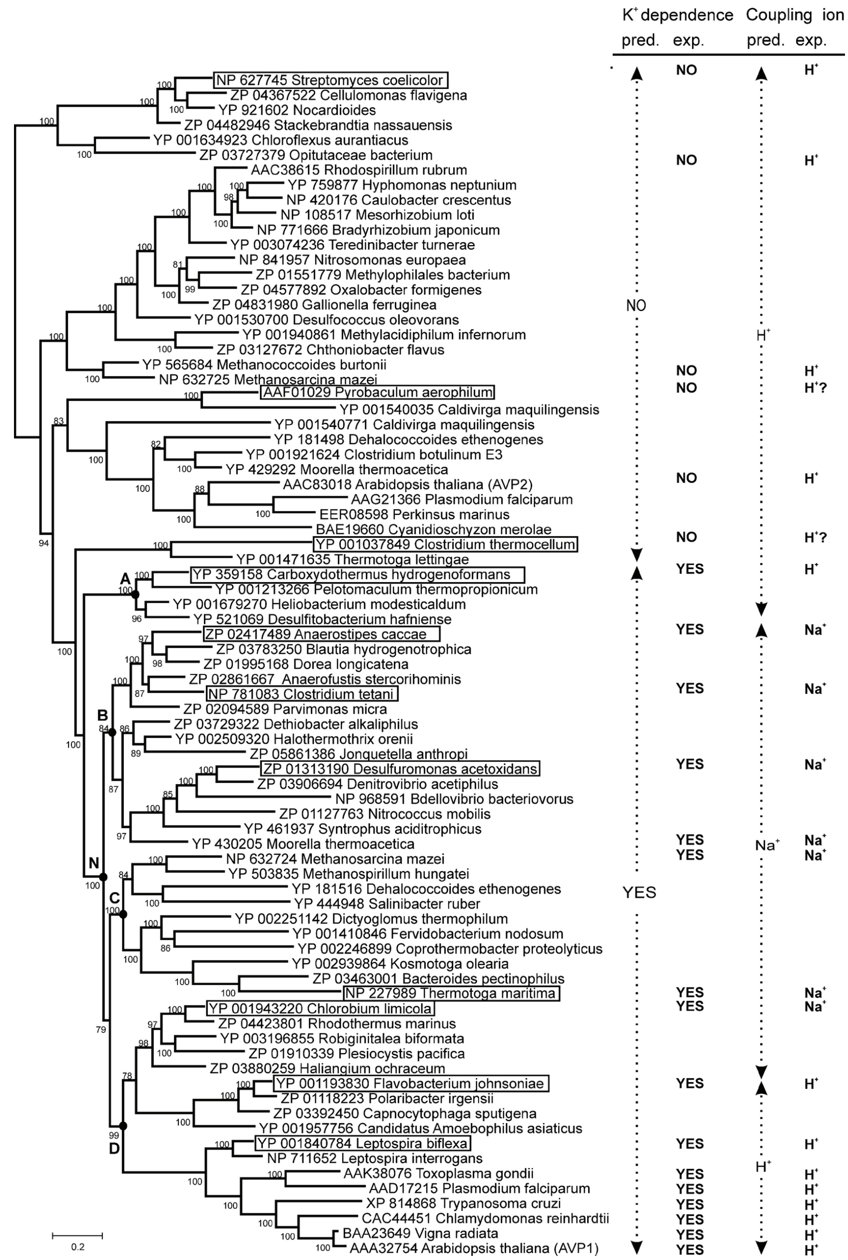

Figure 1. Phylogenetic tree of M-PPases (reprinted from Luoto et al., 2011 with permission). The tree is arbitrarily rooted with the clade leading to the *S. coelicolor* H^+-likely been Na^+-PPases. PPase and shows the GenBank^{TM} protein sequence numbers for the M-PPases before the species name. The experimentally verified and predicted K^+ -dependence and coupling ion specificity of the M-PPases are shown on the right side.

have likely been Na^+-PPases. The primacy of Na^+-PPases is backed by phylogenetic analysis (see 1.3.3. and Figure 1), which shows that the Na^+-PPases form a monophyletic clade, while the H^+-PPases form at least six independent clades (Luoto et al., 2011). The primacy of Na^+-PPases is also suggested by their presence in anaerobic prokaryotes, which have ancient evolutionary origins (Luoto et al., 2011). The last group of M-PPases to evolve would then have been the K^+-independent H^+-PPases, which would have evolved after the development of H^+-pumping activity (Luoto et al., 2011). The evolution of Na^+, H^+-PPases has likely been due to mutation of four residues (see 1.3.3), which has created enzymes with dual pumping specificity (Luoto et al., 2013).

PPi, the substrate of M-PPases, is mostly created by anabolic processes such as protein, DNA and RNA synthesis in which this compound is released during ATP hydrolysis (Baykov et al., 1999). The role of M-PPases in PPi metabolism of different organisms will be further discussed in the follow sections.

Table 1. Distribution of M-PPases in prokaryotes and protozoans (Modified from Malinen, 2009).

Archae	M-PPases	**Bacteria**	M-PPases	**Protozoans**	M-PPases
Crenearcheota	**Yes**	Actinobacteria	**Yes**	Alveolata	**Yes**
Euryarcheota	**Yes**	Aquificae	No	Amoebozoa	**Yes**
Korarcheota	**Yes**	Bacteroidetes/Cholorobi	**Yes**	Apusozoa	No
Nanoarcheota	No	Chlamydiae/Verrucomicrobia	**Yes**	Centroheliozoa	No
		Choloroflexi	**Yes**	Diplomonadida	No
		Chrysiogenetes	No	Euglenozoa	**Yes**
		Cyanobacteria	No	Heteroblosea	No
		Deferribacteres	No	Jacobida	No
		Deinococcus-Thermus	No	Katablepharidophyta	No
		Dictyloglomi	**Yes**	Malawimonididae	No
		Fibrobacteres/Acidobacteria	No	Nucleariidae	No
		Firmicutes	**Yes**	Oxymonadida	No
		Fusobacteria	**Yes**	Parabasalidea	No
		Gemmatimonadetes	No	Rhizaria	**Yes**
		Nitrospirae	No		
		Plantomycetes	**Yes**		
		Proteobacteria	**Yes**		
		Spirochaetes	**Yes**		
		Synergistetes	No		
		Tenericutes	No		
		Thermodesulphobacteria	No		
		Thermotogae	**Yes**		

1.1.1 Physiological role of M-PPases

1.1.1.1 M-PPases in plants and algae

In plants and algae, proton pumping M-PPases are found in the vacuolar and Golgi membranes, with the concentration of vacuolar M-PPase being around 500-fold higher than that of the Golgi M-PPase (Segami et al., 2010; Gaxiola et al., 2012). As different isoforms are found in the vacuole and the Golgi, the possibility that the Golgi M-PPases are only an artefact of vacuolar trafficking can be ruled out (Segami et al., 2010). M-PPases are also found in the plasma membrane (PM) of root and cotyledon phloem cells (Gaxiola et al., 2012). The levels of vacuolar M-PPases are upregulated in young plant tissues and the expression of M-PPase is crucial for plant maturation (Maeshima et al., 2000). As substitution of the vacuolar M-PPase by a soluble PPase reinstates wild-type maturation, it seems that it is the pyrophosphatase activity of this protein that is necessary for proper plant development (Ferjani et al., 2011). This is because pyrophosphate hydrolysis is required for driving various anabolic processes (Baykov et al., 1999). Studies on plants lacking vacuolar pyrophosphatase have shown increased cytoplasmic pyrophosphate concentrations and lowered cytoplasmic sucrose concentrations. This would indicate that the inhibition of gluconeogenesis is the major cause for the stunted maturation of mutant plants (Ferjani et al., 2011).

Besides their role in plant maturation, vacuolar M-PPases are important for stress tolerance under abiotic stress conditions (see 1.1.1.4.), as are PM M-PPases and possibly also Golgi M-PPases (Segami et al. 2010). Studies on *Arabidopsis thaliana* lacking V-ATPase activity have also shown that the tonoplast energization carried out by a vacuolar M-PPase is enough for maintaining the viability of the plant. The mutated plant did, however, suffer from day-length-dependent growth retardation and showed reduced tolerance for zinc (Krebs et al., 2010). As acidification of Golgi by V-ATPases is necessary for the proper function of the organelle (Forgac, 2007), Golgi M-PPases might, like vacuolar M-PPases, similarly complement V-ATPase activity. This might be especially important in energy-constrained stress conditions (see 1.1.1.4.).

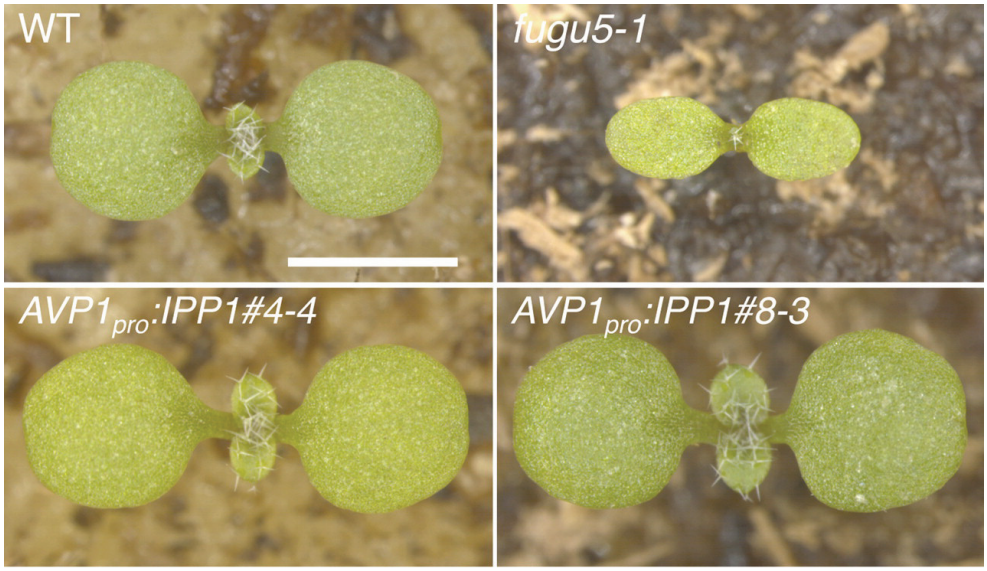

Figure 2. The effect of the loss of pyrophosphatase activity on the maturation of *Arabidopsis thaliana* (reprinted from Ferjani et al., 2011 with permission),. The upper pictures show seedlings of a wild-type plant and a *fugu5-1* mutant lacking vacuolar M-PPase. The two bottom pictures show the restoration of wild-type like maturation when soluble pyrophosphatase (IPP1) is heterologously expressed in the *fugu5-1* plant.

In citrus plants, M-PPases seem to have a differing physiological role. For instance, the vacuolar M-PPase of orange seems to be involved in the synthesis of PPi during development (Marsh et al., 2000), while the vacuolar M-PPase of lime does not show any proton pumping activity (Marsh et al., 2001). In orange the synthesized PPi could act as substrate for PPi utilising phosphofructokinase and UTP—glucose-1-phosphate uridylyltransferase (Marsh et al., 2000).

1.1.1.2 M-PPases in protozoans

In protozoans, proton pumping M-PPases are found in the membranes of acidocalcisomes and in some cases in the plasma membrane and membranes of Golgi and digestive vacuoles. As in plants, the activity of H^+-PPases in these membranes is thought to complement the proton pumping activity of proton pumping ATPases. In contrast to plants, where the vacuolar M-PPase is the most abundant form of the protein, in protozoans the most abundant form is the acidocalcisomal M-PPase (Moreno and Docampo, 2009).

The vacuole-like acidocalcisomes are organelles that are important for pH homeostasis, osmoregulation and the storage of phosphorus and cations, and contain high concentrations of phosphate either as polyphosphate or pyrophosphate and Mg^{2+}, Ca^{2+},

Zn^{2+} and in some cases iron. As the polyphosphate content of aciodocalcisomes changes during the life cycle of trypanosomatids and transmission of these organisms from invertebrate to vertebrate host requires osmoregulatory adjustment to hypoosmotic shock, acidocalcisomes are thought to have an important role in the differentiation and life cycle of protozoans. Related to this, defective transport of Ca^{2+} into the acidocalciomes decreases the virulence of *Toxoplasma gondii* (Moreno and Docampo, 2009).

Studies have been carried out on strains of *Trypanosoma brucei* and *Leishmania major* that lack acidocalcisomal M-PPase either because of loss of expression through RNA interference (Lemercier et al., 2002) or because of defective trafficking (Besteiro et al., 2008), respectively. The *T. brucei* strain shows reduction in the organism's ability to regulate cytoplasmic pH, loss of functional acidocalcisomes and reduction in growth rate, while the *L. major* strain could no longer infect mice. Additionally, the presence of M-PPase inhibitors (Figure 3) has been shown to reduce the growth of protozoans (McIntosh and Vaidya, 2002). These results indicate that M-PPases are a possible drug target against protozoans responsible for diseases such as malaria, sleeping sickness and visceral leishmaniasis. The fact that humans lack M-PPases makes these proteins especially attractive targets for anti-protozoan drugs.

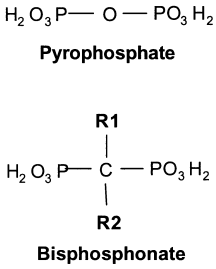

Compound	R1	R2
AMDP	H	NH_2
Etidronate	OH	CH_3
Clodronate	Cl	Cl
Pamidronate	OH	$(CH_2)_2NH_2$
Tiludronate	H	CH_2-S-  -Cl
Risidronate	OH	CH_2- 

Figure 3. The structure of pyrophosphate and biphosphonate analogues that are M-PPase inhibitors (Figure reproduced from McIntosh and Vaidya, 2002 with permission from Elsevier) . Of the bisphosphophosphonates shown, AMDP, pamidronate and risidronate inhibit the growth of protozoans (McIntosh and Vaidya, 2002).

1.1.1.3 M-PPases in prokaryotes

M-PPases in prokaryotes occur in invaginations of the plasma membrane (Serrano et al., 2007). Some bacterial species, such as *Rhodspirillum rubrum* and *Agrobacterium tumefaciens,* have acidocalcisome-like organelles and have M-PPases in the membranes of these organelles (Figure 4) (Seufferheld et al., 2003; Seufferheld et al., 2004). These M-

PPases, like M-PPases of the protozoan acidocalcisomes, acidify the lumen of the bacterial organelles (Seufferheld et al., 2004).

In *Rhodspirillum rubrum*, M-PPases are found in invaginations of the plasma membrane called chromatophores (Moyle et al., 1972). Light-dependent synthesis of PPi has been seen with extracted chromatophore membranes (Baltscheffsky et al., 1966; Guillory and Fisher, 1972). This function has been hypothesized to have physiological relevance and to drive the formation of PPi-containing, acidocalcisome-like organelles during light illumination (Nyren and Strid, 1991).

Besides the H^+-pumping pyrophosphatases (H^+-PPases) found in plants and protozoans, some prokaryotes contain additionally or alternatively Na^+-pumping pyrophosphatases (Na^+-PPases) and both Na^+ and H^+-pumping pyrophosphatases (Na^+, H^+-PPases) (Malinen et al., 2007; Luoto et al., 2013). Na^+-PPases are found in organisms such as *Thermotoga maritima,* which employs Na^+ as the biological energy carrier for ATP synthesis (Dimroth and Cook, 2004; Häse et al., 2001, Luoto et al., 2011) and also in halotolerant and anaerobic prokaryotes with H^+-transport-coupled energy metabolism (Luoto et al., 2011). The Na^+-PPases of the halotolerant organisms might help in increasing the salt tolerance of these organisms by extruding cytoplasmic Na^+ (Luoto et al., 2011). The presence of both Na^+-PPases and H^+-PPases in some prokaryotes might be beneficial for these organisms, as it would allow the creation of both Na^+ and H^+-gradients (Luoto et al., 2011).

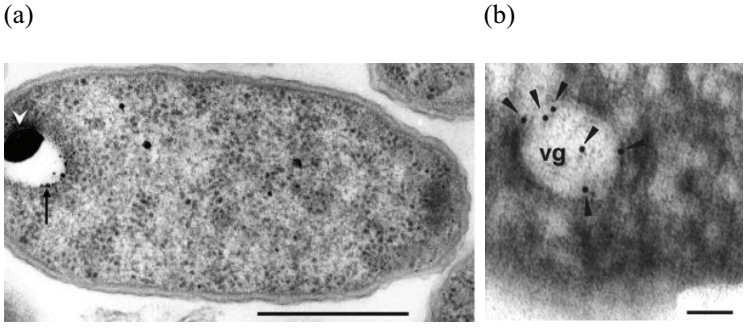

Figure 4. Acidocalcisome-like organelles in *A. tumefaciens* (From Docampo and Moreno, 2011, reproduced with permission from Elsevier). (a) Electron micrograph of bacterium with black arrow pointing to electron-dense material in the periphery of the organelle and white arrowhead pointing to electron-dense inclusion. (b) Immunoelectron microscopy showing the presence of gold-particle labelled M-PPase in the acidocalcisome-like organelle.

Na^+, H^+-PPases are found in anaerobic bacteria (Luoto et al., 2013). As the anaerobic habitat reduces the amount of energy that organisms gain from catabolic reactions, it might have driven the evolution of enzymes that can utilize pyrophosphate, normally a metabolic waste product, for the generations of both Na^+ and H^+ gradients (Luoto et al.,

2013). Many of the Na^+, H^+-PPase containing bacteria are found in the gut flora of humans (Luoto et al., 2013) and some of them are pathogenic, suchs as *Bacteroides fragilis*, which causes brain and gastrointestinal tract abscesses.

1.1.1.4 M-PPases and stress tolerance

The activity of M-PPases is upregulated in abiotic stress conditions. Upregulation has been found to be induced in plants by chilling, anoxia, mineral deficiency and salt stress (Maeshima, 2000) while the expression of M-PPase has been found to be upregulated by low-light exposure, high salt content and anoxia in *Rhodospirillum rubrum* (Garcia-Contreras et al., 2004; Lopéz-Marqués et al., 2004). The cause of this upregulation is thought to be that the cells prefer to use PPi as an energy source under conditions that constrain the availability of energy (Garcia-Contreras et al., 2004; Stitt, 1998). PPi hydrolysis coupled ion-transport relieves the stress as the creation of membrane potential allows the maintenance of membrane integrity and intracellular transport (Stitt, 1998; Greenway and Gibbs, 2003). This hypothesis is supported by mutational studies on *Rhodospirillum rubrum* that have shown that, although the growth of a strain lacking M-PPase is otherwise indistinguishable from that of wild-type cells, its growth-rate is significantly lower under low-light exposure and anoxia (Garcia-Contreras et al., 2004). Due to the necessity of the pyrophosphatase activity of M-PPases for the maturation of plants (Ferjani et al., 2011), the role of the ion-pumping activity of the M-PPases in conferring stress tolerance has not yet been verified by M-PPase knock-out mutations. The recent findings of Ferjani and co-workers (2011), however, make it possible to determine this. Experiments on the role of M-PPases in stress tolerance could be carried out on a mutant strain which has a heterologous soluble pyrophosphate in place of the M-PPase and which shows wild-type like maturation (Ferjani et al., 2011). A conditional M-PPase knockout mutant that is only turned on after maturation would be another approach to answering this question.

An indication of the importance of M-PPases in stress response in plants comes from studies with modified strains that overexpress M-PPase. These strains show increased resistance to the abiotic stress conditions that cause M-PPase upregulation in wild-type plants (Figure 5). M-PPase overexpression in *Arabidopsis thaliana*, alfalfa, tomato, apple, creeping bentgrass, tobacco, rice, maize and cotton makes these plants more drought and salt resistant (Zhao et al., 2006; Lv et al., 2009; Li et al., 2008; Li et al., 2010; Dong et al., 2011; Bao et al., 2009; Gaxiola et al., 2007). Overexpression of M-PPase in tomato, maize and *A. thaliana* leads, in addition, to enhanced growth performance under P_i starvation (Gaxiola et al., 2012). M-PPase overexpression has also been shown to enhance the cold and heat tolerance of apple (Dong et al., 2011) and rice (Zhang et al., 2011), to increase the tolerance of tobacco plants for cadmium (Khoudi et al., 2012) and to improve the nitrogen uptake in romaine lettuce (Paez-Valencia et al., 2013)

The protective effect against drought, salinity and mineral deficiency upon M-PPase overexpression is probably partly due to increased root and shoot growth (Li et al., 2005). This is likely due to the increased levels of auxin seen in the root and shoot tips of these plants (Li et al., 2005). As auxin is a weak acid with a pK_a of 4.75, increased transport of auxin into the cells may be caused by the higher activity of plasma membrane M-PPases: decrease of the extracellular pH by these enzymes drives the protonation of auxin and its transport through the plasma membrane (Li et al., 2005, Malinen, 2009). The M-PPase overexpression increases also rhitzosphere acidification, which enhances nutrient uptake (Yang et al., 2007)

Another factor conferring resistance against stress conditions is the increased proton-motive force created by M-PPases (Duan et al., 2007). This can then be employed by various cotransporters for ion transport into the vacuole (Gaxiola et al., 2001; Khoudi et al., 2012; Duan et al., 2007) and into the cell (Yang et al., 2007; Li et al., 2011). Vacuolar sequestration is not only beneficial for water retention and the removal of toxic ions such as Na^+, which cytoplasmic concentrations rise during drought and in conditions of high salinity (Gaxiola et al., 2007), but can also confer resistance against heavy-metal exposure. For instance, upon exposure to cadmium, tobacco plants overexpressing M-PPase showed higher cadmium accumulation, but at the same time also higher tolerance to cadmium, than wild-type plants (Khoudi et al., 2012).

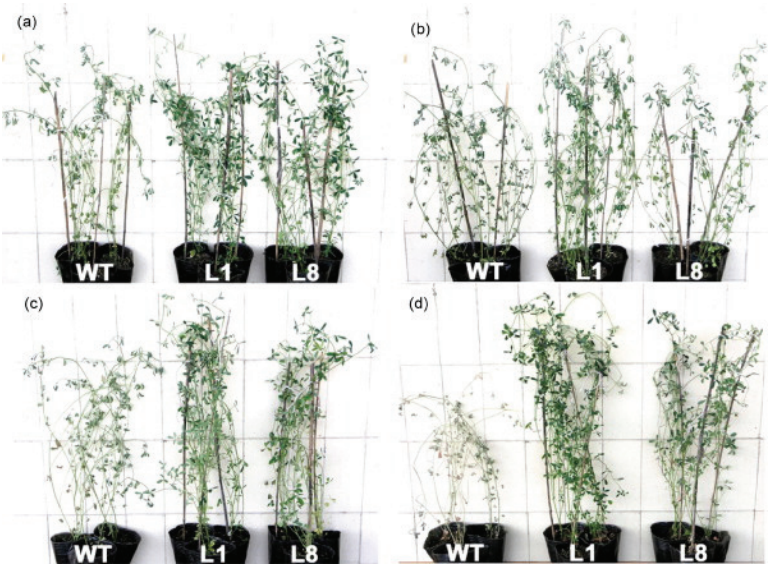

Figure 5. M-PPase overexpression protects alafalfa from drought (reprinted from Bao et al., 2009 with permission from Elsevier). Wildtype (WT) and M-PPase overexpressing plants (L1 and L8) were allowed to dry by withholding water for 6 days (a) and for 8 days (b). After 8 days without water the plants were rewatered for 1 day (c) and 4 days (d).

M-PPase overexpression has also been shown to increase the concentration of proline inside plant cells and lower the concentration of malondialdehyde, a marker for lipid oxidation (Dong et al., 2011; Zhang et al., 2011). As proline stabilises biological membranes (Clause, 2005), its increased concentration may explain the lowering of the malondialdehyde concentration and is probably the reason for the heat and cold resistance of apples (Dong et al., 2011) and rice (Zhang et al., 2011) that overexpress M-PPase. Proline is also known to function as an osmotic balancer and its higher concentration might also help the cells to cope in conditions of drought and high salinity (Clause, 2005).

Overexpression of M-PPases in *Escherichia coli* and *Saccharomyces cerevisiae*, two species, which genomes do not code for M-PPases, shows similar protection against abiotic stress as it does in plants (Yoon et al., 2013). Both in *E. coli* and in *S. cerevisiae* M-PPase overexpression protected the cells against salinity and heavy-metal toxicity and in *E. coli* it also conferred protection against heat and hydrogen peroxide (Yoon et al., 2013). Additionally, the heterologous expression of *Dunaliella viridis*, wheat, tobacco and *A. thaliana* M-PPases in the G19 (Δena1-4) and ena1 mutant strains, respectively, of *S. cerevisiae* suppressed the Na^+ hypersensitivity of the strains (Figure 6) (Gao et al., 2006; Meng et al., 2011; Brini et al., 2005).

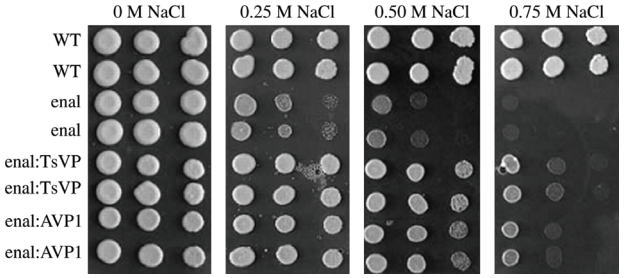

Figure 6. Expression of M-PPases (either tobacco (TsVP) or *A. thaliana* (AVP)) protects the ena1-mutant strain of *S. cerevisiae* from high salt concentrations (reprinted from Gao et al., 2006 by permission of Oxford University press).

1.1.1.5 Complementation by M-PPases

Studies with *S. cerevisiae* have revealed that M-PPases can complement proteins with related activity: yeast strains lacking either soluble pyrophosphatase or V-type ATPase could be revived by the heterologous expression of an M-PPase (Pérez-Castiñeira et al., 2002; Pérez-Castiñeira et al., 2011).

1.2 Enzymatic properties of M-PPases

1.2.1 Substrate and Mg^{2+}-binding

The catalytically active substrate for M-PPases is Mg_2PPi (Baykov et al., 1993a). The K_m for this substrate varies from 2 μM to 8 μM depending on the enzyme and the conditions of the enzymatic assay (Baykov et al., 1993a; Hirono et al., 2005; Gordon-Weeks et al., 1996; Malinen et al., 2008).

Besides the magnesium that comes with the pyrophosphate, M-PPases require free Mg^{2+} for activity (White et al., 1990). Results of steady-state kinetic measurements and enzyme modification experiments in the presence of Mg^{2+} have indicated that M-PPases have two distinct activating binding sites for Mg^{2+} (Baykov et al., 1993a; Baykov et al., 1996). One of these sites is a high-affinity binding site with a K_d = 20 – 42 μM, while the other is a low affinity binding site with a K_d = 0.25 – 0.46 mM (Maeshima, 2000). Experiments with *Methnanosarcina mazei* M-PPase have indicated the presence of a third, inhibitory binding site for Mg^{2+} with a very low binding affinity ($K_d \approx$ 100 mM, Malinen et al., 2008).

Besides Mg^{2+}, Mn^{2+}, Zn^{2+} and La^{3+} (and Co^{2+} in the case of *R. rubrum*) can support the hydrolytic activity of M-PPases, albeit at much reduced levels (PPase activity with Mn^{2+}, Zn^{2+} and La^{3+} 4 - 20 %, 0 – 5 % and 7 % of the Mg^{2+}-activity, respectively) (Velázquez et al., 1993; Celis and Romero, 1987; Romero and Celis, 1995; Malinen et al., 2008; Pérez-Castiñeira et al., 2001; Hirono et al., 2005; Drozdowicz et al., 1999). An exception to this is the K^+-indep H^+-PPase AtVHP2 of *A. thaliana*, which has higher PPase activity with Zn^{2+} than with Mg^{2+} (Segami et al., 2010). Ca^{2+} is a strong inhibitor of M-PPase (Maeshima, 2000). Its inhibitory effect is thought to be caused either by the binding of the free Ca^{2+}-ion (K_i = 0.2 μM, Rea et al., 1992a) or by the binding of CaPPi (Maeshima, 1991) to the enzyme. Of the other tri -or divalent cations, Cd^{2+}, Co^{2+}, Cu^{2+}, Sr^{2+} and Ni^2 have been found to inhibit the K^+-dep H^+-PPase of *V. radiata* (Maeshima, 1991; Nakanishi et al., 2003), while Al^{3+}, but not Ni^{2+}, inhibited the K^+–indep H^+-PPase of *S. coelicolor* (Hirono et al., 2005). Also, Co^{2+} and Ni^{2+} have been shown to bind *M. mazei* Na^+-PPase as they protect it from trypsin digestion and mersalyl inactivation (Malinen et al., 2008).

1.2.2 K^+-dependence

The activity of K^+-dependent Na^+ -and H^+-PPase is stimulated 2-14-fold by K^+ with the maximal activity attained with 30 - 50 mM K^+ (Maeshima, 2000). Three other monovalent cations, Cs^+, Rb^+ and NH_4^+, have been found to have similar, albeit lower, activating effects to K^+ (Obermeyer et al., 1996; Wang et al., 1986; Gordon-Weeks et al., 1997; Zhen

et al., 1997b; Zhen et al., 1997a). The K^+-dependence of M-PPases is dictated by a conserved GNXX(K/A)AX(G/T/A)-motif found in a putative loop between helices 11 and 12 (Belogurov and Lahti, 2002). The K^+-dependent enzymes have an alanine in the first variable position and either an alanine or glycine in the second, while K^+-independent enzymes have a lysine and a threonine. Studies on the *Carboxythermus hydrogenformans* M-PPase have shown that the K^+-dependence of this enzyme can be abolished by the A460K mutation (Belogurov and Lahti, 2002), where the alanine in the first variable position is replaced by a lysine. This indicated that the activating effect of the bound K^+ can be replaced by the positively charged lysine side chain in K^+-independent enzymes.

1.2.3 Effect of Na^+ on M-PPase activity

Na^+-PPase has an absolute requirement for either Na^+ or Li^+ for activity (Belogurov et al., 2005). In the absence of K^+, the effect of Li^+ is similar to Na^+; on the other hand, K^+ does not increase the activity in the presence of Li^+. Some Na^+-PPases have a single binding site for Na^+ (Luoto et al., 2011), while other Na^+-PPase have two (Figure 7, Belogurov et al., 2005). The K_d of single Na^+-binding has been measured to be 9 - 80 mM in the absence of K^+, depending on the enzyme, while binding of K^+ brings the K_d down to 0.036 – 0.45 mM (Malinen et al., 2007; Malinen et al., 2008; Luoto et al., 2011). TmPPase has putatively two binding sites for Na^+ and the K_d of these is 3 mM and 26 mM in the absence of K^+ and 0.4 mM and 3 mM in the presence of K^+ (Belogurov et al., 2005). Like Na^+-PPases, Na^+, H^+-PPases also require Na^+ for activity and their K_d for Na^+ binding is also lowered by K^+ (Luoto et al., 2013).

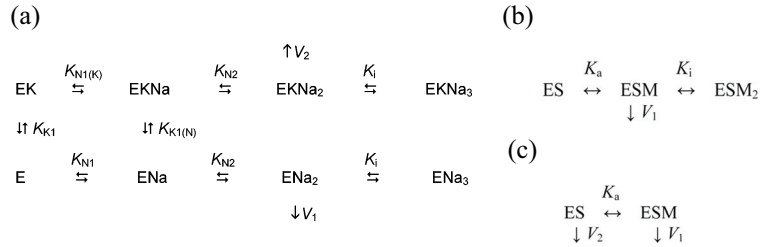

Figure 7. Reaction schemes of Na^+-PPases binding either two (a) or one (b), (c) sodium ion (Reaction scheme (a) reprinted with permission from Belogurov et al., 2005. Copyright 2005 Americal Chemical Society. Reaction schemes (b) and (c) from Luoto et al., 2011, reprinted with permission). The reaction scheme for Na^+-PPases binding two Na^+ (a) shows that the enzyme is capable of catalysis after it has bound two Na^+. The binding of K^+ activates the enzyme (activity constant V_1 changes to V_2) and the binding of the third Na^+ inhibits the enzyme. (b) and (c) show the reaction schemes for monovalent cation binding in the one Na^+ binding Na^+-PPases. (b) Shows the reaction scheme for Na^+-binding, while (c) shows the reaction scheme for K^+-binding (in (b) and (c) M signifies Na^+ and K^+, respectively).

Na^+ has been found to inhibit some K^+-dep H^+-PPases (Maeshima, 2000), while it has a slight activating effect on others in the absence of K^+ (Obermeyer et al., 1996; Gordon-Weeks et al., 1997; Rea and Poole, 1985). The inhibitory or slightly activating effect is probably due to the binding of the Na^+ to the potassium ion binding site. A similar kind of inhibitory effect is also seen in the K^+-dependent Na^+-PPases and Na^+, H^+-PPases, as the activity of these enzymes is inhibited by high Na^+-concentrations (Belogurov et al., 2005; Malinen et al., 2007; Malinen et al., 2008; Luoto et al., 2011; Luoto et al., 2013). The D703N mutation in TmPPase creates an enzyme that is inhibited by K^+ concentrations greater than 10 mM. The altered kinetic properties of the D703N-mutant of TmPPase could be caused by the conversion of one Na^+-site to an inhibitory K^+-binding site (Belogurov et al., 2005).

1.2.4 Ion pumping activity

While reconstitution of purified H^+-PPases has proved that they pump protons (Britten et al., 1992; Nyren et al., 1991b), no Na^+ pumping experiments have yet been carried out on purified and reconstituted Na^+-PPases. The pumping specificity of the Na^+-PPases has been verified, however, by carrying out experiments on Na^+-PPase enriched bacterial membranes in the presence of the proton gradient dissipator carbonyl cyanide *m*-cholorophenylhydrazone (Malinen et al., 2007). As Na^+-PPases show pumping of $^{22}Na^+$ in the presence of this protonophore, the transport of Na^+ through exchange of a transient H^+ gradient by, for example, Na^+/H^+-antiporters can be ruled out. Similar experiments with Na^+ and H^+ ionophores have also confirmed the dual pumping specificity of Na^+, H^+-PPases (Luoto et al., 2013).

H^+-PPases, Na^+-PPases and Na^+, H^+-PPases are all electrogenic pumps (Guillory and Fisher, 1972; Malinen et al., 2007; Luoto et al., 2013). Studies on plant tonoplast H^+-PPases have shown that these enzymes can produce a 270 mV membrane potential (Ros et al., 1995) and can pump protons against a 10,000-fold concentration gradient (Hedrich et al., 1989; Johannes and Felle, 1990). Studies to measure the membrane potential that Na^+-PPase and Na^+, H^+-PPases can generate have not yet been carried out. The H^+/PPi stoichiometry has been calculated to be one for the plant enzymes. Johannes and Felle (1989) calculated this stoichiometry based on the maximal proton-motive force that can be created from the free energy of pyrophosphate hydrolysis, while Schmidt and Briskin (1993) calculated the same value based on mathematical models of ΔpH formation, the rate of pyrophosphate hydrolysis and on the rate of H^+ leakage after H^+ pump inhibition at a steady state ΔpH. Finally, Nakanishi and coworkers' (2003) patch-clamp studies of heterologously produced VrPPAse also revealed an H^+/PPi stoichiometry of one. The H^+/PPi stoichiometry of RrPPase has been reported to be two (Sosa and Celis, 1995). This suits the hypothesized reversibility of RrPPase, as a stoichimetry of two protons per PPi would allow the synthesis of PPi with lower membrane potential than if the stochiometry were one (Malinen, 2009). This can be understood on the basis of an equation describing the thermodynamics of PPi synthesis by M-PPases: $n=\Delta G_{PPi}/\Delta\mu_{H^+}$, where *n* is the minimal

number of transported protons required for the synthesis of one PPi molecule, ΔG_{PPi} is the free-energy required for the synthesis of one PPi molecule and $\Delta\mu_H^+$ is the proton electrochemical potential or proton-motive force (Malinen, 2009). If the equation is changed to the form: $\Delta\mu_H^+ = \Delta G_{PPi}/n$, we can see that when *n* increases, a weaker proton-motive force is sufficient for PPi synthesis (Sosa and Celis, 1995).

The Na^+-PPases and H^+-PPases do not show cross specificity in their pumping activity (Malinen et al., 2007; Luoto et al., 2011); H^+-pumping by Na^+-PPases does not occur even at pH 5.5. As Malinen and co-workers have pointed out (2007), in contrast to this, Na^+/K^+-ATPases and the Na^+-pumping F_oF_1-ATPases show proton pumping at low pH or at low Na^+-concentrations (Polvani and Blostein, 1988; Laubringer and Dimroth, 1989) and H^+/K^+-ATPases show sodium pumping at high pH (Polvani et al., 1989). Changes in pH or in Na^+ concentration had no effect on the ratio of Na^+ and H^+ transport activities of Na^+, H^+-PPases, which indicates simultaneous, non-competetive pumping of both Na^+ and H^+ by these enzymes (Luoto et al., 2013). Na^+-PPases do not show pumping of $^{86}Rb^+$, showing that Na^+-PPases do not pump the higher atomic mass congeners of Na^+ (Malinen et al., 2007). As Li^+ can substitute for Na^+ in activating M-PPases (Belogurov et al., 2005), Na^+-PPase might nevertheless pump Li^+. This is, however, difficult to study as Li^+-specific dyes and stable radioisotopes of Li^+ do not exist.

1.3 Residue conservation in M-PPases

Most of the conserved residues in M-PPases occur in the cytoplasmic part of the protein. Mutation studies of these residues on a number of different M-PPases have revealed a large group of conserved aspartates, lysines and glutamates that are important for enzyme activity (Table 2). Mutation studies have also revealed four conserved residues where mutation leads to selective impairment of ion pumping (Table 3).

Three conserved, charged motifs can be identified in all M-PPases (Figure 8). These all occur in the cytoplasmic part of M-PPases, including the DX_7KXE and DX_3DX_3D-motifs found in the middle of the protein and a second DX_3DX_3D-motif in the C-terminal part of the protein. The N-terminal and C-terminal DX_3DX_3D-motifs are also called acidic motifs I and II, respectively.

Antibodies raised against the DVGADLVGKVE (DX_7KXE)-motif of VrPPase (Takasu et al., 1997) are able to recognize all M-PPases (Maeshima, 2000) due to the universality of the DX_7KXE-motif. The antibodies strongly suppressed both the hydrolytic and proton pumping activities of VrPPase (Takasu et al., 1997). Studies have also shown that VrPPase mutated at either the lysine or the glutamate of the DVGADLGKVE-motif (K261A or E263A, corresponding to TmPPase K210 and E212) is, in contrast to wild-type enzyme, not protected from trypsin digestion by Mg_2PPi, (Nakanishi et al., 2001). The E263D mutation of VrPPase has also been shown to increase the K_M for Mg_2PPi from 4.6 μM to 10.6 μM (Nakanishi et al., 2003). These results suggest that the residues of the

DX_7KXE-motif take part in substrate binding and hence it has been called as a PPi-binding motif (Baltscheffsky et al., 1999).

Table 2. Mutational studies on conserved aspartate, glutamate and lysine residues of M-PPases that affect both hydrolysis and pumping.

Residue in TmPPase	Residue in (M-PPase)	Mutation	Specific activity (% of wt)	Coupling ratio (% of wt)*
Lys199	Lys250 (VrPPase)	K to A (Lee et al., 2011)	15 %	n.d.p.
	Lys250 (VrPPase)	K to R (Lee et al., 2011)	n.d.a	n.d.p.
Asp202	Asp218 (ScPPase)	D to G (Hirono et al., 2007b)	n.d.a	n.d.p.
	Asp253 (VrPPase)	D to A (Nakanishi et al., 2001)	10 %	n.d.p.
	Asp253 (VrPPase)	D to E (Nakanishi et al., 2001)	n.d.a	n.d.p.
Asp206	Asp222 (ScPPase)	D to G (Hirono et al., 2007b)	5 %	n.d.p.
Lys210	Lys261 (VrPPase)	K to A (Nakanishi et al., 2001)	5 %	n.d.p.
	Lys261 (VrPPase)	K to R (Nakanishi et al., 2001)	30 %	n.d.p.
Glu212	Glu263 (VrPPase)	E to A (Nakanishi et al., 2001)	10 %	n.d.p.
	Glu263 (VrPPase)	E to D (Nakanishi et al., 2001, 2003)	67 %	n.d.p.
	Glu197 (RrPPase)	E to A (Malinen et al., 2004)	60 %	-
	Glu197 (RrPPase)	E to D (Malinen et al., 2004)	60 %	-
Asp228	Asp244 (ScPPase)	D to G (Hirono et al., 2007b)	2 %	n.d.p.
	Asp279 (VrPPase)	D to E (Nakanishi et al., 2001)	n.d.a.	n.d.p.
Asp232	Asp248 (ScPPase)	D to G (Hirono et al., 2007b)	2 %	n.d.p.
	Asp283 (VrPPase)	D to A (Nakanishi et al., 2001)	n.d.a	n.d.p.
	Asp283 (VrPPase)	D to E (Nakanishi et al., 2001)	n.d.a	n.d.p.
	Asp217 (RrPPase)	D to A (Schultz and Baltscheffsky, 2003)	2.5 %	n.d.p.
Asp236	Asp252 (ScPPase)	D to G (Hirono et al., 2007b)	2 %	n.d.p.
	Asp287 (VrPPase)	D to A (Nakanishi et al., 2001)	n.d.a	n.d.p.
	Asp287 (VrPPase)	D to E (Nakanishi et al., 2001)	n.d.a	n.d.p.
Asp243	Asp259 (ScPPase)	D to G (Hirono et al., 2007b)	2 %	n.d.p.
	Asp294 (VrPPase)	D to E (Lin et al., 2012)	6 %	n.d.p.
Asp488	Asp500 (ScPPase)	D to G (Hirono et al., 2007b)	2 %	n.d.p.
Lys499	Lys541 (VrPPase)	K to A (Lee et al., 2011)	10 %	n.d.p.
	Lys469 (RrPPase)	K to A (Schultz and Baltscheffsky, 2003)	2 %	n.d.p.
	Lys469 (RrPPase)	K to R (Schultz and Baltscheffsky, 2003)	7 %	60 %.
Lys663	Lys694 (VrPPase)	K to A (Lee et al., 2011)	20 %	n.d.p.
Lys664	Lys695 (VrPPase)	K to A (Lee et al., 2011)	20 %	n.d.p.
Asp688	Asp723 (VrPPase)	D to A (Nakanishi et al., 2001)	n.d.a.	n.d.p.
	Asp723 (VrPPase)	D to E (Nakanishi et al., 2001)	n.d.a	n.d.p.
Asp692	Asp727 (VrPPase)	D to A (Nakanishi et al., 2001)	15 %	n.d.p.
	Asp727 (VrPPase)	D to E (Nakanishi et al., 2001)	n.d.a	n.d.p.
Lys695	Lys730 (VrPPase)	K to A (Lee et al., 2011)	20 %	n.d.p.
Asp696	Asp731 (VrPPase)	D to A (Nakanishi et al., 2001)	n.d.a	n.d.p.
	Asp731 (VrPPase)	D to E (Nakanishi et al., 2001)	15 %	n.d.p.
Lys707	Lys742 (VrPPase)	K to A (Lin et al., 2012)	7 %	n.d.p.

n.d.a. = no detectable PPase activity, .n.d.p. = no detectable pumping. * = coupling ratio is measured as the ratio between PPase and proton pumping activities, with wt coupling ratio being 100 %.

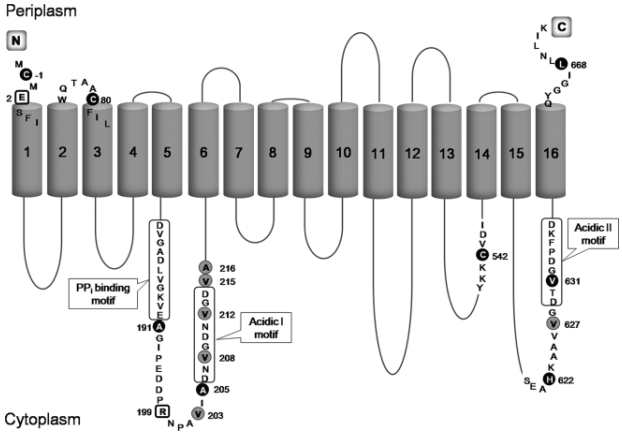

Figure 8. Topological model of a *Clostridium tetani* M-PPase showing the DX_7KXE (PPi-binding) motif and acidic motifs I and II (Figure from Huang et al., 2010, reprinted with permission)

Table 3. M-PPase residues which mutations affect the coupling of pyrophosphate hydrolysis to ion pumping.

Residue in TmPPase	Residue in (M-PPase)	Mutation	Specific activity (% of wt)	Coupling ratio (% of wt)*
Arg191	Arg246 (AtPPase)	R to A(Zancani et al., 2007)	26 %	16 %
	Arg246 (AtPPase)	R to K(Zancani et al., 2007)	46 %	6 %
	Arg242 (VrPPase)	R to A (Hsiao et al., 2007)	7 %	n.d.p.
	Arg207 (ScPPase)	R to A (Hirono et al., 2007b)	n.d.a.	n.d.p.
	Arg207 (ScPPase)	R to K (Hirono et al., 2007b)	40 %	45 %
	Arg176 (RrPPase)	R to A (Schultz and Baltscheffsky, 2003)	4 %	n.d.p
	Arg176 (RrPPase)	R to K (Schultz and Baltscheffsky, 2003)	22 %	48 %
Glys193	Glys178 (RrPPase)	G to A (Schultz and Baltscheffsky, 2003)	50 %	12 %
Ser247	Ser263 (ScPPase)	S to A (Hirono et al., 2007b)	30 %	n.d.p.
	Ser263 (ScPPase)	S to E (Hirono et al., 2007b)	n.d.a.	n.d.p.
	Ser263 (ScPPase)	S to C (Mimura et al., 2004)	n.d.a.	n.d.p.
	Ser298 (VrPPase)	S to A (Pan et al., 2011)	10 %	80 %
Pro290	Pro287 (ScPPase)	P to A (Hirono et al., 2007b)	50 %	n.d.p.

n.d.a. = no detectable PPase activity, .n.d.p. = no detectable pumping. * = coupling ratio is measured as the ratio between PPase and proton pumping activities, with wt coupling ratio being 100 %.

1.3.1 Differences between K^+-dependent and independent enzymes

Besides the K/A and G/T/A dichtomy in the GNXX(K/A)AX(G/T/A)-motif, K^+-dependent and independent enzymes show a difference in the position of a conserved cysteine (see 1.2.2.). These cysteines are found in the positions corresponding to TmPPase residues 237 and 599 in K^+-independent and dependent enzymes, respectively.

1.3.2 Semi-conserved glutamate

Phylogenetic analysis of M-PPases has revealed a semi-conserved glutamate that is found in three different positions in M-PPases (Luoto et al., 2011). In K^+-indep H^+-PPases and in Na^+-PPases, it is found in the position equivalent to TmPPase Glu246. In protozoan and plant K^+-dep H^+-PPases, it occurs in the position equivalent to TmPPase 250, while in prokayrotic K^+-dep H^+-PPases it occurs in the position equivalent to TmPPase 184, 246 or 250. E185S (equivalent to TmPPase 184) and E235S (equivalent to TmPPase 250) mutants of the H^+-PPases of *Flavobacterium johnsoniae* and *Lebtopsira biflexa*, respectively, led to enzymes with 20-30 % of wild-type PPase activity, but no ion-pumping activity (Luoto et al., 2011). Mutation of the semi-conserved glutamate E242 to serine in the Na^+-PPase of *Cholorobium limicola* abolished expression of the enzyme, but the Glu to Asp mutant had a 450-fold reduction in Na^+-binding affinity (Luoto et al., 2011). Glu to Gln mutations of the ScPPase E262 and its equivalent in RrPPase (both equivalent to TmPPase 246) had 3 % and 10 % of wt PPase activity, respectively, while neither mutant showed proton pumping activity (Schultz and Baltscheffsky, 2003; Hirono et al., 2007b). Glu to Ala mutations of the VrPPase E301 (TmPPase 250) and its equivalent in AtPPase had 30 % and 10 % of the wt PPase activity, respectively, while the coupling ratio in VrPPAse was only 33 % of the wt and pumping activity was abolished in AtPPase (Zhen et al., 1997b; Pan et al., 2011). These results show the importance of this semi-conserved glutamate for the ion-pumping activity of M-PPases.

1.3.3 Conserved residues in Na^+, H^+-PPases

Na^+, H^+-PPases contain four conserved residues not found in other M-PPases: Thr/Ser, Phe, Asp and Met in positions equivalent to TmPPase 82, 86, 140 and 176 (Luoto et al., 2013). M-PPases which phylogenetically group with the Na^+, H^+-PPases, but which do not have all of the four conserved residues (M-PPases of *Verrucomicrobiae bacterium* and *Clostridium sp. 7_2_43FAA*, for example) show only Na^+ pumping activity (Luoto et al., 2013). These results implicate the necessity of these four residues for the dual pumping specificity of Na^+, H^+-PPases.

1.4 Relation of M-PPases to other proteins

1.4.1 M-PPases and soluble pyrophosphatases

M-PPases resemble type I soluble pyrophosphatases (sPPases) in that they both use Mg_2PPi as a substrate, require Mg^{2+} for catalysis and are inhibited by Ca^{2+} (Maeshima, 2000). However, they differ in their response to the inhibitory effects of fluoride and

aminomethylenediphosphonate. The soluble pyrophosphatases are inhibited by low concentrations of fluoride (K_i values of 15–80 µM, Baykov et al., 2000; Pohjanjoki et al., 2001), while K_i values of 3.4–4.8 mM or IC(50) values of 1-2 mM have been measured for the fluoride inhibition of M-PPases (Wang et al., 1986; Baykov et al., 1993b). The opposite is true for AMDP inhibition, as the measured K_i of this compound for M-PPases is 1-1.8 µM while for the sPPases it is 11-20 µM (Zhen et al., 1994). An exception to this is the K^+-indep H^+-PPase of *Pyrobaculum aerophilum*, which shows only weak inhibition by AMDP (Drozdowicz et al., 1999).

1.4.2 M-PPases and other phosphoanhydride utilizing pumps

The catalytic mechanism of M-PPases does not resemble that of the other high-energy phosphoanhydride utilising ion pumps, the P, V, F – and A-type ATPases. In P-type ATPases, a catalytic intermediate is formed upon covalent attachement of the terminal phosphoryl group of ATP to a conserved aspartate residue (Palmgren and Nissen, 2011). There is no evidence of a covalent reaction intermediate in M-PPases and therefore their catalytic mechanism must be different from that of the P-type ATPases (Baykov et al., 1994). In F, A and V-type ATPases, movement of the mobile, rotor part of the protein relative to the stator part of the protein drives either ATP synthesis or ion-pumping (Duncan et al., 1995; Stock et al., 1999). As M-PPases are dimers consisting of just one type of subunit, such a rotary mechanism is not possible for them. However the coupling mechanism of M-PPases could possibly resemble the ´binding-change´mechanism of F, A and V-type ATPases, in which binding of the substrate molecule, and not its synthesis/hydrolysis, is energetically coupled to ion-movement (Abrahams et al., 1994, Boyer, 1993).

1.5 Isolation of membrane proteins

1.5.1 Expression of membrane proteins

Heterologous expression of membrane proteins is difficult as the expression levels are often very low (Bill et al., 2011). This is especially problematic when membrane proteins are produced for structural studies, which require large amounts of protein. The main reason for the low expression levels is the limited capacity of cells for handling non-native expression of membrane protein. In *Escherichia coli*, over-expression of membrane proteins is in many cases toxic (Wagner et al., 2006). This is most likely due to saturation of the protein translocation machinery (Valent et al., 1997), which decreases the levels of respiratory complexes in the cytoplasmic membrane (Wagner et al., 2007). In eukaryotes, over-expression of membrane proteins can induce the unfolded protein response (UPR),

which has a detrimental effect on the expression level of the heterologous protein (Griffith et al., 2003).

Besides the toxicity and the UPR, over-expression of membrane proteins can lead to accumulation of non-functional protein inside cytoplasmic aggregates or in the cellular membranes (Tate, 2001; Wagner et al., 2006). In eukaryotes, these misfolded proteins are usually arrested in the ER and not transported to the right membrane compartment (Tate, 2001). The presence of non-functional protein can nonetheless be problematic as it can co-purify with functional protein and interfere with its use.

The problems of toxicity, UPR and production of non-functional protein can be alleviated by tuning the expression of the membrane protein. This tuning can be done, for example, by employing expression plasmids with promoters that allow tight control of the expression level (such as the arabinose inducible promoters) or by using tunable integration vectors (Griffith et al., 2003; Schlegel et al., 2012; Wang et al., 2003). Enhancing the expression of membrane proteins can also be done using the ”Walker strains”, C43 and C41, of *E. coli* (Miroux and Walker, 1996). These strains contain mutations in the *lac*UV5 promoter controlling the expression of T7 polymerase that reduce the amount of mRNA produced. This reduces the toxicity of the membrane protein expression and thus leads to higher yields of the expressed proteins (Wagner et al., 2008). A mutant strain of yeast that has respiratory metabolism, not the wild-type fermentative metabolism, has been shown to have enhanced expression levels of certain membrane proteins (Griffith et al., 2003), as has a strain lacking ubiquitin ligases (Flegelova et al., 2006).

Expression of functional membrane proteins can also be enhanced with an N-terminal insertion of a signal sequence of a highly expressed protein (Weiss et al., 1995; Andre et al., 2006) or by the addition of ’chemical chaperones’ such as glycerol or dimethyl sulphoxide to the growth media (Figler et al., 2000; Andre et al., 2006; Newstead et al., 2007).

As an alternative to optimising the expression of one membrane protein, expression screening can be done on a group of similar membrane proteins. In these cases, instead of trying to tune the metabolism of the cell to facilitate the expression of the selected membrane protein, a search is carried out to find a membrane protein whose expression is suited to the metabolism of the cell (see eg. Newstead et al., 2007).

1.5.2 Purification of membrane proteins

Only a very few membrane proteins, such as bacteriorhodpsin (Oesterhelt and Stoekenius, 1974), can be purified in their membrane-bound form. The purification of the vast majority of membrane proteins requires that the protein be first solubilised from the membrane bilayer (Figure 9). This is carried out by detergent molecules, which are

amphipathic, containing both a hydrophobic tail and hydrophilic head-group. During solubilisation, the hydrophobic tails of the detergent molecules cover the hydrophobic parts of the membrane protein while the hydrophilic head-groups are in contact with the watery environment. The detergent micelles surrounding the protein mimic poorly a number of properties of the lipid bilayers, such as their lateral pressure, water exclusion, topological constraints and acyl chain packing. Consequently, detergent solubilisation can inactivate the protein (Marsh, 1996). Certain conditions, such as the right pH or right ionic strength or the presence of chemical stabilisers such as glycerol or sucrose or stabilising ligands (Pikula et al., 1988; Ottolenghi et al., 1986; Hayashi et al., 1988), can stabilise the solubilised membrane protein. The nature of the detergent has also a strong effect on the stability of the membrane protein, with detergents with short hydrophobic tails and charged head-groups being usually more denaturing (Privé, 2007). The stability of some proteins is dependent on the presence of lipids in the protein-detergent complex (Esmann and Skou, 1984; Esmann, 1984; Banerjee et al., 1995; Breyton et al., 1997). Due to this, the solubilisation of proteins with too high detergent concentration or with the wrong detergent can lead to their inactivation (Figure 10), as excess amounts or the wrong type of a detergent can remove the lipids necessary for activity and/or stability (Esmann and Skou, 1984; Esmann, 1984; Privé, 2007; Banerjee et al., 1995).

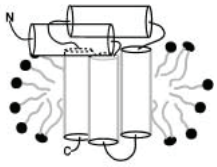

Figure 9. Detergent solubilised membrane protein (Figure from Sanders et al., 2004, reprinted with permission). The solubilised protein is shown as a cartoon with the detergent surrounding the hydrophobic portion of the protein.

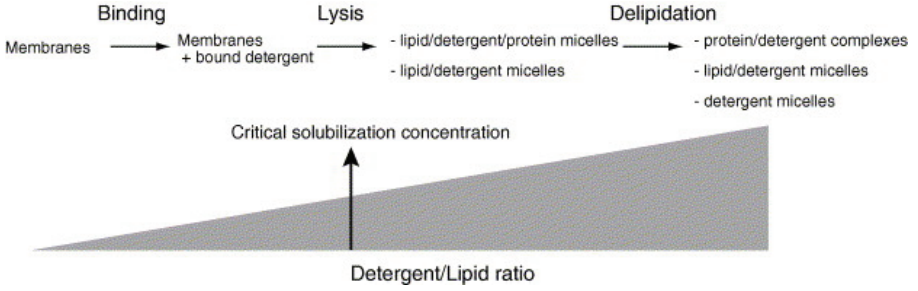

Figure 10. The role of detergent concentration in membrane protein solubilisation (Figure from Privé, 2007, reprinted with permission from Elsevier). The suitable detergent concentration, the critical solubilisation concentration, is high enough so that the protein is solubilised but low enough that it does not undergo delipidation.

Once solubilised, purification of membrane proteins can be carried out using the same techniques as for soluble proteins. However, some conditions can inactivate proteins that require lipids for stability (Esmann, 1984; Scägger, 2003). These techniques usually

include different chromatographies during which lipids can be either washed away or bound to the chromatography matrix (Esmann, 1984; Scägger, 2003).

1.5.3 Expression of M-PPases

Heterologous expression of M-PPases has been carried out in *S. cerevisiae* and *E. coli*. As both of these organisms lack innate M-PPases, functional characterisation of the expressed M-PPases does not require purification, but can be carried out with M-PPase enriched membranes.

So far 19 M-PPases have been heterologously expressed in *E. coli* and 11 in *S. cerevisiae* (Drozdowicz et al., 1999; Yang et al., 2000; Belogurov et al., 2002; Pérez-Castiñeira et al., 2001; Ikeda et al., 2002; Pérez-Castiñeira et al., 2002; Belogurov and Lahti, 2002; Mimura et al., 2004; Belogurov et al., 2005; Malinen et al., 2007; Malinen et al., 2008; Drake et al., 2010; Huang et al., 2010; Meng et al., 2011; Luoto et al., 2011; Luoto et al. 2013). All of the *E. coli* expressed M-PPases so far have been prokaryotic M-PPases, while M-PPases from all source organisms (plants, algae, protozoans, bacteria and archae) have been expressed in yeast.

The bacterial expression of M-PPases has been carried out both in membrane-protein specific (such as C41(DE3)) and more conventional expression strains (BL21(DE3)) under either T7 (Studier and Moffat, 1986) or the T7*lac* promoter (Dubendorff and Studier, 1991). The expression in *S. cerevisiae* was carried out in either wild type (such as W303-1A) or in protein expression specific, protease deficient strains (such as BJ2168). Yeast expression was carried out either under the GAL-promoter (Oberto and Davison, 1985) or a constitutive PMA1-promoter (Villalba et al., 1992). Expression of certain M-PPases in *S. cerevisiae* could be improved by fusing the signal-sequences of either *Trypanosoma cruzi* M-PPase or *S. cerevisiae* Suc2p invertase to their N-termini (Drake et al., 2010). Such chimaeric variants of RrPPase and TgPPase showed 3-10 fold higher levels of functional protein than the respective wild-type proteins.

1.5.4 Purification of M-PPases

As both the tonoplast membranes of young plant tissues and chromatophore membranes of *Rhodospirullum rubrum* were found to contain reasonably high amounts of M-PPase, the first purified M-PPases were isolated from native sources. These purified proteins included the M-PPases of plants *Vigna radiata* (mung bean, Maeshima and Yoshida, 1989), *Beta Vulgaris* (BvPPAse, red beet, Sarafian and Poole, 1989), *Cucurbita sp*. (CsPPAse, pumpkin, Sato et al., 1991) and *Pyrus communis* (PcPPase, pear fruit, Suzuki et al., 1999) and of the bacterium *Rhodospirullum rubrum* (Nyren et al., 1991b).

The purification of the enzymes was carried out by first solubilising the protein from isolated tonoplast or chromatophore membranes either with lysophospatidylcholine (VrPPase and CsPPase), Triton X-100 (BvPPase) or with a mixture of Nonanoyl-N-Methylglucamide (MEGA-9) and cholate (RrPPase). The presence of 20 % glycerol or 25 % ethyleneglycol, 0.75 - 4 mM $MgCl_2$ or $MgSO_4$ and 0.5 - 1 mM EDTA was necessary for the stabilisation of the proteins during the solubilisation. During the purification of VrPPase and CsPPase, prior to their solubilisation, membranes were purified with deoxycholate or Triton X-100 to remove contaminating proteins.

After solubilisation, the proteins were purified to homogeneity either by ion-exchange chromatography (VrPPase and CsPPase), gel filtration and anion-exchange chromatography (BvPPase and PcPPase) or by PEG 4000 precipitation, hydroxyapatite chromatography and affinity chromatography (RrPPase).

Heterologous production has been successfully employed for the purification of VrPPase (Hsu et al., 2009), TmPPase (López-Marqués et al., 2005) and *Clostridium tetani* M-PPase (CtPPase) (Huang et al., 2010). The expression of VrPPase and TmPPase was carried out in *S. cerevisiae* while CtPPase was expressed in *E. coli*. All three enzymes were modified to contain either N- or C-terminal His-tags and were purified by Nickel-affinity purification after solubilisation with n-dodecyl maltoside.

During purification, all M-PPases seem to lose essential lipids, as lipids need to be supplemented for maximal activity. In addition to this, lipids had to be added to the buffers used in the purification of BvPPase and PcPPase as otherwise these proteins would be inactivated. The specific activities of the enzymes purified from plant vacuolar membranes vary from 14 – 33 µmol Pi/mg/min depending on the protein, while that of the RrPPase is 20 µmol Pi/mg/min. The specific activities of the purified, heterologously produced TmPPase and VrPPase were 10 µmol Pi/mg/min and 1.5 µmol Pi/mg/min, respectively.

1.6 X-ray crystallography of membrane proteins

1.6.1 Crystallisation of membrane proteins

At the moment, membrane protein structures account only for ≈1 % of all of the solved protein structures (http://blanco.biomol.uci.edu/mpstruc/listAll/list). This is not only because of the difficulty of expressing and purifying membrane proteins (see 1.5.1. and 1.5.2.), but also because of the difficulty of crystallising them. This is due to the detergent envelope surrounding the protein. As the detergent belt is mostly unordered, ordered crystal contacts are formed by the extramembraneous parts of the protein located outside of the detergent envelope (Wiener, 2004). The size of the detergent envelope can be

reduced by employing detergents with a smaller micelle size (Figure 11) but these detergents are usually more denaturing (Sonoda et al., 2011), and, in addition, detergents with shorter hydrophobic tails tend to be worse at solubilising membrane proteins than detergents with longer hydrophobic tails (White et al., 2007). Because of this, the search for the right detergent that has as small a micelle size as possible, but can still stabilise the membrane protein, is of crucial importance in the crystallisation of membrane proteins (Newstead et al., 2007). Problems with poor solubilisation properties can be circumvented by first employing a well solubilising detergent and then exchanging it for another during purification. This has been successfully employed in the crystallisation of a number of membrane-proteins (see eg. Screpanti et al., 2006; Dang et al., 2010; Umena et al., 2011). Instead of employing a detergent with a small micellar size, an alternative strategy is to increase the hydrophilic surface of the protein. This strategy can rely either on employing co-crystallisation with an antibody (Carpenter et al., 2008) or on crystallisation of a chimaeric construct of a well-behaving soluble protein and the membrane protein. Chimaeric constructs containing T4-lysozyme have been successfully employed in the structure determination of many G-protein coupled receptors (GPCRs) (see eg. Rosenbaum et al., 2007; Jaakola et al., 2008; Wu et al., 2010).

Besides the micelle size and stabilising effect of the detergent, the crystallisation of membrane proteins can be affected by detergent-detergent interactions (Loll, 2003). In some cases, the detergent micelles can fuse to form 3D-crystals with layered bilayer like sheets. These type I crystals have usually better diffraction properties due to their denser packing and lower solvent content (Caffrey and Cherezov, 2009). The fusion of the detergent envelopes usually takes place in conditions that are close to the cloud-point of the detergent (Loll, 2003).

1.6.2 Lipids and membrane protein crystallisation

Instead of trying to crystallise the membrane protein solubilised in detergent, lipidic mesophase based crystallisation can be employed. These methods, which include lipidic cubic phase (LPC) (Landau and Rosenbusch, 1996), bicelles (Faham and Bowie, 2002) and sponge phase (Wadsten et al., 2006), have been very succesful in the crystallisation of GPCRs. They have two advantages in comparison to the more conventional crystallisation procedures: first, the crystals obtained are of type I (Figure 12) and can therefore theoretically pack tighter and, secondly, the membrane protein is reconstituted into a lipid membrane prior to crystallisation which circumvents the denaturing effects of the detergent micelle.

In lipidic mesophase based crystallisation, the lipid membrane adopts a certain structure amenable for protein crystallisation if certain conditions are met. The narrow window of conditions in which the lipidic mesophases are stable, which include having the right type of lipid, right water content and right temperature, has in the past made their use less common.

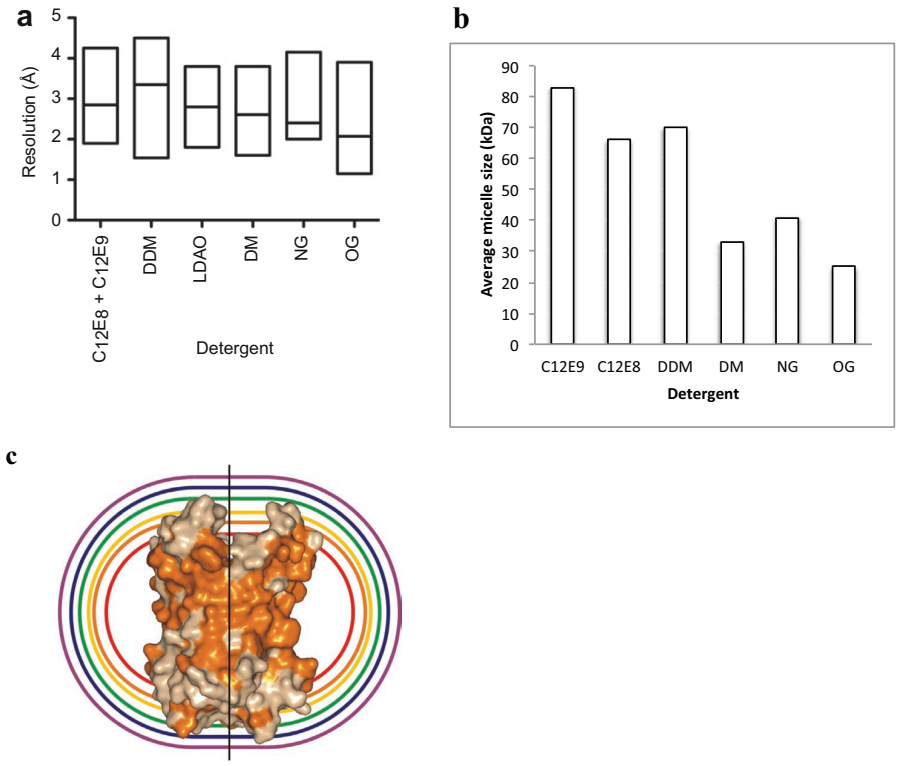

Figure 11. The role of detergent and micelle size in membrane protein crystallisation. (a) Boxplot of the resolution of membrane protein structures obtained with different detergents. Horizontal line signifies the median value of resolution (Figure from Sonoda et al., 2011, reprinted with permission from Elsevier). (b) The micellar sizes of the detergents. (c) The relative sizes of the detergent micelles (alkyl-maltoside series with decreasing hydrocarbon chain length from tridecylmaltoside (purple) to octylmaltoside (red) surrounding the 30 kDa mitochondrial ATP/ADP carrier (Figure from Bill et al., 2011, reprinted with permission from Macmillian publishers Ltd.).

Crystallisation of membrane proteins can be also carried out with a protein sample supplemented with lipids (Jidenko et al., 2005; Long et al., 2005; Efremov et al., 2010; Gourdon et al., 2011b; Andersen et al., 2011). Addition of lipids can have the stabilising and packing enhancing effects of the lipidic mesophase methods, while it does not restrict the allowable crystallisation conditions. A good example of the use of the lipid addition is the employment of `HiLiDe´-method (Gourdon et al., 2011a) for the crystallisation of a number of P-type ATPases (Jidenko et al., 2005; Gourdon et al., 2011b; Andersen et al., 2011). Gourdon and coworkers (2011a) mention that they were able to grow crystals of Cu^{2+} and Ca^{2+}-ATPase only in the presence of added lipids and that the levels of the

supplemented lipid in these conditions closely resemble the levels seen in some of the crystals grown from proteins extracted from natural sources.

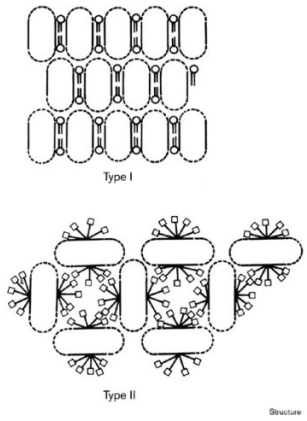

Figure 12. Type I and type II membrane protein crystals (Figure from Gouaux, 1998, reprinted with permission from Elsevier). In type I crystals, the membrane proteins are arranged in bilayer like sheets which pack on top of each other, while in type II crystals the packing is solely formed by the crystal contacts between the hydrophilic parts of the proteins.

1.7 Structure of M-PPases

1.7.1 Subunit and oligomeric structure

Purification of M-PPases from natural sources, their subsequent characterisation by PPase activity measurements and proton-pumping experiments with reconstituted protein showed that M-PPases require only a single polypeptide chain for activity (Sato et al., 1994; Nyren et al., 1991a). This characteristic has also been confirmed by expression studies where the expression of M-PPase genes coding for just one polypeptide chain produced proteins capable of both PPi hydrolysis and H^+-pumping (Kim et al., 1994).

Gel filtration, radiation inactivation, chemical crosslinking, electron microscopy and atomic force microscopy (AFM) have all shown that the oligomeric state of an M-PPase is a dimer (Maeshima, 1990; Tzeng et al., 1996; Mimura et al., 2005a; Sato et al., 1991; López-Marqués et al., 2005; Liu et al., 2009). The position of the dimer interface in the structure has been studied by crosslinking experiments (Mimura et al., 2005a) and AFM (Liu et al., 2009). In these studies, cysteines were introduced by site-directed mutagenesis into otherwise cysteine-free ScPPase and crosslinking between the two ScPPase subunits was analysed by SDS-PAGE. These experiments show crosslinking between monomers through a cysteine replacement of serine 545. AFM indicated that the dimer interface is situated in the C-terminal part of the protein.

Many experiments have indicated that the dimeric structure of an M-PPase is important for its function. Radiation inactivation studies showed that a functional dimer is required

for H^+-pumping activity, while either a dimeric or mononomeric structure is needed for the pyrophosphatase activity (Fraichard et al., 1993; Tzeng et al., 1996). Also, inactivation of one sub-unit of the dimer leads to reduced stability and activity of the remaining subunit (Yang et al., 2004; Mimura et al., 2005b).

1.7.2 Topology

To determine the topology of M-PPases, Mimura and coworkers (2004) used cysteine-scanning mutagenesis of ScPPase with subsequent labelling of residues with either membrane permeable or impermeable sulphydryl reagents. This experiment indicated that ScPPase has 17 transmembrane helices (TMHs) and an N-out C-in orientation (Figure 13). As ScPPase has a C-terminal extension not found in most of the other M-PPases, the archetypal M-PPase thus has 16 TMHs and an N-out C-out orientation. Some M-PPases have an extra N-terminal TMH, which forms a cleavable signal sequence (Drake et al., 2004) and others are predicted to have 15 TMHs either through the loss of TMH1 or TMH16 (Au et al., 2006).

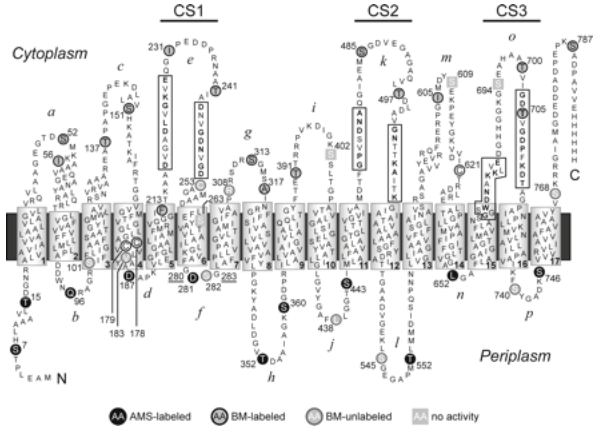

Figure 13. Topology of ScPPase determined by cysteine scanning mutagenesis (Figure from Mimura et al., 2004, reprinted with permission). Residues marked with black and dark and light grey circles and light grey boxes were mutated to cysteines. Mutation of residues marked with light grey boxes caused loss of activity. Residues marked with dark grey circles were accessible to labelling with a membrane-permeable reagent (3-(N-maleimidylpropionyl)biocytin), while those marked with black circles could only be labelled with the membrane-impermeable 4-acetamido-4'maleimidylstilbene-2,2'-disulphonic acid. Residues marked with light grey circles could not be labelled with either dye. White boxes show the place of conserved segments in the protein located in the three cytoplasmic loops.

1.7.3 Possible evolution through gene triplication

Au and coworkers (2006) have proposed that M-PPases arose through gene triplication. The evidence for this comes from the discovery that the sequence for TMHs1-6 is similar

to that of TMHs 11-16 and that regions containing TMHs 1-4 and 7-10 are similar. The proposed gene triplication would have thus happened by duplication of an element containing 6 TMHs to create the N-terminal TMH 1-6 region and the C-terminal TMH 11-16 region, while the middle segment containing TMHs 7-10 would have resulted from either the duplication of only the first 4 TMHs or from deletion of the last two TMHs from a 18 TMH protein precursor (Au et al. 2006).

1.7.4 Conformational changes upon ligand binding

Förster resonance energy transfer (FRET) measurements on *Clostridum tetani* Na^+-PPase using cysteine mutations and Alexa fluorophores show that, upon substrate binding the distance between the A205C residues in the homodimer increases from ≈ 57 Å to ≈ 67 Å, while the distance between the H622C residues increases from ≈54 Å to ≈ 61 Å. These two residues correspond to A227 and H681 of TmPPase and are located in the vicinity of acidic motifs I and II. The two A191Cs (TmPPase L204) located near the DX_7KXL-motif move closer to each other; the distance changes from ≈ 71 Å to 57 Å (Huang et al., 2010). Binding of K^+ had a similar effect on the movement of the A191C residues and also caused the H622Cs to move ≈ 2-3 Å away from each other (Huang et al., 2010).

Ligand binding has been shown to protect M-PPases from modification by covalent inhibitors and from trypsin proteolysis (Table 4). As the modification and proteolysis experiments have been carried out on different M-PPases and in different ways, only a crude comparison of the different experiments can be done (Table 4). However, the magnesium complex of the substrate PPi or its analogue aminomethylene diphosphonate (AMDP) protects the best, while Mg^{2+} together with phosphate or Mg^{2+} alone afforded somewhat lower protection. This is true in all cases, except for the FITC and DEPC modifications of VrPPase, where Mg^{2+} plus phosphate did not show any protection at all. Curiously, conflicting results are seen for the DEPC modification of VrPPase, as one experiment shows protection by Mg_2PPi while the other experiment does not. The discrepancy is probably because in one case the experiments were carried out with purified protein and in the other with M-PPase containing tonoplast membranes. Additionally, the reaction conditions were different.

Mutagensis studies or residue labelling by fluorescent or radioactive modifiers have revealed the target residues of seven covalent inhibitors (Table 4). Mutagenesis studies have shown that neither the phenylglyoxal reactive histidine (Hsiao et al., 2004) nor the *N*-ethylmaleimide or *N*-(1-pyrenyl)maleimide -reactive cysteine are necessary for enzymatic activity (Kim et al., 1995) as H716A VrPPase and C632A AtPPase had 40 % and 100 % of wild-type activity, respectively. With these reagents, the inactivating effect of the compound thus likely comes from the steric blocking that the modifier adduct causes.

Table 4. The protective effect of ligand binding against covalent inhibition and proteolysis of M-PPases.

Modifier	Probable target residue (corresponding TmPPase residue)	Modified M-PPase	Protection against modification⌘				
			Mg	Mg + PPi	Mg + AMDP	Mg + AMDP + Na	Mg + Pi
FITC	K250[1] (K199)	VrPPase	-	-	-	-	-
	K541 (K499)	VrPPase	-	+++[2]	-	-	0[2]
	Lys[1,2]	RrPPase	+[3]	+++[3]	-	-	-
DEPC	H716[4] (H681)	VrPPase	-	+++[5]	-	-	++[5]
	His, Cys, Lys or Tyr[6]	RrPPase	+[3]	+++[3]	-	-	-
	H716[4] (H681)	VrPPase	0[7]	0[7]	-	-	-
Rose Bengal	His[8]	VrPPase	0[7]	0[7]	-	-	-
BPB	His[9]	RrPPase	++ [3]	+++[3]	-	-	-
DCCD	D283[10] (D232)	VrPPase	-	+++[10]	-	-	0[10]
	E305, D287 (250, D232)[11]	AtPPase	+++ [11]	-	-	-	-
	Asp or Glu[10,11]	RrPPase	++[3]	+++[3]	-	-	-
Mersalyl	Any Cys[12]	RrPPase	+[12]	+++[12]	-	-	-
	Cys[12]	MmPPase	+[13]	+++[13]	+++[13]	++++[13]	++[13]
TNM	Tyr[14]	VrPPase	-	+++[14]	-	-	++[14]
PGO	R242[15] (R191)	VrPPase	-	++++[16]	-	-	++[16]
Trypsin	K250[1] (K199)	VrPPase	+[17]	+++[17]	-	-	++[17]
	Lys or Arg	MmPPase	+[13]	+++[13]	-	-	++[13]
NEM	C634[18] (C599)	AtPPase	++[19]	+++[18,19]	-	-	-
	Cys[18]	VrPPase	++[20]	-	-	-	-
	Cys[18]	VrPPase	++[19]	+++[19]	-	-	-
	Cys[18]	BvPPase	++[19]	+++[19]	-	-	-
NPM	C632[21] (C599)	CmPPase	-	-	-	-	-
EDAC	E or D[7]	VrPPase	++[7]	+++[7]	-	-	-

[1](Lee et al., 2011)[2](Yang et al., 2000)[3](Schultz and Baltscheffsky, 2004)[4]Hsiao et al., 2004, [5](Hsiao et al., 2002)[6](Miler, 1977)[7](Gordon-Weeks et al., 1996)[8](Eyzaguirre, 1987)[9](Dennis, 1983)[10](Yang et al., 1999)[11](Zhen et al., 1997b)[12](Belogurov et al., 2002)[13](Malinen et al., 2008) [14](Yang et al., 1996)[15](Hsiao et al., 2007)[16](Kuo and Pan, 1990)[17](Kuo and Pan, 1990)[18](Kim et al., 1995)[19](Rea et al., 1992b)[20](Baykov et al., 1993a)[21](Maruyama et al., 1998)

⌘ Level of protection: Very high = ++++, High = +++, Medium = ++. Low = +, None = 0, Measurement not done = -. These arbitrary values are used to denote the level of protection because the experiments have been done differently by different people.

On the basis of both the FRET and modification experiments a rough model can be devised for the conformational changes in M-PPases upon substrate binding. In this model

the movement of the DX_7KXL -and acidic motifs upon substrate binding will either hide or order the residues R191, K199, D232, K499, C599 and H681 (TmPPase numbering).

1.7.5 Structure of *Vigna radiata* M-PPase

1.7.5.1 Overview of the structure

In 2012 Lin and coworkers solved the structure of a K^+-dep H^+-PPase of *Vigna radiata* with the bound substrate analogue imidodiphosphonate (Figure 14). The C-terminally His-tagged protein was produced heterologously in *S. cerevisiae* and purified with Ni-affinity chromatography. The structure shows a dimeric protein with each monomer consisting of 16 transmembrane spanning helices, which extend up to 25 Å into the cytoplasmic space. The protein contains a large, cytoplasmic active site cavity surrounded by helices 5, 6, 11, 12, 15 and 16 and closed by loop 5-6. On the vacuolar side of this cavity are a series of smaller cavities that lead to the vacuolar lumen. The cytoplasmic end of the active site cavity contains the bound imidodiphosphonate (IDP) and metal ions (Mg^{2+} and K^+).

As the structure shows a dimeric protein it confirms earlier findings (Maeshima, 1990; Tzeng et al., 1996; Mimura et al., 2005a; Sato et al., 1991; López-Marqués et al., 2005; Liu et al., 2009). The structure also confirms the findings of earlier studies about the position of the dimer interface. Although ScPPase S545, found to be in the dimer interface based on crosslinking experiments (Mimura et al., 2005a), is not conserved in VrPPase, this area contains a loop between TMHs 12 and 13 (loop 12-13) and residues of this loop make monomer-monomer contacts (Lin et al., 2012). The other residues that are found in the dimer interface reside mostly in the TMHs 10, 12, 13, 15 and 16 (Lin et al., 2012). As residues of the dimer interface in TMH16 are close to the C-terminus of the protein this gives credence to the findings of AFM, which indicated the proximity of the C-terminus to the dimer interface (Liu et al., 2009).

The crystal structure also confirms that the number of helices is indeed 16 as suggested by Mimura and coworkers (2004). However, the topological model did not predict the extension of the membrane helices into the cytoplasm seen in the VrPPase structure (Lin et al., 2012). This error in the cysteine-scanning based topology is mostly due to the inaccurate predictions of the membane protein topology prediction programs that predict the membrane helices to be the height of a membrane bilayer (Tusnady and Simon, 2010)

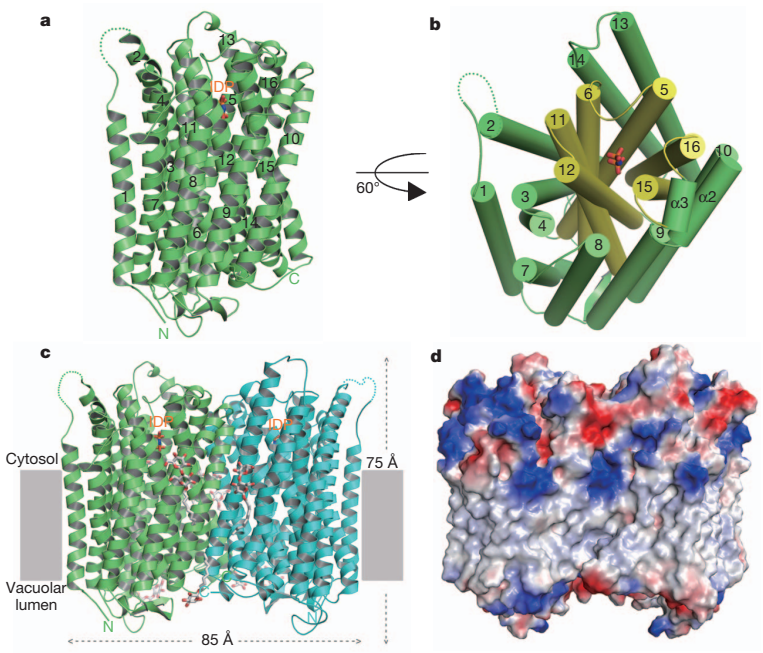

Figure 14. The crystal structure of a Vr-PPase (Figure from Lin et al. 2012, reprinted with permission from Macmillian publishers Ltd.). (a) Structure of a monomer showing the site of the bound substrate analogue, imidodiphosphonate (IDP). (b) View of the monomer from the cytoplasm with six helices (in yellow) lining the active site containing IDP (in red). (c) Structure of the dimer showing the membrane-embedded, cytosolic and vacuolar parts of the protein. (d) Surface representation of the dimer.

1.7.5.2 Substrate and cofactor binding

The VrPPase structure shows an imidiodiphosphonate (IDP)- molecule with five complexed Mg^{2+} in the active site of the enzyme (Figure 15). The binding of the IDP to the protein is facilitated almost entirely through the complexing metal ions which themselves are bound by the conserved aspartates of TMHs 5, 6, 11, 15 and 16 (Asp253, 257, 283, 507, 691 and 727) and the conserved Asn534 of TMH12. The only residues of VrPPase that are in direct contact with the IDP are lysines 250, 694 and 730, which reside in TMHs 5, 15 and 16, respectively. Studies have shown drastically decreased enzyme activity upon the mutation of the aforementioned aspartates and lysines (Table 2). Two aspartates in TMH5, Asp253 and Asp257, which take part in Mg^{2+} binding, are part of the conserved DVGADLGKVE-motif (see 1.2.1.). This fits the results of Takasu and coworkers (1997), which show inhibition upon binding of an antibody that has been raised against the motif. Based on mutagenesis studies, K261 and E263 in the motif should take part in substrate binding (Nakanishi et al., 2001; Nakanishi et al., 2003), but they do not directly bind IDP or Mg^{2+}. These two residues seem to exert their effect on substrate

binding by forming salt-bridges with other, conserved residues (Table 5), and the salt-bridges probably stabilise the substrate-bound state of the enzyme (Lin et al., 2012).

The five Mg^{2+}-ions seen in the active site of VrPPase seem to validate the previous experimental models about the number of magnesium ions bound by M-PPases. Of the total five, two would come from the Mg_2PPi-complex, two would be the activating Mg^{2+} (Baykov et al., 1993a) and one an inhibiting Mg^{2+} (Malinen et al., 2008). Even though the binding affinity of the inhibiting Mg^{2+} is low ($K_d \approx 100$ mM, Malinen et al., 2008) the crystallisation of VrPPase was carried out in the presence of high concentrations of magnesium ions (0.2 M) and in these conditions the fifth magnesium could well bind to the enzyme.

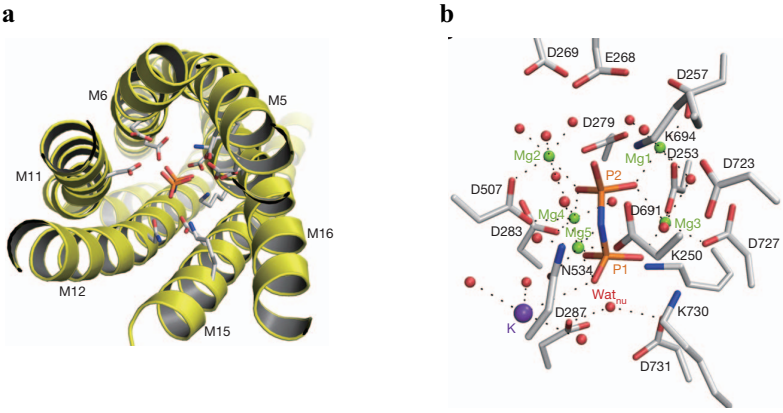

Figure 15. The substrate binding site of VrPPase (Figure from Lin et al., 2012, reprinted with permission from Macmillian publishers Ltd.). (a) The binding site with the surrounding helices, active site residues and bound IDP. (b) The architecture of the active site showing the bound IDP (P2 and P1), Mg^{2+} (Mg1-5) and K^+ (K) together with the binding coordinating residues. Also shown is the activated nucleophilic water (Wat_{nu}) coordinated by Asp287 and Asp731.

Table 5. Salt-bridge network in the active site of VrPPase (Modified from Lin et al., 2012).

Cationic/donor			Anionic/acceptor			Distance (Å)
Position	Residue	Atom	Position	Residue	Atom	
TMH5	K261	NZ	Loop 5-6	E268	OE1	2.4
TMH5	K261	NZ	TMH15	E698	OE2	2.9
TMH12	R523	NH1	Loop 5-6	D269	OD2	3.1
TMH12	R523	NH2	Loop 5-6	E268	OE2	3.0
TMH12	R523	NH2	TMH12	D527	OD1	3.5
TMH15	K695	NZ	TMH12	D527	OD1	2.5
TMH13	R609	NH2	Loop 5-6	E263	OE2	2.8

In the solved VrPPase structure, K^+ is also seen in the active site. K^+ coordinates the P1 phosphate of the IDP (Figure 15) (Lin et al., 2012). The activating effect of the potassium seems to be because it increases the electrophilicity of this phosphate group. However, as the activating effect of K^+ in the crystallized C-terminally H_6-tagged VrPPase is drastically reduced compared to the wild-type enzyme (Hsu et al., 2009) the K^+ might occupy a different position in the wild-type protein. The structure reveals why Mg_2PPi protects the Arg242, Lys250, Asp283 Lys541 and His716 from modification (see 1.7.4.): all of these residues are located inside the closed active site cavity (Figure 16).

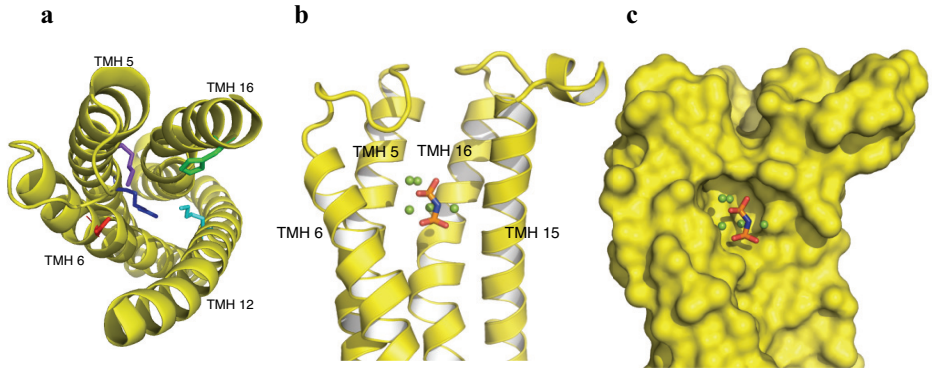

Figure 16. The position of VrPPase residues protected from covalent inhibition by Mg_2PPi binding. (a) Residues Arg242 (purple), Lys250 (blue), Asp283 (red), Lys541 (cyan) and His761 (green) inside the active site cavity. TMHs 5, 6 12 and 16 are shown. (b), (c) Closure of the active site. IDP (in red and orange) and Mg^{2+} (in green) are shown inside the active site. (b) TMHs 5, 6, 15 and 16 in cartoon form. (c) Surface representation of TMHs 5-6 and 15-16 areas of VrPPase showing the closure of the active site.

1.7.5.3 Mechanism of pyrophosphate hydrolysis and proton pumping

The structure of the IDP:VrPPase-complex shows a water molecule close to the leaving-group phosphate of the IDP. This water molecule is coordinated by two conserved aspartates, Asp287 and Asp731. Lin and coworkers (2012) propose that this coordination would activate the water molecule and lead to nucleophilic attack on the bound substrate molecule causing pyrophosphate hydrolysis.

This hydrolysis mechanism would explain the at least 300-fold difference between sPPases and M-PPases in the K_i of fluoride inhibition. In sPPases, a water molecule is activated by bound metal ions (Heikinheimo et al., 1996) to generate an hydroxide ion. This then attacks the electrophilic phosphate moiety of the PPi molecule leading to PPi hydrolysis. A fluoride ion can substitute for the nucleophilic hydroxide ion and thus inhibit the reaction (Heikinheimo et al., 2001). On the basis of the solved VrPPase structure (Lin et al., 2012), this type of inhibition could not take place in M-PPases as the fluoride would be repelled by the negative charge of the aspartates. The low level of

fluoride inhibition of M-PPases seen so far (Wang et al., 1986; Baykov et al., 1993b) could then perhaps be due to the sequestration of Mg^{2+} by F^- or inhibition by the phosphate mimicking $Mg(H_2O)F_3^-$ and $Mg(H_2O)_2F_2$ (Palmgren & Nissen, 2011).

Lin and coworkers (2012) proposed that proton pumping is driven by the pyrophosphate hydrolysis and the release of a proton from the activated water that attacks the pyrophosphate (Figure 18). The proton is then transferred through the activity of four charged residues, R242, D294, K742, E301, to the vacuolar space (Figures 17 and 18).

Mutations of both R242 and E301 have been shown to reduce the H^+-pumping activity drastically (see 1.3.), while mutations of the D294 and K742 decrease the enzyme activity to less than 10 % of wt (Table 3). Due to its importance for H^+-pumping activity, the proton donor/acceptor is proposed to be E301. Besides these four residues, the proton transport pathway is thought to include two waters of which one, Wat1, is hydrogen bonded to Arg242 and Asp294 and the other, Wat2, to Ser298, Ser547 and Asn738 (Figure 17b). The necessity of Ser298 for the coordination of the Wat2 would explain the drastic reduction in activity seen upon its mutation (Table 3).

In the catalytic model of Lin and coworkers (2012), the enzyme is first in a resting state with the active site cavity open and the vacuolar channel closed. Glu301 is protonated, Asp294 and Lys742 form a salt bridge and Wat1 and Wat2 occupy their positions in the proton-transfer pathway. After PPi binds in the active site, the active site is closed by loop 5-6 and an intermediate state forms. PPi hydrolysis by nucleophilic attack by the activated water molecule and the transfer of a proton from the activated water to the proton transfer pathway results in a short-lived state. In this state, the energy released from the hydrolysis reaction causes the vacuolar channel to open up. Proton pumping takes place during this and is initiated by the protonation of Asp294. This causes the reorganisation of the residues of the transfer pathway, which leads to formation of a salt-bridge between Lys742 and Glu301 and drives the Glu301 to pass its proton trough the opened channel to the vacuolar lumen.

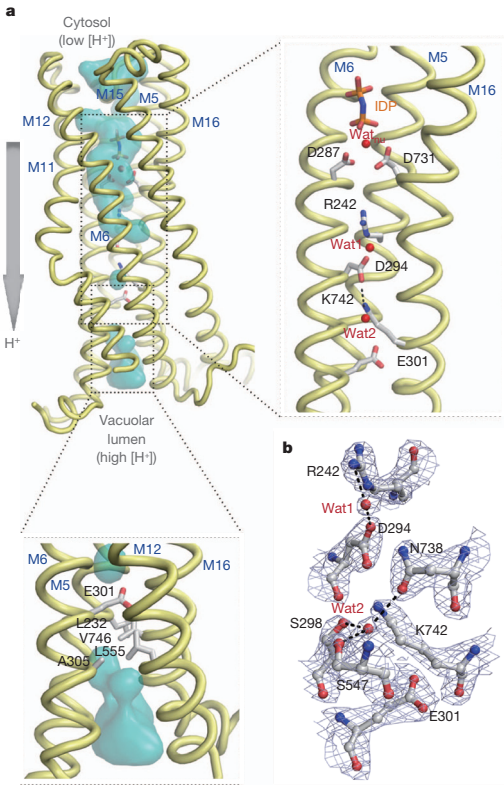

Figure 17. Proton transfer pathway in VrPPase (Figure from Lin et al., 2012, reprinted with permission from Macmillian publishers Ltd.). (a) Proton transfer pathway consisting of residues Arg242, Asp294, Lys742 and Glu301 and two bound waters (Wat1 and Wat2) is enclosed by TMHs 5,6, 12 and 16 (M5, M6, M15 and M16). The proton is donated to the pathway from the activated water molecule (Wat1) when it attacks the bound substrate molecule. The non-hydrolysable substrate analogue IDP is shown above the Wat. The proton is pumped into the vacuolar lumen through the vacuolar channel (shown in blue). (b) The coordination of water molecules in the proton transfer pathway. Wat1 is hydrogen-bonded to Arg242 and Asp294 and Wat2 to Ser298, Ser547 and Asn738.

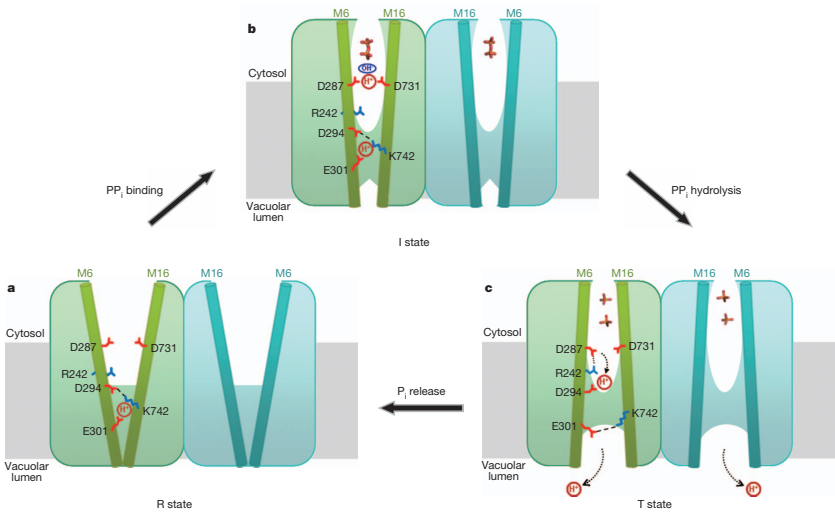

Figure 18. Reaction mechanism of proton pumping by VrPPase proposed by Lin and coworkers 2012 (reprinted with permission from Macmillian publishers Ltd.). The two subunits of VrPPAse dimer are shown in green and blue. The critical residues for proton pumping are shown as sticks and the two TMHs (M6 and M16) in which they reside as cylinders. Protons are shown as H^+ surrounded by a red circle, and salt bridges as blue lines. (a) In the resting state (R state) the active site is open and the proton is bound to Glu301. (b) In the initiated state (I state) PPi (shown in sticks) binds and closes the active site. An activated water molecule binds close to the leaving group phosphate of the PPi. (c) PPi hydrolysis causes the formation of a transient state (T state) where a channel leading to the vacuolar lumen opens up and a proton released from the activated water causes the reorganisation of the residues of the proton-transfer pathway. The combined effect of these two changes leads to pumping of a proton to the vacuolar lumen.

2 Aims of this study

The aim of this study was to solve the structure of an M-PPase through X-ray crystallography. This would not only have medical relevance, as the protein is a possible target protein against protozoan parasites, but would also be interesting from an enzymological point of view as the catalytic mechanism of an M-PPase is unlike that of any of the other phosphoanhydride utilising ion pumps.

As the crystallisation of membrane proteins is difficult, I chose a strategy that has been successfully used in determining the structure of other membrane proteins. In this strategy a group of homologous proteins, in this case eight M-PPases, are selected as target proteins. Starting with a group of homologous proteins enhances the chance that one of them is suitable for structural studies. Finding the correct target can be done by screening the target proteins by successive expression, purification and crystallisation trials. Of the eight selected target proteins of this study, the two best expressing proteins, the Na^+-PPase of *Thermotoga maritima* (TmPPase) and the K^+-independent H^+-PPase of *Pyrobaculum aerophilum* (PaPPase), could be purified with the ”hot-solve” method (López-Marqués et al., 2005). Both proteins crystallised in the presence of different detergents and well diffracting crystals of TmPPase were obtained that allowed the determination of its molecular structure. Recently, Lin et al. (2012) solved the structure of a plant H^+-PPase with substrate bound. The comparison of the resting-state and product bound conformations of TmPPase reported in this study with the plant H^+-PPase structure allowed me to devise a potential catalytic model of M-PPase function.

3 Materials and methods

Detailed descriptions of the materials and methods can be found in the original publications (Studies I-III). The methods of the unpublished work are described below.

3.1 Expression of selenomethionylated TmPPase

To produce selenomethionylated protein for finding the phases, plasmids pRS1024 and pYES2 containing TmPPase were transformed into the BG1484 strain of *S. cerevisiae* (Malkowski et al., 2007). The TmPPase-pRS1024-containing cells were first precultured in 300 ml of SCD-media lacking leucine and supplemented with 64 µM S-adenosyl methionine. This culture was then used to inoculate 6 l of SCD-media lacking leucine and containing 64 µM S-adenosyl methionine and 120 µM selenomethionine (Se-Met) and the cells were grown in this media to OD(600) ≈ 2. To express TmPPase under the GAL1-promoter, SalI and XbaI-digested $MRSGH_6$-tagged TmPPase gene was ligated into a pYES2-plasmid that had been digested with XhoI and XbaI restriction enzymes (all restriction enzymes from Fermentas). BG1484-cells were then transformed with the TmPPase containing pYES2-plasmid and the expression of TmPPase was carried out as described by Malkowski and coworkers (2007).

3.2 Characterisation of TmPPase

To measure the activity of TmPPase at 30°C, 3-5 µl of heat-solubilized TmPPase or TmPPase purified either in 1 % OGNPG, 0.5 % CYMAL-5 or 0.05 % DDM was mixed with 16-14 µl of buffer containing 50 mM MES-NaOH, 50 mM KCl, 20 % glycerol, 5 mM $MgCl_2$ and 1 mM DTT. The mixed samples were incubated at 30°C for 5 min after which 1 µl of 40 mM Na_2PPi was added to them. The PPi supplemented samples were then incubated at 30°C for 1 min – 1 h and after this the released phosphate was quantified as described by Baginski and coworkers (1967).

A novel lipid supplementation method was tested for TmPPase purified in 1 % OGNPG. 4 - 6 µl 30 mg/ml asolectin was mixed with 0.75 - 2.25 µl 20 % DDM. The mixture was heated at 55°C for 15 minutes and then 3.75 µl of purified protein was added. 1 µl of this protein, DDM and lipid containing sample was then added to a 239 µl reaction mixture containing 20 mM Tris pH 8, 20 mM NaCl, 2.6 mM $MgCl_2$ and 100 mM KCl. The reaction mixture was heated for 5 min at 71°C after which 10 µl of 10 mM PPi was added to it. The pyrophosphatase reaction was let to proceed for 2 - 5 min at 71°C and after this the released phosphate was quantified as described by Baginski and coworkers (1967).

3.3 Derivatization of TmPPase crystals

To determine the phases, I tried to derivatise the TmPPase crystals by soaking the protein crystals with a range of different heavy-metal reagents. The soakings were done by adding different reagents to the well solution and then overlaying the drop (0.4 – 2 µl) with 0.5 – 3 µl of heavy metal containing well solution. I tested the following reagents: 0.1 – 5 mM HgCl, 1 -2 mM CH_3HgCl, 1 mM tetrakis(mercuriacetoxy)methane, 5 – 20 mM trimethyl lead acetate, 1 mM phenyl mercury acetate, 1 - 5 mM Thiomersal, 1 - 5 mM chloro-(4-sulphophenyl)mercury, 2 – 5 mM K_2PtCl_4, 1 – 5 mM $KAu(CN)_2$, 1 mM Ta_6Br_{12}, 1 mM platinum orange, 5 -50 mM Na_2WO_4, 5 – 20 mM $EuCl_3$, 5 -20 mM $SmCl_3$ and 5 – 50 mM $GdCl_3$. The derivatization was then let to proceed from 1h to overnight, after which the crystals were frozen by flash freezing with liquid nitrogen and taken to the European Synchrotron Radiation Facility (ESRF, Grenoble, France), the National Electron Accelerator Laboratory for Synchrotron Radiation Research, Nuclear Physics and Accelerator Physics (MAX-lab, Lund, Sweden), or the Berliner Elektronenspeicherring-Gesellschaft für Synchrotronstrahlung (BESSY, Berlin Germany) for X-ray diffraction experiments. X-ray diffraction experiments were carried out on beamlines BM-14, ID-14/1, ID-14/2 and ID-29 at ESRF, I911-3 at MAX-lab and MX-14-2 at BESSY.

4 Results and discussion

4.1 Expression and purification of M-PPases (Studies I & II)

4.1.1 Expression of M-PPases in *S. cerevisiae* (Study I)

As the yeast *S. cerevisiae* has been shown to be a good host for the heterologous expression of M-PPases of different organisms (see 1.5.3.), it was chosen as the host organism for the expression of M-PPases carried out in this study. To find suitable targets for X-ray crystallography, I expressed eight M-PPases in the BJ1991-strain of *S. cerevisiae* under the constitutive PMA1-promoter. The eight selected target proteins contained M-PPases from archae, bacteria and protozoans and from all three functional groups known at the start of my study: Na^+-PPases and K^+-dependent -and K^+-independent H^+-PPases.

Pyrophosphatase activity measurements were carried out to assess the expression levels of the target M-PPases. These measurements were carried out with the extracted, M-PPase enriched yeast membranes. The optimal temperatures for PPase activity were known for two M-PPases: TmPPase (71°C) and PaPPase (81°C) and their activities were measured at these temperatures. The PPase activity measurements of the M-PPases from thermophilic organims (MtPPase and StPPase) were carried out at 55°C and from mesophilic organisms at 37°C (TdPPase) or at 33°C (MaPPase, TgPPase and TcPPase). Either based on the yield of the purified protein (TmPPase and PaPPase) or on the level of the PPase activity measured from yeast membranes (TdPPase), three M-PPases expressed at levels ≥ 0.5 mg/liter: TmPPase, PaPPase and TdPPase. The two best expressing M-PPases came from hyperthermophilic source organisms (TmPPase and PaPPase) which would indicate that highly thermotolerant M-PPases have a propensity for high expression levels in *S. cerevisiae*.

As fusions of T4 lysozyme to the i3-loop of G-protein coupled receptors had been shown to be beneficial for the crystallisation of many of these proteins (see 1.6.1), a similar approach was tested for TmPPase. Mutated T4 lysozyme (C54S, C97A) was inserted into the loop regions of TmPPase predicted not to contain conserved motifs necessary for the protein functions. Even though some of these chimaeric proteins expressed well (expression at up to 55% of the wt level), work on these proteins was not continued. This was because they all showed reduced levels of pyrophosphatase activity, indicating that the structure of the protein was perturbed by the T4L insertion.

4.1.2 Purification of PaPPase and TmPPase (Studies I & II)

After expression under the PMA1-promoter in BJ1991, both TmPPase and PaPPase could be purified by a modified version of the ”hot-solve” method (López-Marqués et al., 2005). The protein was first solubilised with DDM at 75°C from the pelleted yeast membrane fraction and then purified by nickel-affinity chromatography. Based on Bradford assay (Bradford, 1976) with bovine plasma gamma globulin as the standard, up to 2.5 mg/liter of pure TmPPase and 1.5 mg/liter of pure PaPPase could be obtained. A_{280} measurements carried out after buffer exchange of the purified protein showed the real protein yields to be 1.25 mg/liter of TmPPase and 0.75 mg/liter of PaPPase. These yields are similar to the the yields of other membrane proteins heterogously expressed in *S. cerevisiae* (see eg. White et al., 2007). The yield of TmPPase obtained with expression in BJ1991 was higher than with the w303a-strain used in the original ”hot-solve” purification. This could be due to the lack of vacuolar proteases in BJ1991.

In the beginning, the purification of PaPPase was marred by sporadic co-purification of two contaminating proteins (Figure 19). N-terminal sequencing showed these proteins to be ubiquitinylated derivatives of PaPPase. As ubiquitinylation of some membrane proteins has been shown to take place during the post-diauxic growth phase of *S. cerevisiae* (Hershko and Ciechanover, 1998), the formation of ubiquitunylated PaPPase could be stopped by harvesting the cells well before they reached the diauxic shift.

I could recover 100 % of the total activity of TmPPase and up to 85 % of the total activity of PaPPase after solubilisation when the activities of the proteins were measured at temperatures optimal for their activity in membrane-bound state (71°C for TmPPase and 81°C for PaPPase). To regain full activity in its solubilised state, PaPPase had to be supplemented with 0.12 mM soybean lecithin.

After the nickel affinity purification, both proteins required lipid supplementation for full activity. TmPPase had to be supplemented with both DDM (0.015 %) and soybean lecithin (0.12 mM), while, as in the case of the solubilised protein, PaPPase required solely 0.12 mM soybean lecithin. A similar requirement for reactivation with either lipid or lipid and detergent addition has been reported for all purified M-PPases (see 1.5.4.). After reactivation, the specific activities of TmPPase and PaPPase were 20 µmolPi/mg/min and 60 µmolPi/mg/min, respectively (40 µmolPi/mg/min and 120 µmolPi/mg/min if A_{280}-measured protein concentrations are used).

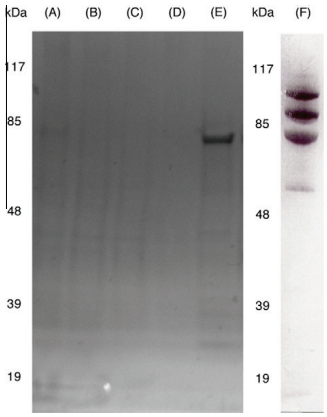

Figure 19. Analysis of PaPPase purification by SDS-PAGE (From Study I, reprinted with permission from Elsevier). The lanes are (A) 25 µg membranes after heat-solubilisation, (B) 15 µl of flow-through and (C), (D) wash fractions from the Nickel-affinity chromatography and (E) 10 µg of purified protein. (F) 30 µg of purified PaPPase from another batch of purification showing partial ubiquitinylation.

During Ni-affinity purification, I carried out detergent exchange into 17 different detergents for TmPPase and 7 different detergents for PaPPase. TmPPase showed high activity in 12 of these, while PaPPase showed high activity in all 7 (Table 6). Of the 7 detergents in which TmPPase showed low activity even after reactivation, most had either short acyl chain (OG), small, zwitter-ionic or ionic headgroups (Fos-12, CyFos-6) or small micelle size (OG, CHAPSO) all of which are characteristics of `harsh´ detergents (Privé, 2007). Whether the protein is actually denatured in the presence of these detergents or requires a different re-activation procedure remains to be tested.

We also tested the effect of detergent on the stability of TmPPase by circular dichroism (CD)-thermal denaturation measurements. Measurements were carried out with TmPPase in either 0.05 % DDM or 1.5 % OG and showed lower T_m of denaturation for TmPPase OG (≈60°C *vs* ≈80°C, Figure 20). This fits the results of the activity measurements, which showed significantly lower activity for TmPPase OG in comparison to TmPPase DDM (Table 6). The complexity of the denaturation behaviour of TmPPase (Figure 20) might be due to the protein having possibly two transition midpoints for denaturation; one (possibly for dimer dissociation) with a T_m≈70°C and the second with a T_m≈85°C.

In order to characterise the oligomeric state of the purified proteins, we carried out size-exclusion coupled multi-angle laser light scattering (SEC-MALLS) measurements on DDM purified protein. With this method one can attain molecular masses of protein-detergent complexes and measure the oligomericity of membrane proteins by measuring the UV-signal, refractive index and light scattering of the gel-filtrated protein samples (Slotboom et al. 2008). These measurements showed that both proteins were dimeric with the ≈150 kDa dimer surrounded in the case of TmPPase and PaPPase by ≈100 kDa and ≈150 kDa detergent belt, respectively (Figure 21).

Table 6. Effect of detergent exchange on the activity of TmPPase and PaPPase (Studies I and II).

Protein	Detergent	Concentration of detergent (%)	Concentration of detergent (× CMC)	Specific activity (μmolPi/mg/min)	Activity (%)
TmPPase	DDM	0.02 – 0.08	2.3-9.2	40	100
	UDM	0.145	5		100
	DM	0.175 - 0.45	2-5.2		98
	αUDM	0.145	2		95
	αDM	0.45	5		96
	d-thio-DM	0.225	10		95
	NM	0.56	2		100
	C12E8	0.072	5		24
	HEGA-10	0.52	2		83
	C-HEGA-10	2.6	2		10
	CYM-6	0.056 - 0.14	2.1-5		100
	CYM-5	0.24 - 0.6	2-5		85
	CYM-4	0.74	2		80
	NG	0.4	2		90
	FosC-12	0.235	5		22
	CyFos-6	0.47	5		20
	OG	1	2		14
	CHAPSO	1	2		25
	DMNPG	0.2	59		98
	OGNPG	1	17		90
PaPPase	DDM	0.05 – 0.08	2.3-9.2	120	100
	DM	0.45	5		99
	NM	0.56	2		105
	αUDM	0.145	5		95
	αDM	0.45	5		96
	OM	1.8	2		98
	C-HEGA-10	2.6	2		43
	OG	1	2		110
	CYM-6	0.14	5		102
	CYM-5	0.6	5		101
	CHAPSO	1	2		97
	OGNPG	1	17		95

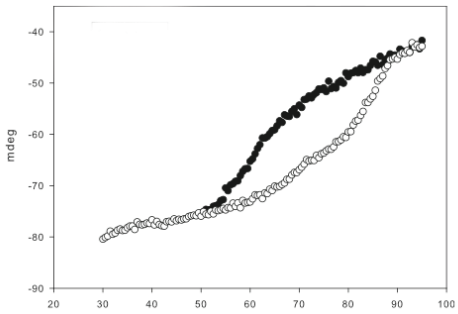

Figure 20. Results of CD-thermal denaturation measurements of TmPPase OG (black spheres) and DDM (white spheres) (From Study I, reprinted with permission from Elsevier).

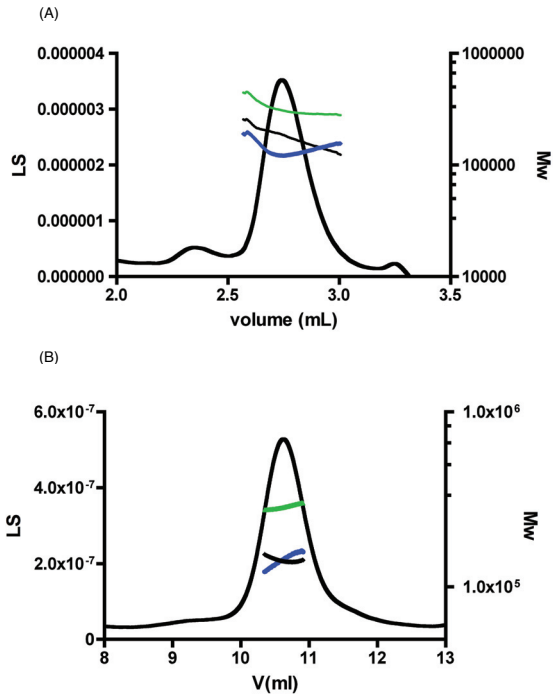

Figure 21. Analysis of purified (a) TmPPase and (b) PaPPase DDM with SEC-MALLS (From Study I, reprinted with permission from Elsevier). The black trace shows the trace of the light scattering (left axis), while the green, black and blue curves show the calculated molecular masses (right axis) of the protein detergent complex, protein and detergent micelle, respectively.

4.2 Crystallisation of TmPPase and PaPPase (Study II)

4.2.1 Crystal optimization

After Ni-affinity purification, both TmPPase and PaPPase were buffer exchanged into a buffer containing all of the ligands of M-PPases (Mg^{2+}, Pi, Na^{+} and K^{+}) and subjected to

crystallisation trials by hanging-drop vapour diffusion. Initial crystallisation screens of TmPPase and PaPPase in DDM used 0.2 µl drops at room temperature with a crystal screen with conditions similar to those described by Iwata (2003). Crystals of TmPPase and PaPPase grew in various PEG 400 containing conditions and they diffracted at best to 7.5 Å and 28 Å, respectively.

Optimisation of these initial conditions was carried out by varying the PEG 400 concentration (20 - 40 %), salt concentration (0 – 0.7 M NaCl) and pH (4 – 9), by testing the addition of secondary detergents and additives, by crystallising at 4°C, by using bigger drops (0.5 µl protein solution + 0.5 µl well solution), and by varying the DDM concentration (0.08 – 0.02 % DDM) used in the Ni-affinity purification and buffer exchange. Also crystallisation with different precipitants (PEG 200, PEG 550 MME, PEG 1000, PEG 3350 and PEG 4000) was tested. These optimisation steps produced better diffracting crystals: for example, one TmPPase crystal grown at 4°C diffracted to 6.5 Å and TmPPase crystals with nonyl glucoside and CHAPSO as secondary detergents also brought an improvement in resolution, while one PaPPase crystal diffracting to 9 Å was grown, but the diffraction still remained poor and/or highly anisotropic (see Study II). Also, the reproducibility of the crystallisation was very poor; crystallisation results varied wildly not only between different purification batches, but even between identical drops.

Due to the problems with poor diffraction and poor reproducibility with crystals of both TmPPase DDM and PaPPase DDM, optimisation of crystallisation by detergent exchange was then tested. This detergent exchange was carried out on DDM solubilised protein during Ni-affinity chromatography.

Detergent exchange of TmPPase and PaPPase was tested in three rounds. In the first round, seven detergents were tested with TmPPase and three with PaPPase. Of these detergents DM gave a marked increase in TmPPase and PaPPase diffraction to 5 Å and 5.8 Å, respectively (Tables 7 and 8). Lipid addition by the `HiLiDe´-method (see 1.6.2.) improved the diffraction of TmPPase DM further to 4.3 Å (Table 7). In the second round of detergent exchange, six detergents were tested with TmPPase and three with PaPPase. Of these detergents, both CYM-6 and CYM-5 increased the diffraction of TmPPase to 3.9 Å (Table 7), while none increased the diffraction of PaPPase (Table 8). As with DDM, TmPPase and PaPPase crystallisation with the detergents of the first and the second round was marred by very poor reproducibility. In the third round of detergent exchange, three detergents were tested with TmPPase and one with PaPPase. One of these detergents, OGNPG, gave marked enhancement not only to TmPPase diffraction, with the best crystal diffracting to 2.6 Å (Figure 22, Table 7), but also to the reproducibility of crystallisation; with this detergent we could reproducibly grow TmPPase crystals diffracting to around 3 Å.

Table 7. Crystallisation of TmPPase after detergent exchange (Study II).

Detergent	Well solution	Crystallisation temperature	Diffraction	Space group
0.072 % C12E8	(No crystals)	-	-	-
0.145 % UDM	30 % PEG 400, 0.1 M Novelle buffer 4 pH 6.5, 0.1 M $LiSO_4$, 0.1 M NaCl	21°C	7 Å	n.d.
0.45 % DM	30 % PEG 400, 0.1 M Novelle buffer 4 pH 7, 0.1 M Li_2SO_4, 0.1 M NaCl	21°C	5 Å	P422[§]
0.175 % DM	30 % PEG 400, 0.1 M Factorial citrate pH 7, 0.1 M NaCl	21°C	28 Å	n.d.
0.45 % DM (0.1 mg/ml DOPC)	35 % PEG 400, 0.05 M Tris pH 8, 0.05 M Na_2SO_4, 0.05 M Li_2SO_4	21°C	4.3 Å	$P2_1$
0.56 % NM	35 % PEG 400, 0.1 M Novelle buffer 4 pH 9, 0.1 M Li_2SO_4, 0.1 M NaCl.	21°C	15 Å	n.d.
0.225 % D-thio-M	30 % PEG 400, 0.1 M Novelle buffer 4 pH 8, 0.1 M $LiSO_4$, 0.1 M NaCl	21°C	3.7- 8 Å[*]	$P2_1$
0.4 % NG	(No crystals)	-	-	-
0.52 % HEGA-10	(No crystals)	-	-	-
2.6 % C-HEGA-10	35 % PEG 400, 0.1 M Novelle buffer 4 pH 6.5, 0.1 M $LiSO_4$, 0.1 M NaCl	21°C	no diff.	-
1 % CHAPSO	(No crystals)	-	-	-
0.47 % CyFos-6	35 % PEG 400, 0.05 M Tris pH 8, 0.22 Na-Citrate	21°C	no diff.	-
0.235 % FosC-12	(No crystals)	-	-	-
0.14 % CYM-6	18 % PEG 3350. 0.64 M NaAcetate pH 4.6	21°C	3.9 Å	P6[§]
0.06 % CYM-6	14 % PEG 3350 0.8 M NaAcetate pH 4.0	21°C	no diff.	-
0.5 % CYM-5	35 % PEG 400, 0.05 M Tris pH 8, 0.05 M Na_2SO_4, 0.05 M Li_2SO_4	21°C	3.9 Å	$P2_1$
0.24 % CYM-5	35 % PEG 400, 0.05 M Tris pH 8, 0.05 M Na_2SO_4, 0.05 M Li_2SO_4	21°C	no diff.	-
0.74 % CYM-4	33 % PEG 400, 0.1 M HEPES pH 7, 0.2 M $CaCl_2$.	4°C	4.5 Å	$P2_1$
0.2 % DMNPG	29 % PEG 400, 0.1 M Tris pH 9.5, 0.05 M Na_2SO_4, 0.05 M Li_2SO_4	21°C	4 – 7 Å[*]	n.d.
1 % OGNPG	19 % PEG 350 MME, 0.1 M MES pH 6.5, 0.2 M $CaCl_2$. 2 mM DTT	4°C	2.6 Å	$P2_1$

[*] = Anisotropically diffracting crystal, no diff. = No diffraction detected, [§] = Not possible to assign the space group with the lattice form, n.d. = Not determined.

With some of the detergents, different detergent concentrations were tested during the Ni-affinity chromatography and buffer exchange (Tables 7 & 8). These results showed the optimal detergent concentration to be in each of these cases ≈ 4-5 x cmc. This high detergent concentration might be beneficial to crystal formation either because it facilitates formation of detergent-detergent contacts (Loll, 2003) or because it washes away lipid from the protein-detergent complex and thus decreases the size of the detergent envelope.

Table 8. Crystallisation of PaPPase after detergent exchange (Study II).

Detergent	Well solution	Crystallisation temperature	Diffraction	Space group
0.45 % DM	35 % PEG 400, 0.1 M Tris pH 8, 0.1 M KCl	21°C	5.8 Å	$C222/C222_1$
0.175 % DM	(No crystals)	-	-	-
0.56 % NM	32 % PEG 400, 0.1 M HEPES pH 7, 0.2 M $CaCl_2$.	21°C	no diff.	-
1 % OG	(No crystals)	-	-	-
1 % CHAPSO	(No crystals)	-	-	-
0.14 % CYM-6	(No crystals)	-	-	-
0.5 % CYM-5	(No crystals)	-	-	-
1 % OGNPG	(No crystals)	-	-	-

no diff. = No diffraction detected.

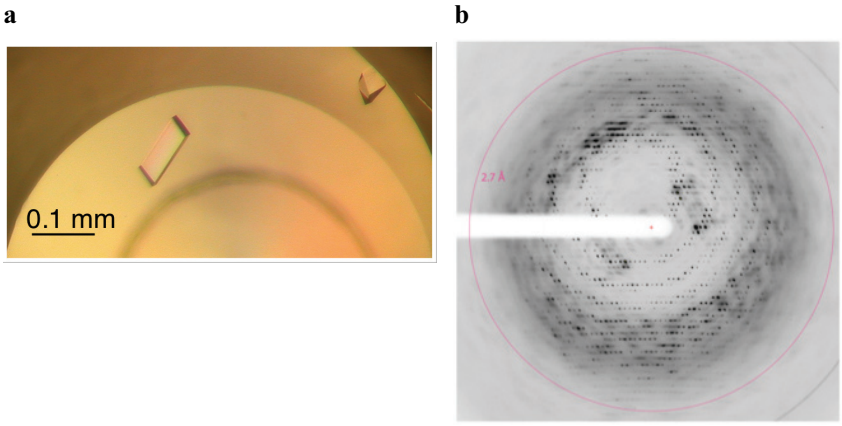

Figure 22. Crystallisation of TmPPase in the presence of OGNPG (from Study II, reprinted with permission). (a) TmPPasa OGNPG crystals. (b) Diffraction of TmPPase OGNPG crystal measured at I911-3 beamline of Nuclear Physics and Accelerator Physics (MAX-lab, Lund, Sweden).

4.2.2 Crystal properties

From the initial crystallisation trials of TmPPase, I obtained DDM crystals in different space groups: depending on the conditions, crystals in primitive orthorhombic, monoclinic, hexagonal or tetragonal groups grew (see Study II). After detergent exchange, TmPPase crystallised either in space group $P2_1$, P6 or P422 depending on the detergent

used (Table 7). Addition of the lipid dioleylphosphatidyl choline to TmPPase DM caused the space group to change from P422 to $P2_1$ (Table 7).

Packing of the TmPPase molecules in the OGNPG-containing $P2_1$-space group crystals is of type I (Figure 23). The formation of the layered, bilayer like sheets in these crystals seems to be driven by favourable detergent-detergent interactions. As similar type I packing is also seen in the TmPPase CYM-5 crystals, which also crystallised in space group $P2_1$ (data not shown), it is likely that all TmPPase crystals with this space group are of type I (Table 7). The change of the space group from P422 to $P2_1$ after the lipidation of TmPPase DM might thus be due to the change of the crystal packing from type II to type I, where the added lipid drives the formation of bilayer like sheets.

Figure 23. Electron density of a 2.6 Å diffracting TmPPase OGNPG crystal showing type I crystal packing (From Study II, reprinted with permission).

With TmPPase, low pyrophosphatase activity in detergent was associated with poor crystallisation behaviour; the detergents in which the protein had 25 % or less of the activity of TmPPase DDM either did not facilitate the formation of crystals or the crystals that did grow did not diffract (Tables 6 and 7).

With detergents in which TmPPase had over 80 % of the activity of TmPPase DDM, however, there was no correlation between activity and crystallisation behaviour. For example, TmPPase CYM-5 and CYM-4 had 85 % and 80 % of TmPPase DDM activity (Table 6), respectively, and produced better diffracting crystals than TmPPase NM (Table 7), which had the same activity as TmPPase DDM (Table 6). With these detergents, detergent-detergent interactions and small micellar size seems to have stronger effect on their crystallisation behaviour than the stabilising effect of the detergent.

PaPPase showed similar activity in all of the detergents that were tested (Table 6). However, it crystallised in only DDM and DM, and the best crystals, in DM, diffracted only to 5.8 Å (Table 8). This poor crystallisation behaviour could be due to loss of activity during the solubilisation of the protein; we could recover only ≈80 % of the total activity after this step.

In CHAPSO, C-HEGA-10 and HEGA-10 both TmPPase and PaPPase started to aggregate during concentration. In the case of CHAPSO and C-HEGA-10, in which TmPPase showed low PPase activity (Table 6), the aggregation is probably a sign that the protein is inactivated in them.

4.3 Structure of TmPPase in resting and product bound states (Study III)

4.3.1 Structure determination of TmPPase (Study III)

Having obtained well diffracting crystals of TmPPase OGNPG, the structure had to be solved. To do so, derivatization with various heavy-metal reagents was tested (See 3.3) and crystallization of Se-Met labelled TmPPase was carried out (See 4.4.1) because there were no structures of homologous proteins to be used for molecular replacement. Of the tested heavy-metal derivatives, only TMLA and Na_2WO_4 showed interpretable differences. We then used these for solving the high-resolution (2.6 Å, R_{work}/R_{free} = 20.5/24.5%) protein structure. The structure was determined by multiple isomorphous replacement with anomalous scattering phasing. The heavy-atom substructures were solved with SHELXC/D (Schneider and Sheldrick, 2002) at 6 Å. The protein structure was phased using SHARP (Bricogne et al., 2003) and the phases were extended to 3.5 Å with SOLOMON (Abrahams and Leslie, 1996). The two-fold axis of the protein dimer was discovered based on the electron density and anomalous signal peaks of the initial maps and these maps were further improved to a resolution of 3.3 Å by non-crystallographic two-fold averaging in DM (Cowtan, 2001). As the direction of helices was still unclear and no side-chains could be built in to this map, building the sequence into the structure required the use of Rosetta molecular replacement method (DiMaio et al., 2011).

Even though the initial crystallisation conditions of TmPPase OGNPG contained 1 mM phosphate, we could not see it in the active site. This was probably due to the high Ca^{2+} concentration in the drop (initially 0.1 M), which caused precipitation of the phosphate. For this reason we solved the structure of TmPPase CYM-5 at 4 Å resolution using molecular replacement from our high resolution structure (R_{work}/R_{free} = 29.5/36.5%). In this low-resolution structure we could see the density for a Mg_4Pi_2K-complex in the active site of the protein (Figure 24).

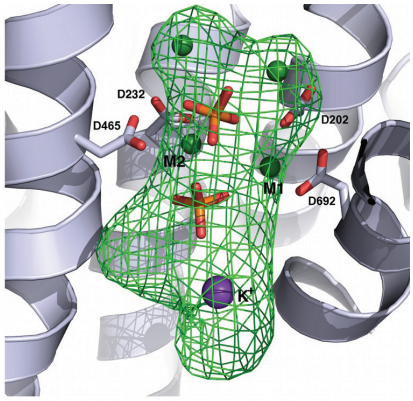

Figure 24. Mg_4Pi_2 complex and K^+ in the activesite of the product bound state of TmPPase (From Study III, reprinted with permission from AAAS). The map shown in the figure is a Fo-Fc map of product complex structure with a contour of 2.6 δ.

4.3.2 Analysis of TmPPase structures

4.3.2.1 TmPPase in a metal-bound, resting state

The structure of TmPPase in the metal-bound, resting state solved at 2.6 Å reveals that the protein has 16 TM-helices, some of which extend 27 Å into the cytoplasmic space (Figure 25). The cytoplasmic part of the protein contains an active site cavity lined by conserved, charged residues. The cavity ends at a cluster of conserved residues that separates the active site cavity from a series of small cavities leading to the periplasmic space (Figure 25). Cytoplasmic loops between helices 5-6 and 13-14 (loop 5-6 and loop 13-14) near the active site cavity were not visible in the structure.

In the upper part of the active-site cavity is the 'hydrolytic centre' in which the cofactors (Mg^{2+} and K^+) and substrate (Mg_2PPi) bind (Figure 25). The resting state TmPPase structure contains two bound metal ions (Figure 26). The bond lengths suggest that one of them (M1) is a Ca^{2+} coordinated by conserved D688, D660 and D692 (2.9 Å, 2.1 Å and 2.8 Å away from M1, respectively) and the second one (M2) is a Mg^{2+} coordinated by conserved D232 and D465 (1.7 and 2.9 Å away from the M2, respectively). The D688, D660 and D692 themselves are positioned by the conserved K663, K664 and K695. Although the $GdCl_3$ derivative could not be used to solve the structure, anomalous difference Fourier electron density was seen for Gd^{3+} in the same positions as M1 and M2 of the native structure. This supports the metal binding role of these two sites (Figure 26).

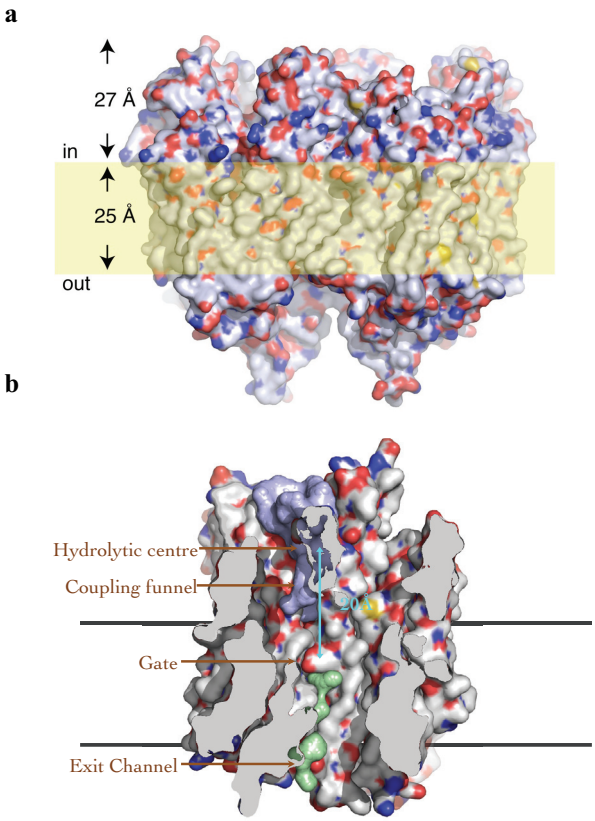

Figure 25. Overview of the resting state TmPPase structure (From Study III, reprinted with permission from AAAS). (a) Surface representation of the TmPPase structure with the TM-area shown in yellow. (b) Cut-away of the protein showing its four-part structure and with the active site cavity (blue) and periplasmic cavites (green) visible.

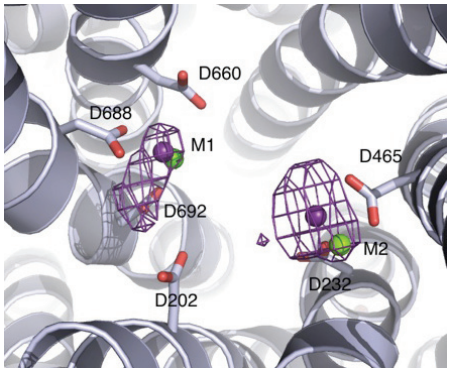

Figure 26. Coordination of metal binding in the resting state TmPPase (From Study III, reprinted with permission from AAAS). Ca^{2+} and Mg^{2+} are shown in green and the anomalous difference Fourier electron density of the bound Gd^{3+} is shown purple (displayed at 7.0 δ). The position of the Gd sites are shown as purple spheres.

Below the hydrolytic centre is a chain of conserved, charged residues (Figure 27). Mutagenesis studies have shown that, besides the conserved residues of the hydrolytic centre, these residues are also necessary for the catalytic activity of M-PPases (see 1.3.). For this reason it seems that the chain of the conserved residues below the active site forms a 'coupling funnel', which couples the pyrophosphate hydrolysis to ion pumping (Figure 25). This chain leads down to the charged ionic triplet of D243, E246 and K707 that form a 'gate ' that separates the cytoplasmic and periplasmic cavities (Figure 27) and that, when opened, allows the transfer of the Na^+ or H^+ to the periplasmic space (Figure 25). In the vicinity of the charged residues of the gate are two conserved serines, S184 and S247, which form hydrogen bonds with K707.

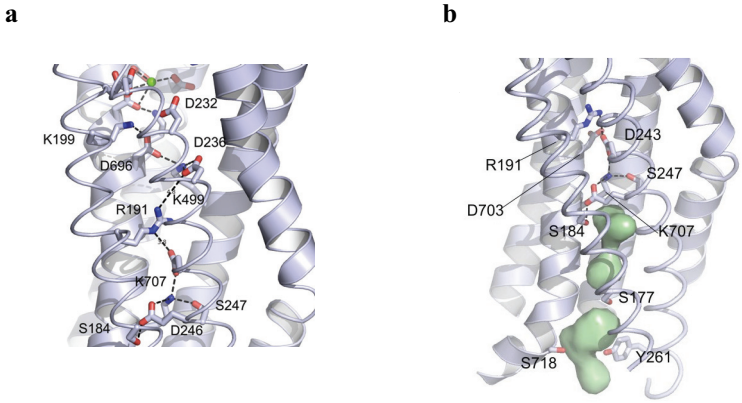

Figure 27. Coupling funnel in the resting state TmPPase (From Study III, reprinted with permission from AAAS). (a) Chain of conserved, charged residues leading down from the hydrolytic centre to the gate. M2 in the hydrolytic centre is shown in green. (b) Periplasmic cavites (in green) below the gate leading to the periplasm.

On the cytoplasmic side of the gate is a conserved R191, which occupies an unusual position in between D236 and D243 as it forms only very long and weak ionic bonds to both (Figure 28). As mutation of this residue to lysine in AtPPase lowers the coupling ratio of the protein to 6 % of wt enzyme (see 1.3.), this residue seems to play a part in the coupling of pyrophosphate hydrolysis to ion pumping.

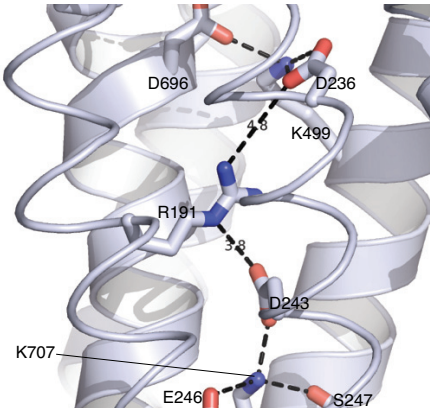

Figure 28. Position of R191 in the resting state TmPPase. Distances from R191 to D236 and D243 are shown in Ångströms.

4.3.2.2 TmPPase in the product bound state

The product bound state of TmPPase shows a complex of Mg_4:K:Pi_2 in the active site. The Mg^{2+} ions in the structure are coordinated by D202, D688 and D692, while the magnesium ions and K199, K664 and N493 coordinate the binding of the two phosphate ions (Figure 29). The potassium ion coordinates D696 and the leaving group phosphate.

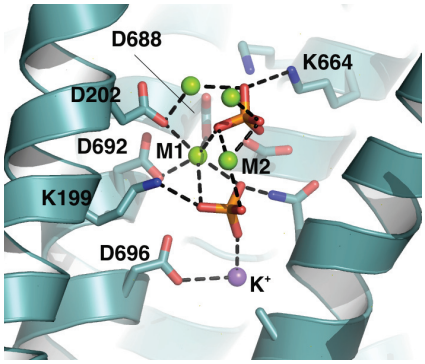

Figure 29. Mg_4:Pi_2:K-complex and its coordinating residues in the active site of the product bound state of TmPPase (From Study III, reprinted with permission from AAAS).

4.3.2.3 Gene triplication in M-PPases

Superposition of the helices 3-6, 9-12 and 13-16 shows these four-helix motifs to have a similar structure with an r.m.s.d per Cα for the 3-6 and 9-12 versus 13-16 of 2.1 Å (120/169) and 2.9 Å (113/119), respectively (Figure 29). The structure-based sequence alignment aligns conserved active site regions that contain the functionally important residues D202, D206, D228, D232, D236, D243, S247, D465, D488, D660, K663, D688, D692, D696 and K707 (Tables 2 and 3, Figure 30). These facts prove that M-PPases have evolved through gene triplication as previously hypothesised (Au et al., 2006).

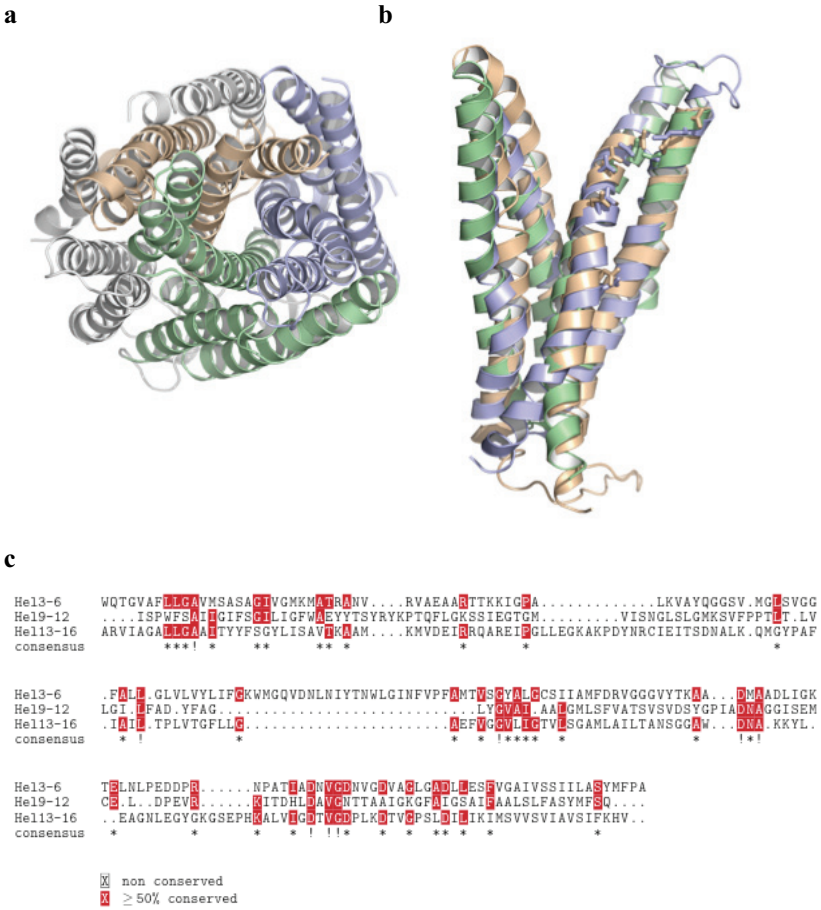

Figure 30. Evidence for gene triplication in M-PPases (from Study III, reprinted with permission from AAAS). (a), (b) Superimposition of TMHs 3-6 (sand), 9-12 (green) and 13-16 (blue). (c) Sequence alignment of TMHs 3-6 (Hel3-6), 9-12 (Hel9-12) and 13-16 (Hel13-16) showing conserved residues.

4.3.2.4 Comparison of TmPPase structures with the VrPPase structure

A DALI-search (Holm and Sander, 1997) with the 2.6 Å TmPPase structure showed the structure to be similar only to that of the 2.35 Å VrPPase structure that had just been published (Lin et al. 2012). Superposition of these two structures shows them to be very similar and gives an r.m.s.d. of 1.57 Å for 517/618 aligned Cαs (Figure 31) and 1.01 Å if only the core of 319 Cαs is taken.

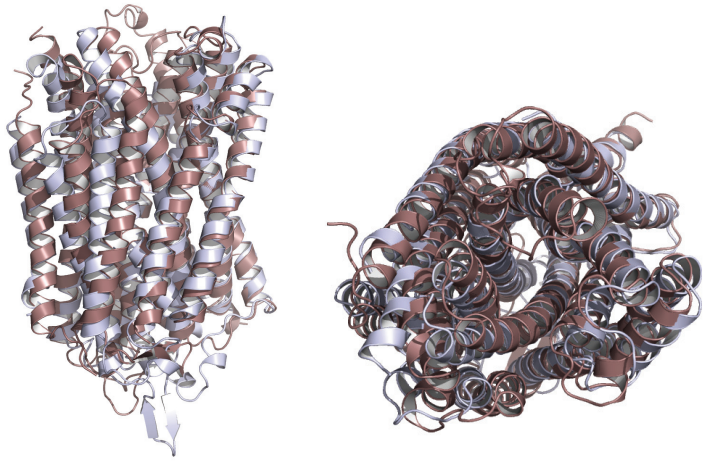

Figure 31. Superimposition of TmPPase resting state structure (in blue) and the product bound state of VrPPase (in brown).

The largest differences between the VrPPase and resting state TmPPase structures are seen at the cytoplasmic end of the active-site cavity (Figure 32). In the VrPPase structure, binding of the substrate causes the cytoplasmic 5-6-loop to order and thus close the active site (Figures 16 and 32), while this loop is not visible in the TmPPase structure (Figure 32). The closure of the active site is also facilitated by the movement of the cytoplasmic ends of helices 11 and 12 towards the active site's centre (Figure 32). In the product bound TmPPase structure, TMH 11 is in the same position as in the VrPPase structure, while TMH 12 is further away from the centre of the active site as it is in the resting state TmPPase structure (Figure 32). As the opening of active site to the cytoplasm in the product bound state is thus midway between the resting and substrate bound states, the full opening of the active site takes place when the enzyme returns to the resting state at the end of the catalytic cycle.

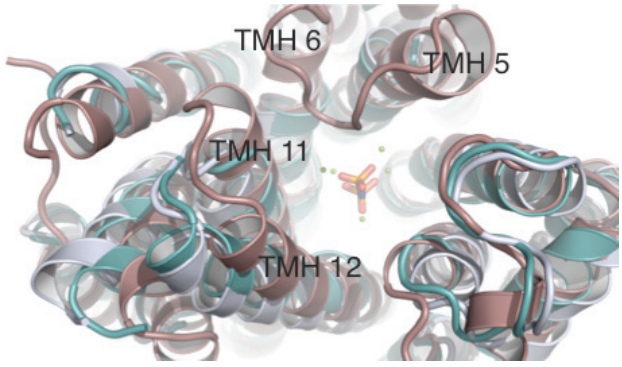

Figure 32. Opening of the active site between the resting, substrate and product bound states of an M-PPase. The resting state TmPPase structure is shown in light blue, VrPPase structure in brown and the product-bound state of TmPPase in cyan. The TMHs 5, 6, 11 and 12 are marked. IDP:Mg-complex of the VrPPase structure is shown in the active site.

The binding of the substrate seems to cause slight reorganisation of the bound divalent cations as the coordination of the metals is different in the TmPPase and VrPPase structures (Figure 33). Two ions in the VrPPase structure seem to have about the same coordination as the metals in the resting state TmPPase structure. These are M3 and M2, which, due to different numbering of metal ions in the two structures, have similar coordination to that of M1 and M2 of the resting state TmPPase, respectively (Figure 33). After hydrolysis, the coordination of the Mg_4:Pi_2:K-complex seems to be similar to the coordination of the substrate complex, with M1 occupying the same position and having the same coordination in both of the structures (Figure 33), but with the position and coordination of the phosphate groups and the other metals changing slightly (Figure 33). The tungstate derivative occupies roughly the same position as the leaving group of the PPi-analogue in the VrPPase:IDP-structure (Figure 33), which is reasonable given that tungstate and phosphate are isosteric.

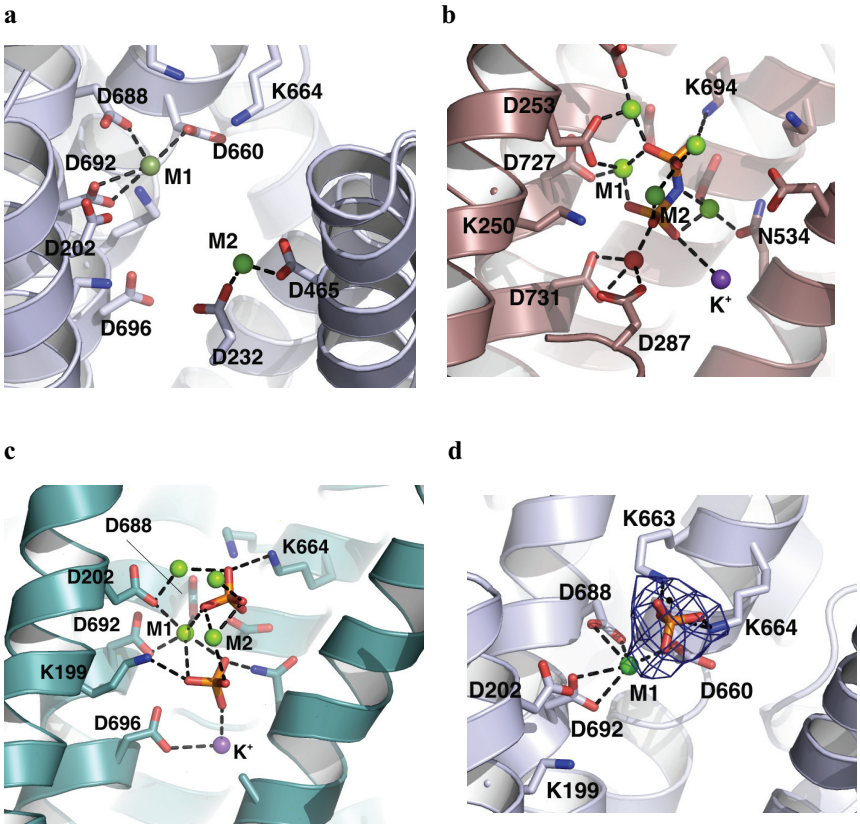

Figure 33. Ligand binding in the hydrolytic centres of (a) resting state TmPPase, (b) substrate-bound VrPPase and (c) product-bound TmPPase (From Study III, reprinted with permission from AAAS). Metal numbering is according to that of the resting state TmPPase. (d) Anomalous difference Fourier electron density map of tungstate derivative showing the position of the bound ion.

In comparison to the position of R191 in the resting-state TmPPase, which is in between D236 and D243, the equivalent arginine in VrPPase, R242, is in the ”down” position in a salt bridge with D294 (Figure 34). Below the arginine, the gate of the VrPPase almost wholly superimposes with that of TmPPase. The only difference is in the place of the semi-conserved glutamate in the two proteins: in VrPPase the semi-conserved glutamate E301 is in position equivalent to residue 250 of TmPPase and therefore one α-helix turn below the other gate residues (Figure 35).

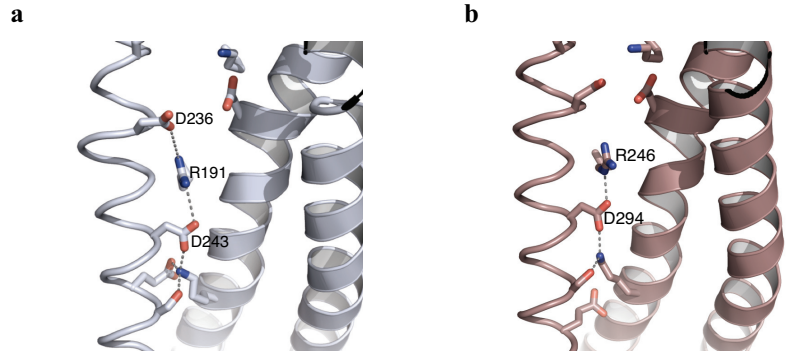

Figure 34. Position of conserved arginine in the resting state TmPPase and substrate bound VrPPase. (a) In the resting state TmPPase the R191 is coordinated by both D236 and D243, while the equivalent arginine (b), R246, in VrPPase is coordinated only by D294.

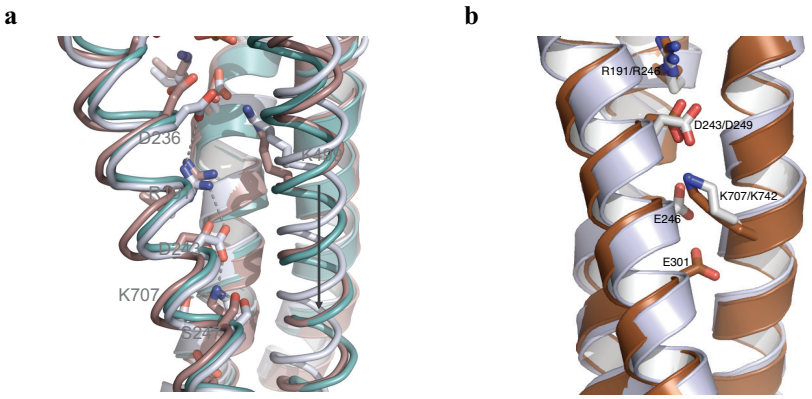

Figure 35. Gate and movement of TMH12. (a) Superimposition of the gate residues of TmPPase (blue) and VrPPase (brown) shows the difference in the position of the semi-conserved glutamates E246 and E301. (b) Superimposition of the resting (blue) and product-bound (green) states of TmPPase and substrate-bound state of VrPPase (brown) shows the movement of TMH12 in the vicinity of the gate down towards the periplasm/vacuolar lumen in the product- and substrate-bound states (From Study III, reprinted with permission).

Superposition of the three different M-PPase structures shows that the helix 12 is shifted 2 Å towards the periplasmic/vacuolar part of the protein in the VrPPase:PNP and TmPPase:Pi-structures (Figure 35). The side of helix 12 that faces into the active site cavity is lined by hydrophobic residues (A502, I503, A506, and I507). These hydrophobic residues can possibly form a flat, oily face that can lubricate the surface of the helix and thus facilitate its movement during the catalytic cycle of the enzyme.

4.3.2.5 Catalytic model of how sodium pumping occurs

By combining the structural information gained from the TmPPase:Mg:Ca, TmPPase:Pi and VrPPase:PNP-structures (Figure 36), I could put forward a catalytic model to explain pyrophosphate-driven sodium pumping (Kellosalo et al., 2012). In this model, Mg_2PPi binds to the resting state enzyme. The binding of the substrate closes the active site cavity and causes the formation of a short-lived transition state. In this transition state, I hypothesize that movement of R191 and helix 12 towards the periplasm (Figures 34 and 35) opens the gate and the exit channel and leads to ion pumping. As stated before (See 4.3.2.4.), the hydrophobic surface of the helix 12 could help this movement as its hydrophobic residues could act as a lubricatant, enabling the TMH12 to slide past TMH6 and TMH16. The opening of the gate and the exit channel could also involve the movement of helix 11, as it has a short break in the middle that could act as a hinge. After the sodium ion has passed out into the solvent, the gate and the exit channel close as the short lived transient state reverts to the substrate-bound state. The pyrophosphate is then hydrolysed by nucleophilic attack of an activated water molecule. Hydrolysis and the proton released from the activated water molecule cause the reorganisation of the residues of the coupling funnel, thus drawing R191 back up to its position in between D236 and D243 (Figure 34). The hydrolysis also allows the opening of the active-site cavity by breaking the salt-bridge network that holds loop 5-6 in place (see 1.7.5.2). As a single tungstate molecule was seen in the position of the leaving group phosphate (Figure 33), I propose that after the opening of the active site, the first phosphate to leave is the electrophilic one, followed by the the leaving group phosphate. After this, the protein reverts back to its resting state. As the tungstate derivative and the resting state have the same structure, the movement of helix 12 back towards the cytoplasm takes place after the release of the electrophilic phosphate group.

An alternative mechanism put forward by Lin et al. (2012) suggests that pumping is directly coupled to pyrophosphate hydrolysis (see 1.7.4.3.). In this model, the transfer of a proton released from an activated water molecule causes the movement of the conserved arginine down towards the gate, which leads to the gate opening and ion pumping.

I prefer the binding change mechanism, as it explains better the reversibility of the enzyme. The direct model favoured by Lin et al. (2012) would be analogous to that of bacteriorhodpsin, where the activity is not reversible (Lanyi, 2006). A similar case where the energy from the binding of the substrate drives the ion-pumping is seen with the F,V

and A-type ATPases in which the binding or release of a substrate from the active site is an energy releasing or requiring process (Stock et al., 2000).

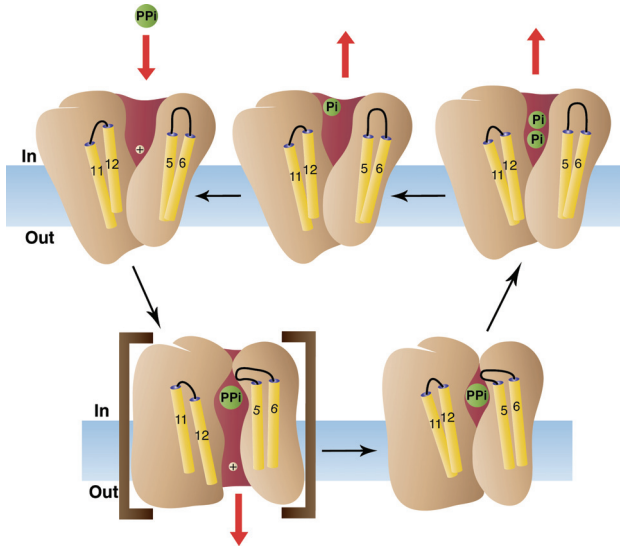

Figure 36. Model of M-PPase catalysis (From Study III, reprinted with permission from AAAS). Helices 5, 6, 11 and 12 are shown as yellow cylinders. Binding of PPi to the resting state enzyme (upper left) causes the closure of the active site and the formation of a short-lived transient state (lower left). In this state movement of TMH12 towards the periplasm opens the periplasmic channel and leads to pumping of the ion. After this, the periplasmic channel closes (lower right) and the PPi is hydrolysed (upper right). Hydrolysis of pyrophosphate opens the active site cavity and allows first the electrophilic phosphate (upper middle) and then the leaving group phosphate to leave, thus returning the enzyme back to the resting state.

4.4 Unpublished results

4.4.1 Production of Se-Met TmPPase

Se-Met TmPPase was produced both under a constitutive PMA1-promoter and under a galactose inducible GAL1-promoter in a Se-Met tolerant yeast strain BG1484 (Malkowski et al., 2007). In both cases production of the protein was marred by low yield (0.05 – 0.2 mg/liter), variability in specific activity (activity varied between 5 to 40 µmolPi/mg prot./min between different purification batches) and low incorporation rate (20 %). One

data set was collected, but no interpretable peaks were found. I therefore did not continue with this approach for obtaining phases.

4.4.2 Necessity of L351 and G395 for the thermostability of TmPPase

The TmPPase I worked with contained two amino acid changes, V351L and S395G, compared to the sequence of TmPPase Q9S5X0. These changes were crucial for the stability of the enzyme during its purification, as while the L353 and G395-containing enzyme did not lose any activity after the ”hot-solve” step, the total activity of the solubilised wild-type enzyme was only 20 % of that of the membrane-bound protein (Figure 37).

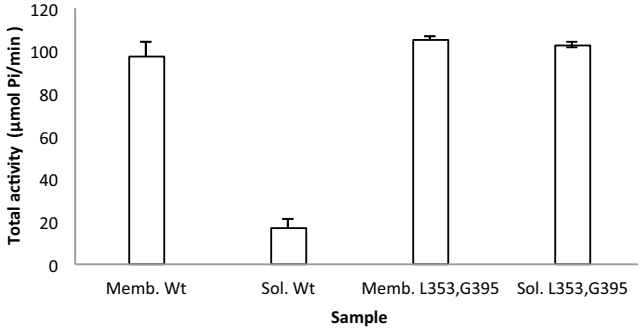

Figure 37. The stability of wt and L353,G395 TmPPase. The total PPase activity of wt and L353,G395 TmPPase from 1 liter of yeast growth was measured at 71°C in membrane-bound state and after heat-solubilisation.

The increased thermostability of the TmPPase L353, G395 might be explained by the better packing of the TMH9 against the TMH15 in the G395 containing protein (Figure 38).

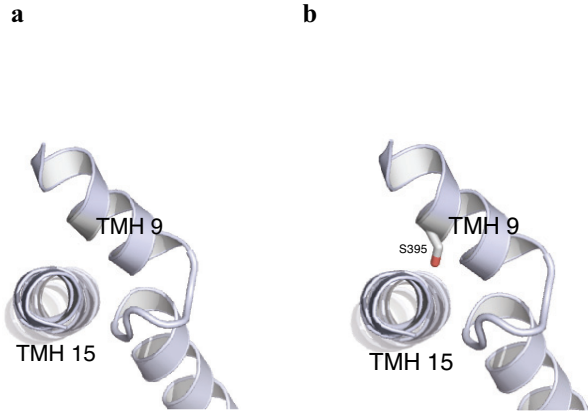

Figure 38. Packing of TMH9 against TMH15. (a) TMH9 with G395 and (b) S395.

4.4.3 Characterisation of TmPPase in 1 % OGNPG and 0.5 % CYM-5

I found that if the washing and elution buffers of the nickel affinity chromatography were supplemented with magnesium (5 mM) and phosphate (1 mM), purified TmPPase in 0.05 % DDM showed high activity (25 µmolPi/mg/min) at 71°C in the absence of supplemented soybean lecithin and DDM. For this reason, in all of the subsequent purifications, the buffers for the nickel affinity purification step were supplemented with these ligands. A similar requirement of ligands for maintaining the activity after the Ni-affinity has been seen with other M-PPases (Malinen, personal communication).

The presence of the ligands in the buffer of Nickel-affinity did not, however, allow TmPPase to retain as high specific activities in 0.05 % CYM-5 and in 1 % OGNPG, the two detergents in which the structure of TmPPase has been solved: their activities were 15 µmolPi/mg/min and 10 µmolPi/mg/min, respectively, without lipid and DDM. These proteins, however, did not show any loss of total activity during the purification when their activities were measured at 30°C (See 3.2, Figure 39), pointing to the necessity of lipid and DDM for the maintenance of the protein's thermostability, but not for the maintenance of its activity. Also, TmPPase DDM showed the same activity at 30°C as TmPPase OGNPG and CYM-5 (Figure 39). These results show that both TmPPase OGNPG and CYM-5 were crystallised in a fully active form.

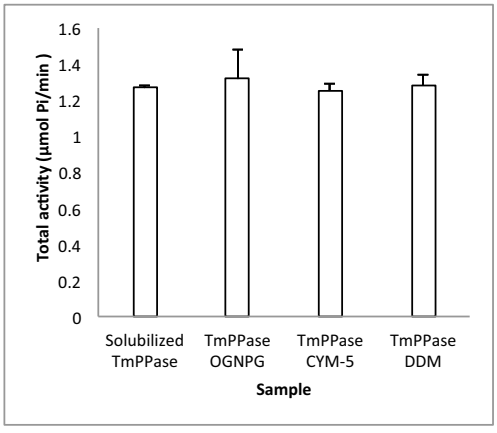

Figure 39. Monitoring TmPPase activity at 30°C during its purification. The total activity of TmPPase from 1 liter yeast culture was measured after heat solubilisation with DDM (Solubilised TmPPase) and after Ni-affinity purification and detergent exchange in to 1 % OGNPG, 0.5 % CYM-5 and 0.05 % DDM (TmPPase OGNPG, CYM-5 and DDM).

Lastly, I was also recently able to devise a lipid supplementation method where the DDM and soybean lecithin mixture is heated to 55°C (See 3.3) to facilitate full solubilisation of the lipid by the large headgroup containing DDM (le Maire et al., 2000). Lipid supplementation with a mixture containing 4 µl 30 mg/ml asolectin and 2.25 µl 20 % DDM gives TmPPase OGNPG a specific activity of 80 µmolPi/mg/min.

Having attained a new value for the specific activity of purified TmPPase I re-calculated the expression levels of the 8 target M-PPases of Study I (Table 9) as these, with the exception of PaPPase, were calculated on the basis of the yield and activity of TmPPase.

Also, the fact that the results of the Bradford assay (Bradford, 1976) with bovine γ-globulin as the standard overestimate the yield of M-PPases in comparison to the results of the A_{280}-measurements (see 4.1.2) was taken in to consideration in the re-calculation of the expression levels.

Table 9. Expression levels of M-PPases in *S. cerevisiae*

Protein	Specific activity (μmolPi/mg/min)*	Expression level (mg/l)
TmPPase	0.83±0.15	≈1.25
PaPPase	0.89±0.13	≈1
StPPase	0.041±0.013	≈0.05
MtPPase	0.0021±0.002	≈0
TdPPase	0.32±0.008	≈0.5
MaPPase	0.001±0.0021	≈0
TgPPase	0.016±0.004	≈0.025
TcPPase	0.021±0.005	≈0.025

* = Specific activity in extracted membranes.

5 Conclusions

So far the membrane-bound pyrophosphatases have remained the only phosphoanhydride utilising ion pumps of unknown structure. This has hampered understanding their mechanism of action, as the only thing known so far is that it is unlike that of any other phosphoanhydride utilising ion pump, and this made the design of anti-protozoan drugs that would target this enzyme difficult.

My work presented in this thesis shows the full span of a project which begun from selection of suitable target proteins for structural studies of M-PPases and resulted finally in a solved M-PPase structure, the first membrane protein structure solved in Finland. This project demonstrates again that it is important to screen numerous homologues of the studied membrane protein in order to find a suitable target protein which expresses well, behaves well during purification and crystallises well. My work has also shown the importance of testing multiple detergents in membrane protein crystallisation; the necessary step for obtaining well diffracting TmPPase crystals was detergent exchange in to a novel neopentyl detergent, octyl glucose neopentyl glycol.

Of the 8 initial target proteins on which I worked with I have been able to purify and crystallise two and of these I have been able to solve the structure of one M-PPase, that of sodium-pumping pyrophosphatase of *Thermotoga maritima*.

The solved TmPPase structure in resting –and product-bound states together with the recently solved VrPPase structure in substrate-bound state have allowed the analysis of the catalytic mechanism of M-PPases. In this mechanism ion pumping seems to be linked to the movement of TMH12 and that of a conserved arginine. These movements cause the opening of a gate formed by a cluster of conserved, charged residues and allow the pumped ion to move from the cytoplasmic active site cavity in to a periplamic exit channel and finally to the periplamic space.

Analysis of the TmPPase structure has also shown that the M-PPases have evolved through gene triplication.

Acknowledgements

This study was carried out between 2006 and 2012 at the Insititute of Biotechnology (University of Helsinki). The work was financially supported by the Academy of Finland, the Sigrid Juselius foundation, European Drug Initiative on Channels and Transporters (EDICT) and National Doctoral Programme in Informational and Structural Biology.

I would like to thank Professor Tomi Mäkelä, the head of Insititute of Biotechnology, and Kari Keinänen, the head of the Biochemistry Division, for their excellent facilities and working environments. I would also like to thank Kari for volunteering to be the custos of my PhD-defence.

I would like to thank warmly my supervisor Adrian Goldman for the opportunity to work on a challenging, but rewarding project and for teaching me science. I would especially like to thank Adrian for the support he has given me during the days when I was ready throw in the towel.

I would like to thank Tommi Kajander for the thorough guidance I have received from him.

I am gratefull to Pirkko Heikinheimo and Mårten Wikström for the advice they have given me during the meetings of the thesis advisory committee.

I am gratefull to Poul Nissen and Peter Henderson not only for the excellent job and the valuable suggestions they have given me as the pre-examiners of my thesis, but also for the benefial advices I have received from them during our annual EDICT-meetings. I would like to extend this gratitude also to Sir John Walker, to whom I am not only gratefull for volunteering to be my opponent, but also for the usefull discussions during the EDICT-meetings.

I owe my gratitude to the current and previous members of the crystallography lab. I especially like to thank Konstantin Kogan, Robert Kolodziejczyk, Esko Oksanen, Danielle Bansfield, Arnab Bhattacharjee, Katja Rosti, Heidi Repo and Sanjay Sarkhel who have been of great help and inspiration.

I owe my gratitude to all of the co-authors of the original publications, Rosa Lopéz, Marqués, Michel Palmgren, Riina Honkanen and Kisun Pokharel, for the helpful discussion and preparation of mansucripts. I would especially like to thank Kisun for the crucial work he did on the *Science*-paper and Riina for the crucial work she did so that we could have the *Science*-paper; I think if we would not have hired you, Riina, it might be that we would not be as far as we now are.

I would like to sincerely thank my family all of my friends. Especially: Riku, Tiukku, Pirjo, Markku, Tummu, Olli (N), Olli (R), Mursu, Antti (H), Lape, Pepin, Wesley, Tuulikki and Juha for support and friendship.

I am especially gratefull to my parents Riitta and Juhani, who have always supported me.

Lastly I would like to thank Satu: you are the love of my life.

In Helsinki, September 2013

-J-

References

Abrahams JP, Leslie AG. (1996). Methods used in the structure determination of bovine mitochondrial F1 ATPase. *Acta Crystallogr D,* 52, 30-42.

Abrahams JP, Leslie AG, Lutter R, Walker JE. (1994) Structures at 2.8 Å resolution of F_1-ATPase from bovine heart mitochondria. *Nature*, 370: 621-628.

Andersen JL, Gourdon P, Møller JV, Morth JP, Nissen P. (2011). Crystallization and preliminary structural analysis of the *Listeria monocytogenes* Ca^{2+}-ATPase LMCA1. *Acta Crystallogr F,* 67, 718-722.

Andre N, Cheroauti N, Prual C, Steffan T, Zeder-Lutz G, Magnin T, Pattus F, Michel H, Wagner R, Reinhart C. (2006). Enhancing functional production of G protein-coupled receptors in *Pichia pastoris* to levels required for strutural studies via a single expression screen. *Protein Sci,* 15, 1115-1126.

Au KM, Barabote RD, Hu KY, Saier MHJ. (2006). Evolutionary apperance of H^+-translocating pyrophosphatase. *Microbiology,* 152, 1243-1247.

Baginski ES, Foa PP, Zak B. (1967). Determination of phosphate: Study of labile organic phosphate interference. *Clinica Chim Acta,* 15, 155 - 158.

Baltscheffsky H, Von Stedingk LV, Heldt HW, Klingenberg M. (1966). Inorganic pyrophosphatase: formation in bacterial photophosphorylation. *Science,* 153, 1120-1122.

Baltscheffsky M, Schultz A, Baltscheffsky H. (1999). H^+-proton-pumping inorganic pyrophosphatase: a tightly membrane-bound family. *FEBS Lett,* 452, 121-127.

Banerjee P, Joo JB, Buse JT, Dawson G. (1995). Differential solubilization of lipids along membrane proteins by different classes of detergents. *Chem Phys Lipids,* 77, 65-78.

Bao A-K, Wang S-M, Wu G-Q, Xi J-J, Zhang J-L, Wang C-M. (2009). Overexpression of the *Arabidopsis* H^+-PPase enhanced the resistance to salt and drought stress in transgenic alfalfa (*Medicago sativa* L.). *Plant Science,* 176, 232-240.

Baykov AA, Fabrichniy IP, Pohjanjoki P, Zyryanov AB, Lahti R. (2000). Fluoride effects along the reactions pathways of pyrophosphatase: evidence for a second enzyme center pyrophosphate intermediate. *Biochemistry,* 39, 11939-11947.

Baykov AA, Bakuleva NP, Rea PA. (1993a). Steady-State Kinetics of Substrate Hydrolysis by Vacuolar H^+-pyrophosphatase - A Simple three-State Model. *Eur J Biochem,* 217, 755-762.

Baykov AA, Dubnova EB, Bakuleva NP, Evtushenko OA, Zhen R-G, Rea PA. (1993b). Differential sensitivity of membrane-associated pyrophosphatases to inhibition by diphosphonates and fluoride delineates two classes of enzyme. *FEBS Lett,* 327, 199-202.

Baykov AA, Kasho VN, Bakuleva NP, Rea PA. (1994). Oxygen exchange reactions catalyzed by vacuolar H^+-translocating pyrophosphatase. *FEBS Lett,* 350, 323-327.

Baykov AA, Sergina NV, Evtushenko OA, Dubnova EB. (1996). Kinetic characterization of the hydrolytic activity of the H^+-pyrophosphatase of *Rhodospirillum rubrum* in the membrane-bound and isolated states. *Eur J Biochem,* 236, 121-127.

Baykov AA, Cooperman BS, Goldman A, Lahti R (1999) Cytoplasmic Inorganic Pyrophosphatase. In *Inorganic polyphosphates(23),* (Ed, Schröder HC) Springer Verlag, Berlin, pp. 127-150.

Belogurov GA, Lahti R. (2002). A lysine substitute for K^+. A460K mutation eliminates K^+ dependence in H^+-pyrophosphatase of *Carboxydothermus hydrogenoformans*. *J Biol Chem,* 277, 49651-49654.

Belogurov GA, Malinen AM, Turkina MV, Jalonen U, Rytkönen K, Baykov AA, Lahti R. (2005). Membrane-bound pyrophosphatase of *Thermotoga maritima* requires sodium for activity. *Biochemistry,* 44, 2088-2096.

Belogurov GA, Turkina MV, Penttinen A, Huopalahti S, Baykov AA, Lahti R. (2002). H^+-pyrophosphatase of *Rhodospirillum rubrum*. High yield expression in *Escherichia coli* and identification of the Cys residues responsible for inactivation by mersalyl. *J Biol Chem,* 277, 22209-22214.

Besteiro S, Tonn D, Tetley L, Coombs GH, Mottram JC. (2008). The AP3 adaptor is involved in the transport of membrane proteins to acidocalcisomes of *Leishmania*. *J Cell Sci,* 121, 561-570.

Bill RM, Henderson PF, Iwata S, Kunji ERS, Michel H, Neutze R, Newstead S, Poolman B, Tate CG, Vogel H. (2011). Overcoming barriers to membrane protein structure determination. *Nat Biotech,* 29, 335-340.

Boyer PD (1993) The binding change mechams for ATP synthase - some probabilities and possibilities. *Biochim Biophys Acta,* 1140, 215-250.

Bradford MM. (1976). A rapid and sensitive method for the quantitation of microgram quantities of protein utilizing the principle of protein-dye binding. *Anal Biochem,* 72, 248-254.

Breyton C, Tribet C, Olive J, Dubacq JP, Popot JL. (1997). Dimer to monomer conversion of the cytochrome b6 f comples. Causes and consequences. *J Biol Chem,* 272, 21892-21900.

Bricogne G, Vonrhein C, Flensburg C, Schiltz, M, Paciorek W. (2003). Generation, representation and flow of phase information in structure determination: recent developments in and around SHARP 2.0. *Acta Crystallogr D,* 59, 2023-2030.

Brini F, Gaxiola RA, Berkowitz GA, Masmoudi K. (2005). Cloning and characterization of a wheat vacuolar cation/proton antiporter and pyrophosphatase proton pump. *Plant Physiol Biochem,* 43, 347-454.

Britten CJ, Zhen R-G, Kim EJ, Rea PA. (1992). Reconstitution of transport function of vacuolar H^+-translocating inorganic pyrophosphatase. *J Biol Chem,* 267, 21850-21855.

Caffrey M, Cherezov V. (2009). Crystallizing membrane proteins using lipidic mesophases. *Nat Protoc,* 4, 706-731.

Carpenter EP, Beis K, Cameron AD, Iwata S. (2008). Overcoming the challenges of membrane protein crystallography. *Curr Opin Struct Biol,* 18, 581-586.

Celis H, Romero I. (1987). The phosphate-pyrophosphate exchange and hydrolytic reactions of the membrane-bound pyrophosphatase of *Rhodospirillum rubrum*: effects of pH and divalent cations. *J Bioenerg Biomembr,* 19, 255-272.

Chae PS, Rana RR, Gotfryd K, Rasmussen SG, Kruse AC, Cho KH, Capaldi S, Carlsson E, Kobilka B, Loland CJ, Gether U, Banerjee S, Byrne B, Lee JK, Gellman SH. (2013). Glucose-Neopentyl Glycol (GNG) amphiphiles for membrane protein study. *Chem Commun (Camb),* 49, 2287-2289.

Chae PS, Rasmussen SGF, Rana RR, Gotfryd K, Chandra R, Goren MA, Kruse AC, Nurva S, Loland CJ, Pierre Y. (2010). Maltose-neopentyl glycol (MNG) amphiphiles for solubilization, stabilization and crystallization of membrane proteins. *Nat Methods,* 7, 1003-1008.

Clause W. (2005). Proline as a measure of stress in tomato plants. *Plant Sci,* 168, 241-248.

Cowtan K. (2001). Fast Fourier feature recognition. *Acta Crystallogr D,* 57, 1435-1444.

Dang S, Sun L, Huang Y, Lu F, Liu Y, Gong H, Wang J, Yan N. (2010). Structure of fucose transporter in an outward-open conformation. *Nature,* 476, 734-738.

Dennis EA (1983) Phospholipases. In *The Enzymes vol. XVI,* (Ed, Boyer PD) Academic Press, New York, pp. 307-353.

DiMaio F, Terwilliger TC, Read RJ, Wlodawer A, Oberdorfer G, Wagner U, Valkov E, Alon A, Fass D, Axelrod HL. (2011). Improved molecular replacement by density-and energy-guided protein structure optimization. *Nature,* 473, 540-543.

Dimroth P, Cook GM. (2004). Bacterial Na^+ -or H^+-coupled ATP synthase operating at low electrochemical potential. *Adv Microb Physiol,* 49, 175-218.

Docampo M, Moreno SN. (2011). Acidocalsisomes. *Cell Calcium,* 50, 113-119.

Dong QL, Liu DD, An XH, Hu DG, Yao YX, Hao YJ. (2011). MdVHP1 encodes an apple vacuolar H^+-PPase and enhances stress tolerance in transgenic apple callus and tomato. *J Plant Physiol,* 168, 2124-2133.

Drake R, Serrano A, Péréz-Castineira JR. (2004). Heterologous expression of membrane-bound inorganic pyrophosphatases in *Saccharomyces cerevisiae* is significantly improved by constructing chimeras with N-terminal domain of *Trypanosoma cruzi* H^+-PPase. *Recent advances in Inorganic Pyrophosphatase Research 3rd International Meeting on Inorganic Pyrophosphatases,* 56-59.

Drake R, Serrano A, Perez-Castineira JR. (2010). N-terminal chimaeras with signal sequences enhance the functional expression and alter the subcellular localization of heterologous membrane-bound inorganic pyrophosphatases in yeast. *Biochem J,* 426, 147-157.

Drozdowicz YM, Lu YP, Patel V, Fitz-Gibbon S, Miller JH, Rea PA. (1999). A thermostable vacuolar-type membrane pyrophosphatase from the archaeon *Pyrobaculum aerophilum*: implications for the origins of pyrophosphate-energized pumps. *FEBS Lett,* 460, 505-512.

Duan XG, Yang AF, Gao F, Zhang SL, Zhang JR. (2007). Heterologous expression of vacuolar H^+-PPase enhances the electrochemical gradient across the vacuolar membrane and improves tobacco cell salt tolerance. *Protoplasm,* 232, 87-95.

Dubendorff JW, Studier FW. (1991). Controlling basal expression in an inducible T7 expression system by blocking the target T7 promoter with lac repressor. *J Mol Biol,* 219, 45-59.

Duncan TM, Bulygin VV, Zhou Y, Hutcheon ML, Cross RL (1995) Rotation of subunits during catalysis by *Escherichia coli*. *Proc Natl Acad Sci USA*, 92, 10964-68.

Efremov RG, Baradaran R, Sazanov LA. (2010). The architecture of respiratory complex I. *Nature,* 465, 441-445.

Esmann M. (1984). The distribution of C12E8-solubilized oligomers of the Na^+/K^+-ATPase. *Biochim Biophys Acta,* 787, 81-89.

Esmann M, Skou JC. (1984). Kinetic properties of C12E8-solubilized Na^+/K^+-ATPase. *Biochim Biophys Acta,* 787, 71-80.

Eyzaguirre J (1987) Chemical modification of enzyme. In *Active Site Studies,* (Ed, Eyzaguirre J) Ellis Horwood, London, pp. 9-22.

Faham S, Bowie JU. (2002). Bicelle Crystallization: A New Method for Crystallizing Membrane Proteins Yields a Monomeric Bacteriorhodopsin Structure. *J Mol Biol,* 316, 1-6.

Ferjani A, Segami S, Horiguchi G, Muto Y, Maeshima M, Tsukaya H. (2011). Keep an eye on PPi: the vacuolar-type H^+-pyrophosphatase regulates postgerminative development in *Arabidopsis. Plant Cell,* 23, 2895-2908.

Figler RA, Omote H, Nakamoto RK, Al-Shawi MK. (2000). Use of chemical chaperons in the yeast *Saccharomyces cerevisiae* to enhance heterologous membrane protein expression: high-yield expression and purification of human P-glycoprotein. *Arch Biochem Biophys,* 376, 34-46.

Flegelova H, Haugenauer-Tsapis R, Sychrova H. (2006). Heterologous expression of mammalian Na^+/H^+-antiporters in *Saccharomyces cerevisae*. *Biochim Biophys Acta,* 1760, 504-516.

Forgac M. (2007). Vacuolar ATPase: rotary proton pumps in physiology and pathophysiology. *Nat Rev Mol Cell Biol,* 8, 917-929.

Fraichard A, Magnin T, Trossat C, Pugin A. (1993). Properties of the proton-pumping pyrophosphatase in tonoplast vesciles of *Acer pseudoplatanus* - functional molecular-mass and polypeptide composition. *Plant Physiol Biochem,* 31, 349-359.

Gao F, Gao Q, Duan X, Yue G, Yang A, Zhang J. (2006). Cloning of an H^+-PPase gene from Thellungiella halophila and its heterologous expression to improve tobacco salt tolerance. *J Exp Bot,* 57, 3259-3270.

Garcia-Contreras R, Celis H, Romero I. (2004). Importance of Rhodospirillum rubrum H^+-pyrophosphatase under low-energy conditions. *J Bacteriol,* 186, 6651-6655.

Gaxiola RA, Li J, Undurraga S, Dang LM, Allen GJ, Alper SL, Fink GR. (2001). Drought -and salt-tolerant plants result from overexpression of the AVP1 H^+-pump. *Proc Natl Acad Sci U S A,* 98, 11444-11449.

Gaxiola RA, Sanchez CA, Paez-Valencia J, Ayre BG, Elser JJ. (2012). Genetic manipulation of "vacuolar" H^+-PPase: from salt tolerance to yield enhancement under phosphorous-deficient soils. *Plant Physiol,* 159, 3-11.

Gaxiola RA, Palmgren MG, Schumacher K. (2007). Plant proton pumps. *FEBS Lett,* 581, 2204-2214.

Gordon-Weeks R, Korenkov VD, Steele SH, Leigh RA. (1997). Tris Is a Competitive Inhibitor of K^+ Activation of the Vacuolar H^+-Pumping Pyrophosphatase. *Plant Physiology,* 114, 901-905.

Gordon-Weeks R, Steele SH, Leigh RA. (1996). The role of magnesium, pyrophosphate, and their complexes as substrates and activators of the vacuolar H^+-pumping inorganic pyrophosphatase - Studies using ligand protection from covalent inhibitors. *Plant Physiology,* 111, 195-202.

Gouaux E. (1998). It's not just a phase: crystallization and X-ray structure determination of bacteriorhodopsin in lipidic cubic phases. *Structure,* 6, 5-10.

Gourdon P, J.L. A, Hein KL, Bublitz M, Pedersen BP, Liu XY, Yatime L, Nyblom M, Nielsen TT, Olesen C, Mizuuchi K, Møller JV, Nissen P, Morth JP. (2011a). HiLiDe-Systematic Approach to Membrane Protein Crystallization in Lipid and Detergent: Published as part of the Crystal Growth & Design virtual special issue on the 13th International Conference on the Crystallization of Biological Macromolecules (ICCBM13). *Crystal growth & design,* 11, 2098-2106.

Gourdon P, Liu XY, Skjørringe T, Morth P, Møller LB, Pedersen BP, Nissen P. (2011b). Crystal structure of a copper-transporting PIB-type ATPase. *Nature,* 475, 59-64.

Greenway H, Gibbs J. (2003). Mechanism of anoxia tolerance in plants. II. Energy requirements for maintenance and energy distribution to essential processes. *Funct Plant Biol,* 30, 999-1036.

Griffith DA, Delipala C, Leadsham J, Jarvis SM, Oesterhelt D. (2003). A novel yeast expression system for the overproduction of quality-controlled membrane proteins. *FEBS Lett,* 553, 45-50.

Guillory RJ, Fisher RR. (1972). Studies on the light-dependent synthesis of inorganic pyrophosphatase by *Rhodospirillum rubrum* chromatophores. *Biochem J,* 129, 571-581.

Häse CC, Fedorova ND, Galperin MY, Dibrov PA. (2001). Sodium ion cycle in bacterial pathogens: evidence from cross-genome comparisons. *Microbiol Mol Biol Rev,* 65, 353-370.

Hayashi Y, Mimura K, Matsui H, Takagi T. (1988). High-performance gel chromatography of active solubilized Na^+/K^+-ATPase maintained by exogenous phosphatidylserine. *Prog Clin Biol Res,* 268A, 205-210.

Hedlund J, Cantoni R, Baltscheffsky M, Baltscheffsky H, Persson B. (2006). Analysis of ancient sequence motifs in the H^+-PPase family. *FEBS J,* 273, 5183-5193.

Hedrich R, Kurkdjian A, Guern J, Flügge UI. (1989). Comparative studies on the electrical properties of the H^+-translocating ATPase and pyrophosphatase of the vacuolar-lysosomal compartment. *EMBO J,* 8, 2835-2841.

Heikinheimo P, Lehtonen J, Baykov AA, Lahti R, Cooperman BS, Goldman A. (1996). The Structural Basis for Pyrophosphatase Catalysis. *Structure,* 4, 1491-1508.

Heikinheimo P, Tuominen V, Ahonen A-K, Teplyakov A, Cooperman BS, Baykov AA, Lahti R, Goldman A. (2001). Toward a Quantum-mechanical description of Metal Assisted Phosphoryl Transfer in Pyrophosphatase. *Proc Natl Acad Sci U S A,* 98, 3121-3126.

Hershko A, Ciechanover A. (1998). The ubiquitin system. *Annu Rev Biochem,* 67, 425-479.

Hirono M, Mimura H, Nakanishi Y, Maeshima M. (2005). Expression of functional Streptomyces coelicolor H^+-pyrophosphatase and characterization of its molecular properties. *J Biochem (Tokyo),* 138, 183-191.

Hirono M, Nakanishi Y, Maeshima M. (2007a). Identification of amino acid residues participating in the energy coupling and proton transport of *Streptomyces coelicolor* A3(2) H^+-pyrophosphatase. *Biochim Biophys Acta,* 1767, 1401-1411.

Hirono M, Nakanishi Y, Maeshima M. (2007b). Essential amino acid residues in the central transmembrane domains and loops for energy coupling of *Streptomyces coelicolor* A3(2) H^+-pyrophosphatase. *Biochim Biophys Acta,* 1767, 930-939.

Holm L, Sander C. (1997). Dali/FSSP classification of three-dimensional protein folds. *Nucleic Acids Res,* 25, 231-234.

Holm NG, Baltscheffsky H. (2011). Links between hydrothermal environments, pyrophosphate, Na^+ and early evolution. *Orig Life Evol Biosph,* 41, 489-493.

Hsiao YY, Van RC, Hung SH, Lin HH, Pan RL. (2004). Roles of histidine residues in plant vacuolar H^+-pyrophosphatase. *Biochim Biophys Acta,* 1608, 190-199.

Hsiao YY, Van RC, Hung HH, Pan RL. (2002). Diethylpyrocarbonate inhibition of vacuolar H^+-pyrophosphatase possibly involves a histidine residue. *J Protein Chem,* 21, 51-58.

Hsiao YY, Pan YJ, Hsu SH, Huang YT, Liu TH, Lee CH, Lee CH, Liu PF, Chang WC, Wang YK, Chien LF, Pan RL. (2007). Functional roles of arginine residues in mung bean vacuolar H^+-pyrophosphatase. *Biochim Biophys Acta,* 1767, 965-973.

Hsu SH, Hsiao YY, Liu PF, Lin SM, Luo YY, Pan RL. (2009). Purification, characterization, and spectral analyses of histidine-tagged vacuolar H^+-pyrophosphatase expressed in yeast. *Bot Stud,* 50, 291-301.

Huang YT, Liu TH, Chen YW, Lee CH, Chen HH, Huang TW, Hsu SH, Lin SM, Pan YJ, Lee CH. (2010). Distance variations between active sites of H^+-pyrophosphatase determined by fluorescence resonance energy transfer. *J Biol Chem,* 285, 23655-23664.

Ikeda M, Umami K, Hinohara M, Tanimura Y, Ohmae A, Nakanishi Y, Maeshima M. (2002). Functional expression of *Acetabularia acetabulum* vacuolar H^+-pyrophosphatase in a yeast VMA3-deficient strain. *J Exp Bot,* 53, 2273-2275.

Jaakola V-P, Griffith MT, Hanson MA, Cherezov V, Chien EY, Lane JR, Ijzerman AP, Stevens RC. (2008). The 2.6 Ångstrom Crystal Structure of a Human A2A Adenosine Receptor Bound to an Antagonist. *Science,* 322, 1211-1217.

Jidenko M, Nielsen RC, Sorensen TL, Moller JV, le Maire M, Nissen P, Jaxel C. (2005). Crystallization of a mammalian membrane protein overexpressed in *Saccharomyces cerevisiae. Proc Natl Acad Sci U S A,* 102, 11687-11691.

Johannes E, Felle H. (1990). Proton gradient across the tonoplast of *Riccia fluitans* as a result of the joint action of two electroenzymes. *Plant Physiol,* 93, 412-417.

Karlsson J. (1975). Membrane-bound potassium and magnesium ion-stimulated inorganic pyrophosphatase from roots and cotyledons of sugar beet. *Biochim Biophys Acta,* 399, 356-363.

Kellosalo J, Kajander T, Kogan K, Pokharel K, Goldman A. (2012). The structure and catalytic cycle of a sodium pumping pyrophosphatase. *Science,* 337, 473-476.

Kellosalo J, Kajander T, Honkanen R, Goldman A. (2013). Crystallization and preliminary X-ray analysis of membrane-bound pyrophosphatases. *Mol Membr Biol,* 30, 64-74.

Kellosalo J, Kajander T, Palmgren MG, Lopéz-Marqués RL, Goldman A. (2011). Heterologous expression and purification of membrane-bound pyrophosphatases. *Protein Express Purif,* 79, 25-34.

Khoudi H, Maatar Y, Gouiaa S, Masmoudi K. (2012). Transgenic tobacco plants expressing ectopically wheat H^+-pyrophosphatase (H^+-PPase) gene TaVP1 show enhanced accumulation and tolerance to cadmium. *J Plant Physiol,* 169, 98-103.

Kim EJ, Zhen RG, Rea PA. (1995). Site-directed Mutagenesis of Vacuolar H^+-pyrophosphatase. *J Biol Chem,* 270, 2630-2635.

Kim EJ, Zhen R-G, Rea PA. (1994). Heterologous expression of plant vacuolar pyrophosphatase in yeast demonstrates sufficiency of the substrate-binding subunit for proton transport. *Proc Natl Acad Sci U S A,* 91, 6128-6132.

Krebs M, Beyhl D, Görlich E, Al-Rasheid AS, Marten I, Stierhof Y-D, Hedrich R, Schumacher K. (2010). Arabidopsis V-ATPase activity at the tonoplast is required for efficient nutrient storage bu not for sodium accumulation. *Proc Natl Acad Sci U S A,* 107, 3251-3256.

Kuo SY, Pan RL. (1990). An essential arginyl residue in the tonoplast pyrophosphatase from etiolated mung bean seedlings. *Plant Physiol,* 93, 1128.

Kurilova SA, Bogdanova AV, Nazarova TI, Avaeva S. (1984). Changes in the *Escherichia coli* inorganic pyrophosphatase activity on interaction with magnesium, zinc, calcium and fluoride ions. *Bioorg Khim,* 10, 1153-1160.

Landau EM, Rosenbusch JP. (1996). Lipidic cubic phases: A novel concept for the crystallization of membrane proteins. *Proc Natl Acad Sci U S A,* 93, 14532-14535.

Lanyi JK. (2006). Proton transfers in the bacteriorhodopsin photocycle. *Biochim Biophys Acta,* 1757, 1012-1018.

Laubringer W, Dimroth P. (1989). The sodium ion translocating adenosinetriposphatase of *Propionigenium modestum* pumps protons at low sodium ion concentrations. *Biochemistry,* 28, 7194-7198.

le Maire M, Champeil P, Moller JV. (2000). Interaction of membrane proteins and lipids with solubilizing detergents. *Biochim Biophys Acta,* 1508, 86-111.

Lee CH, Pan YJ, Huang YT, Liu TH, Hsu SH, Lee CH, Chen YW, Lin SM, Huang LK, Pan RL. (2011). Identification of essential lysines involved in substrate binding of vacuolar H^+-pyrophosphatase. *J Biol Chem,* 286, 11970.

Lemercier G, Dutoya S, Luo S, Ruiz FA, Rodrigues CO, Baltz T, Docampo R, Bakalara N. (2002). A vacuolar-type H^+-pyrophosphatase governs maintenance of functional acidocalcisomes and growth of the insect and mammalian forms of *Trypanosoma brucei*. *J Biol Chem,* 277, 37369-37376.

Li B, Wei A, Song C, Li N, Zhang J. (2008). Heterologous expression of the TsVP gene improves the drought resistance of maize. *Plant Biotechnol J,* 6, 146-159.

Li J, Yang H, Peer WA, Richter G, Blakeslee J, A. B, Titapiwantakun B, Undurraga S, Khodakovskaya M, Richards EL, Krizek B, Murphy AS, Gilroy S, Gaxiola R. (2005). Arabidopsis H^+-PPase AVP1 regulates auxin-mediated organ development. *Science,* 310, 121-125.

Li Z, Baldwin CM, Hu Q, Liu H, Luo H. (2010). Heterologous expression of *Arabidopsis* H^+-pyrophosphatase enhances salt tolerance in transgenic bentgrass (*Agrostis stolonifera* L.). *Plant Cell Environ,* 33, 272-289.

Li Z, Gao Q, Liu YC, He C, Zhang X, Zhang J. (2011). Overexpression of transcription factor ZmPTF1 improves low phosphate tolerance of maize by regulating carbon metabolism and root growth. *Planta,* 233, 1129-1143.

Lin SM, Tsai JY, Hsiao CD, Huang YT, Chiu CL, Liu MH, Tung JY, Liu TH, Pan RL, Sun YJ. (2012). Crystals structure of membrane-embedded H^+-translocating pyrophosphatase. *Nature,* 484, 399-403.

Lipmann F. (1965). Projecting backwards from the present stage of evolution of biosyntheses. The origins of prebiological systems. *The Origins of Prebiological Systems and Their Molecular Matrices,* S. W. Fox. Ed. Academic press, New York, 259-280.

Liu TH, Hsu SH, Huang YT, Lin SM, Huang TW, Chuang TH, Fan SK, Fu CC, Tseng FG, Pan RL. (2009). The proximity between C-termini of dimeric vacuolar H^+-pyrophosphatase determined using atomic force microscopy and a gold nanoparticle technique. *FEBS J,* 276, 4381-4394.

Loll PJ. (2003). Membrane protein structural biology: the high throughput challenge. *J Struct Biol,* 142, 144-153.

Long SB, Campbell EB, Mackinnon R. (2005). Crystal structure of a mammalian voltage-dependent Shaker family K^+-channel. *Science,* 309, 897-903.

López-Marqués RL, Pérez-Castiñeira JR, Buch-Pedersen MJ, Marco S, Rigaud JL, Palmgren MG, Serrano A. (2005). Large-scale purification of the proton pumping pyrophosphatase from *Thermotoga maritima*: a "Hot-Solve" method for isolation of recombinant thermophilic membrane proteins. *Biochim Biophys Acta,* 1716, 69-76.

Lopéz-Marqués RL, Péréz-Castineira JR, Losada M, Serrano A. (2004). Differential regulation of soluble and membrane-bound inorganic pyrophosphatases in the photosynthetic bacterium *Rhodospirillum rubrum* provides insights into pyrophosphate-based stress bioenergetics. *J Bacteriol,* 186, 5418-5426.

Luoto HH, Belogurov GA, Baykov AA, Lahti R, Malinen AM. (2011). Na^+-translocating membrane pyrophosphatases are widespread in the microbial world and evolutionarily precede H^+-translocating pyrophosphatases. *J Biol Chem,* 286, 21633-21642.

Luoto HH, Baykov AA, Lahti R, Malinen AM. (2013). Membrane-integral pyrophosphatase subfamily capable of translocating both Na^+ and H^+. *Proc Natl Acad Sci U S A,* 110, 1255-1260.

Lv SL, Lian LJ, Tao PL, Li ZX, Zhang KW, Zhang JR. (2009). Overexpression of Thellungiella halophila H^+-PPase (TsVP) in cotton enhances drought stress resistance of plants. *Planta,* 229, 899-910.

Maeshima M. (1990). Oligomeric structure of H^+-translocating inorganic pyrophosphatase of plant vacuoles. *Biochem Biophys Res Commun,* 168, 1157-1162.

Maeshima M. (1991). H^+-translocating inorganic pyrophosphatase of plant vacuoles. Inhibition by Ca^{2+}, stabilization by Mg^{2+} and immunological comparison with other inorganic pyrophosphatases. *Eur J Biochem,* 196, 11-17.

Maeshima M, Yoshida S. (1989). Purification and properties of vacuolar membrane proton-translocating inorganic pyrophosphatase from mung bean. *J Biol Chem,* 264, 20068-20073.

Maeshima M. (2000). Vacuolar H^+-pyrophosphatase. *Biochim Biophys Acta,* 1465, 37-51.

Malinen AM. (2009) *Discovery and Characterization of Na+-transporting Pyrophosphatases*. Doctoral thesis. University of Turku, Turku.

Malinen AM, Belogurov GA, Salminen M, Baykov AA, Lahti R. (2004). Elucidating the role of conserved glutamates in H^+-pyrophosphatase of *Rhodospirillum rubrum*. *J Biol Chem,* 279, 26811-26816.

Malinen AM, Baykov AA, Lahti R. (2008). Mutual effects of cationic ligands and substrate on activity of the Na^+-transporting pyrophosphatase of *Methanosarcina mazei*. *Biochemistry,* 47, 13447-13454.

Malinen AM, Belogurov GA, Baykov AA, Lahti R. (2007). Na^+-pyrophosphatase: a novel primary sodium pump. *Biochemistry,* 46, 8872-8878.

Malkowski MG, Quartley E, Friedman AE, Babulski J, Kon Y, Wolfley J, Said M, Luft JR, Phizicky EM, DeTitta GT, Grayhack EJ. (2007). Blocking S-adenosylmethionine synthesis in yeast allows selenomethionine incorporation and multiwavelength anomalous dispersion phasing. *Proc Natl Acad Sci U S A,* 104, 6678-6683.

Marsh D. (1996). Peptide models for membrane channels. *Biochem J,* 315, 345-361.

Marsh D, Gonzalez P, Echeverria E. (2000). PPi formation by reversal of the tonoplast-bound H^+-pyrophosphatase from 'Valencia' orange juice cells. *J Amer Soc Hort Sci,* 125, 420-424.

Marsh K, Gonzalez P, Echeverria E. (2001). Partial characterization of H^+-translocating inorganic pyrophosphatase from 3 citrus varieties differing in vacuolar pH. *Physiol Plant,* 111, 519-526.

Maruyama C, Tanaka Y, Takeyasu K, Yoshida M, Sato MH. (1998). Structural studies of the vacuolar H^+-pyrophosphatase: sequence analysis and identification of the residues modified by fluorescent cyclohexylcarbodiimide and maleimide. *Plant Cell Physiol,* 39, 1045-1053.

McIntosh MT, Vaidya AB. (2002). Vacuolar type H^+ pumping pyrophosphatases of parasitic protozoa. *Int J Parasitol,* 32, 1-14.

Meng X, Xu Z, Song R. (2011). Molecular cloning and characterization of vacuolar H+-pyrophosphatase from *Dunaliella viridis*. *Mol Biol Rep,* 38, 3375-3382.

Miler EW. (1977). Modifiifaction of histidyl residues by diethyl pyrocarbonate. *Methods Enzymol,* 47, 431-442.

Mimura H, Nakanishi Y, Hirono M, Maeshima M. (2004). Membrane topology of the H^+-pyrophosphatase of *Streptomyces coelicolor* determined by cysteine-scanning mutagenesis. *J Biol Chem,* 279, 35106-35112.

Mimura H, Nakanishi Y, Maeshima M. (2005a). Oligomerization of H^+-pyrophosphatase and its structural and functional consequences. *Biochim Biophys Acta,* 1708, 393-403.

Mimura H, Nakanishi Y, Maeshima M. (2005b). Disulfide-bond formation in the H^+-pyrophosphatase of Streptomyces coelicolor and its implications for redox control and enzyme structure. *FEBS Lett,* 579, 3625-3631.

Miroux B, Walker JE. (1996). Overproduction of proteins in *Eschrichia coli*: mutant hosts that allow synthesis of some membrane proteins and globular proteins at high level. *J Mol Biol,* 260, 289-298.

Moreno SN, Docampo R. (2009). The role of acidocalcisomes in parasitic protists. *J Eukaryot Microbiol,* 56, 208-213.

Motta LS, da Silva WS, Oliveira DM, de Souza W, Machado EA. (2004). A new model for proton pumping in animal cells: the role of pyrophosphatase. *Insect Biochem Mol Biol,* 34, 19-27.

Motta LS, Ramos IB, Gomes FM, de Souza W, Champagne DE, Santiago MF, Docampo R, Miranda K, Machado EA. (2009). Proton-pyrophosphatase and polyphosphate in acidocalcisome-like vesicles from oocytes and eggs of Periplaneta americana. *Insect Biochem Mol Biol,* 39, 198-206.

Moyle J, Mitchell RS, Mitchell P. (1972). Proton translocating pyrophosphatase of *Rhodospirillim rubrum*. *FEBS Lett,* 23, 233-236.

Nakanishi Y, Saijo T, Wada Y, Maeshima M. (2001). Mutagenic analysis of functional residues in putative substrate-binding site and acidic domains of vacuolar H^+-pyrophosphatase. *J Biol Chem,* 276, 7654-7660.

Nakanishi Y, Yabe I, Maeshima M. (2003). Patch clamp analysis of a H^+-pump heterologously expressed in giant yeast vacuoles. *J Biochem (Tokyo),* 134, 615-623.

Newstead S, Kim H, von Heijne G, Iwata S, Drew D. (2007). High-throughput fluorescent-based optimization of eukaryotic membrane protein overexpression and purification in Saccharomyces cerevisiae. *Proc Natl Acad Sci U S A,* 104, 13936-13941.

Nyren P, Nore BF, Strid Å. (1991). Proton-pumping N,N'-dicyclohexylcarbodiimide-sensitive inorganic pyrophosphate synthase from *Rhodospirillum rubrum*: purification, characterization, and reconstitution. *Biochemistry,* 30, 2883-2887.

Nyren P, Strid Å. (1991). Hypothesis: the physiological role of the membrane-bound proton-translocating pyrophosphatase in some phototropic bacteria. *FEMS Microbiol Lett,* 77, 265-270.

Obermeyer G, Sommer A, Bentrup FW. (1996). Potassium and voltage dependence of the inorganic pyrophosphatase of intact vacuoles from *Chemenopodium rubrum*. *Biochim Biophys Acta,* 1284, 203-212.

Oberto J, Davison J. (1985). Expression of chicken egg white lysozyme by *Saccharomyces cerevisiae*. *Gene,* 40, 57-65.

Oesterhelt D, Stoekenius W. (1974). Isolation of the cell membrane of *Halobacterium halobium* and its fractionation into red and purple membrane. *Methods Enzymol,* 31, 667-678.

Ottolenghi P, Nørby JG, Jensen J. (1986). Solubilization and further chromatographic purification of highly purified, membrane-bound Na^+/K^+-ATPase. *Biochem Biophys Res Commun,* 135, 1008-1014.

Paez-Valencia J, Sanchez-Lares J, Marsh E, Dorneles LT, Santos MP, Sanchez D, Winter A, Murphy S, Cox J, Trzaska M, Metler J, Kozic A, Facanha AR, Schachtman D, Sanchez CA, Gaxiola R. (2013) Enhanced proton translocating pyrophosphatase activity improves nitrogen use efficiency in romain lettuce. *Plant Physiol*, 161, 1557-1569.

Palmgren MG, Nissen P. (2011). P-type ATPases. *Annu Rev Biochem,* 40, 243-266.

Pan YJ, Lee CH, Hsu SH, Huang YT, Lee CH, Liu TH, Chen YW, Lin SM, Pan RL. (2011). The transmembrane domain 6 of vacuolar H^+-pyrophosphatase mediates protein targeting and proton transport. *Biochim Biophys Acta,* 1807, 59-67.

Pérez-Castiñeira JR, Hernandez A, Drake R, Serrano A. (2011). A plant proton-pumping iorganic pyrophosphatase functionally complements the vacuolar ATPase transport activity and confers bafilomycin resistance in yeast. *Biochem J,* 437, 269-278.

Pérez-Castiñeira JR, López-Marqués RL, Losada M, Serrano A. (2001). A thermostable K^+-stimulated vacuolar-type pyrophosphatase from the hyperthermophilic bacterium *Thermotoga maritima*. *FEBS Lett,* 496, 6-11.

Pérez-Castiñeira JR, López-Marqués RL, Villalba JM, Losada M, Serrano A. (2002). Functional complementation of yeast cytosolic pyrophosphatase by bacterial and plant H^+-translocating pyrophosphatases. *Proc Natl Acad Sci U S A,* 99, 15914-15919.

Pikula S, Müllner N, Dux L, Martonosi A. (1988). Stabilization and crystallization of Ca^{2+}-ATPase in detergent-solubilized sarcoplasmic reticulum. *J Biol Chem,* 263, 5277-5286.

Pohjanjoki P, Fabrichniy IP, Kasho VN, Cooperman BS, Goldman A, Baykov AA, Lahti R. (2001). Probing essential water in yeast pyrophosphatase by directed mutagenesis and fluoride inhibition measurements. *J Biol Chem*, 276, 434-441.

Polvani C, Blostein R. (1988). Protons as substitutes for sodium and potassium in the sodium pump reaction. *J Biol Chem,* 263, 16757-16763.

Polvani C, Sachs G, Blostein R. (1989). Sodium ions as substitutes for protons in the gastric H^+,K^+-ATPase. *J Biol Chem,* 264, 17854-17859.

Privé GG. (2007). Detergent for the stabilization and crystallization of membrane proteins. *Methods,* 41, 388-397.

Rea PA, Britten CJ, Jennings IR, Calvert CM, Skiera LA, Leigh RA, Sanders D. (1992a). Regulation of vacuolar H^+-pyrophosphatase by free calsium: a reaction kinetic analysis. *Plant Physiol,* 100, 1706-1715.

Rea PA, Poole RJ. (1985). Proton-translocating inorganic pyrophosphatase in red beet (*Beta vulgaris* L.) tonoplast vesicles. *Plant Physiol,* 77, 46-52.

Rea PA, Britten CJ, Sarafian V. (1992b). Common identity of substrate binding subunit of vacuolar H^+-translocating inorganic pyrophosphatase of higher plant cells. *Plant Physiol,* 100, 723-732.

Romero I, Celis H. (1995). Comparison of the hydrolysis of Zn_2PPi and the Mg_2PPi as substrates and the effect of free cations upon membrane-bound pyrophosphatase of *Rhodspirillum rubrum*. *Biochemie,* 77, 949-952.

Ros R, Romieu C, Gibrat R, Grignon C. (1995). The plant inorganic pyrophosphatase does not transport K^+ in vacuole membrane vesicles multilabeled with fluorescent probes for H^+, K^+, and membrane potential. *J Biol Chem,* 270, 4368-4374.

Rosenbaum DM, Cherezov V, Hanson MA, Rasmussen SG, Thian FS, Kobilka TS, Choi HJ, Yao XJ, Weis WI, Stevens RC, Kobilka BK. (2007). GPCR engineering yields high-resolution structural insights into 2-adrenergic receptor function. *Science,* 318, 1266-1273.

Sanders CR, Hoffmann AK, Gray DN, Keyes MH, Ellis CD. (2004). French swimwear for membrane proteins. *Chem Bio Chem,* 5, 423-426.

Sarafian V, Poole RJ. (1989). Purification of an H^+-translocating inorganic pyrophosphatase from vacuole membranes of red beet. *Plant Physiol,* 91, 34-38.

Sato MH, Kasahara M, Ishii N, Homareda H, Matsui H, Yoshida M. (1994). Purified Vacuolar Inorganic Pyrophosphatase Consisting of a 75-kDa Polypeptide Can Pump H^+ into Reconstituted Proteoliposomes. *J Biol Chem,* 269, 6725-6728.

Sato MH, Maeshima M, Ohsumi Y, Yoshida M. (1991). Dimeric structure of H^+-translocating pyrophosphatase from pumpkin vacuolar membranes. *FEBS Lett,* 290, 177-180.

Schägger H (2003) Techniques and basic operations in membrane protein purification. In *Membrane protein purification and crystallization 2nd edition,* (Eds, Hunte C, von Jagow G, Schägger H) Academic press, San Diego, California, pp. 19-54.

Schlegel S, Löfblom J, Lee C, Hjelm A, Klepsch M, Strous M, Drew D, Slotboom DJ, de Gler JW. (2012). Optimizing membrane protein overexpression in the *Escherichia coli* strain Lemo21(DE3). *J Mol Biol,* 31, (in press).

Schneider TR, Sheldrick GM. (2002). Substructure solution with SHELXD. *Acta Crystallogr D,* 58, 1772-1779.

Schöke L, Schink B. (1998). Membrane-bound proton-translocating pyrophosphatase of *Syntrophus gentianae*, a synthropically benzoate-degrading fermenting bacterium. *Eur J Biochem,* 256, 589-594.

Schultz A, Baltscheffsky M. (2003). Properties of mutated *Rhodospirillum rubrum* H^+-pyrophosphatase expressed in *Escherichia coli*. *Biochim Biophys Acta,* 1607, 141-151.

Schultz A, Baltscheffsky M. (2004). Inhibition studies on Rhodospirillum rubrum H^+-pyrophosphatase expressed in Escherichia coli. *Biochim Biophys Acta,* 1656, 156-165.

Scott DA, de Souza W, Benchimol M, Zhong L, Lu HG, Moreno SN, Docampo R. (1998). Presence of a plant-like proton-pumping pyrophosphatase in acidocalcisomes of Trypanosoma cruzi. *J Biol Chem,* 273, 22151-22158.

Screpanti E, Padan E, Rimon A, Michel H, Hunte C. (2006). Crucial steps in the structure determination of the Na^+/H^+-antiporter NhaA in its native conformation. *J Mol Biol,* 362, 192-202.

Segami S, Nakanishi Y, Sato MH, Maeshima M. (2010). Quantification, organ-specific accumulation and intracellular localization of type II H^+-pyrophosphatase in *Arabidopsis thaliana*. *Plant Cell Physiol,* 51, 1350-1360.

Serrano A, Pérez-Castineira JR, Baltscheffsky M, Baltscheffsky H. (2007). H^+-PPases: yesterday, today and tomorrow. *IUBMB Life,* 59, 76-83.

Seufferheld M, R. LC, Vleira M, Oldfield E, Docampo R. (2004). The H^+-pyrophosphatase of *Rhodospirillum rubrum* is predominantly located in polyphosphate rich acidocalsisomes. *J Biol Chem,* 279, 51193-51202.

Seufferheld M, Vleira MC, Ruiz FA, Rodrigues CO, Moreno SN, Docampo R. (2003). Identification of organelles in bacteria similar to acidocalsisomer of unicellular eukaryotes. *J Biol Chem,* 278, 29971-29978.

Sonoda Y, Cameron A, Newstead S, Omote H, Moriyama Y, Kasahara M, Iwata S, Drew D. (2010). Tricks of the trade used to accelerate high-resolution structure determination of membrane proteins. *FEBS Lett,* 584, 2539-2547.

Sonoda Y, Newstead S, Hu NJ, Alguel Y, Nji E, Beis K, Yashiro S, Lee C, Leung J, Cameron AD. (2011). Benchmarking Membrane Protein Detergent Stability for Improving Throughput of High-Resolution X-ray Structures. *Structure,* 19, 17-25.

Sosa A, Celis H. (1995). H^+/PPi stoichiometry of membrane-bound pyrophosphatase of Rhodospirillum rubrum. *Arch Biochem Biophys,* 316, 421-427.

Stitt M. (1998). Pyrophosphate as an energy donor in the cytosol of plant cells: an enigmatic alternative to ATP. *Bot Acta,* 111, 167-175.

Stock D, Leslie AG, Walker JE. (1999) Molecular architecture of the rotary motor in ATP synthase. *Science,* 286, 1700-1705.

Stock D, Gibbons C, Arechaga I, Leslie AGW, Walker JE. (2000). The rotary mechanism of ATP synthase. *Curr Opin Struct Biol,* 10, 672-679.

Studier FW, Moffat BA. (1986). Use of bacteriophage T7 RNA polymerase to direct selective high-level expression of cloned genes. *J Mol Biol,* 189, 113-130.

Suzuki Y, Kanayama Y, Shiratake K, Yamaki S. (1999). Vacuolar H^+-pyrophosphatase purified from pear fruit. *Phytochemistry,* 50, 535-539.

Takasu A, Nakanishi Y, Yamauchi T, Maeshima M. (1997). Analysis of the susbsrate binding site and carboxyl terminal region of vacuolar H^+-pyrophosphatase of mung bean with peptide antibodies. *J Biochem,* 122, 883-889.

Tate CG. (2001). Overexpression of mammalian integral membrane proteins for structural studies. *FEBS Lett,* 504, 94-98.

Tusnady GE, Simon I. (2010). Topology prediction of helical transmembrane proteins: how far have we reached ? *Curr Protein Pept Sci,* 11, 550-561.

Tzeng CM, Yang CY, Yang SJ, Jiang SS, Kuo SY, Hung SH, Ma JT, Pan RL. (1996). Subunit structure of vacuolar proton-pyrophosphatase as determined by radiation inactivation. *Biochem J,* 316, 143-147.

Umena Y, Kawakami K, Shen JR, Kamiya N. (2011). Crystal structure of oxygen-evolving photosystem II at a resolution of 1.9 Å. *Nature,* 473, 55-60.

Valent QA, de Gler JW, von Heijne G, Kendall DA, ten Hagen-Jongman CM, Oudega B, Luirink J. (1997). Nascent membrane and presecretory proteins synthesized in *Escherichia coli* associates with signal recognition particle and trigger factor. *Mol Microbiol,* 25, 53-64.

Velázquez I, Celis H, Romero I. (1993). Regulation of divalent cations of the membrane-bound pyrophosphatase of *Rhodospirillum rubrum,* as shown by the hydrolysis of tripositive-pyrophosphate complexes. *Biometals,* 6, 143-148.

Villalba JM, Palmgren MG, Berberian GE, Ferguson C, Serrano R. (1992). Functional expression of plant plasma membrane H^+-ATPase in yeast endoplasmic reticulum. *J Biol Chem,* 267, 12341-12349.

Wadsten P, Wöhri AB, Snijder, A, Katona, G, Gardiner AT, Cogdell RJ, Neutze R, EngWiener M. (2006). Lipidic Sponge Phase Crystallization of Membrane Proteins. *J Mol Biol,* 364, 44-53.

Wagner S, Baars L, Ytterberg AJ, Klussmeier A, Wagner CS, Nord O, Nygren PA, van Wijk KJ, de Gler JW. (2007). Consequences of membrane protein overexpression in *Eschericia coli*. *Mol Cell Proteomics,* 6, 1527-1550.

Wagner S, Bader ML, Drew D, de Gier J-W. (2006). Rationalizing membrane protein overexpression. *Trends Biotechnol,* 24, 364-371.

Wagner S, Klepsch MM, Schlegel S, Appel A, Draheim R, Tarry M, Högbom M, van Wijk KJ, Slotboom DJ, Persson JO, de Gier JW. (2008). Tuning *Escherichia coli* for membrane protein overexpression. *Proc Natl Acad Sci U S A,* 105, 14371-14376.

Wang D-N, Safferling M, Lemiuex MJ, Griffth H, Chen Y, Li X-D. (2003). Practical aspects of overexpressing bacterial secondary membrane transporters for structural studies. *Biochem Biophys Acta,* 1610, 23-26.

Wang Y, Leigh RA, Kaestner KH, Sze H. (1986). Electrogenic H^+-pumping pyrophosphatase in tonoplast vesicles of oat roots. *Plant physiol,* 81, 497-502.

Weiss HM, Haase W, Michel H, Reiländer H. (1995). Expression of functional mouse 5-HT5 A serotonin receptor in the methylotrophic yeast *Pichia pastoris*: pharmacological characterization and localization. *FEBS Lett,* 377, 451-456.

White MA, Clarck KM, Grayhack EJ, Dumont ME. (2007). Characteristics affecting expression and solubilization of yeast membrane proteins. *J Mol Biol,* 365, 621-636.

White PJ, Marshall J, Smith JA. (1990). Substrate kinetics of the tonoplast H^+-translocating pyrophosphatase and its activation by free Mg^{2+}. *Plant Physiol,* 93, 1063-1070.

Wiener MC. (2004). A pedestrian guide to membrane protein crystallization. *Methods,* 34, 364-372.

Wilkens S. (2005). Rotary molecular motors. *Adv Protein Chem,* 71, 345-382.

Wu B, Chien EY, D. MC, Fenalti G, Liu WM, Katrich V, Abagyan R, Brooun A, Wells P, Bi FC, Hamel DJ, Kuhn P, Handel TM, Cherezov V, Stevens RC. (2010). Structures of the CXCR4 chemocine GPCR with small-molecule and cyclic peptide antagonists. *Science,* 330, 1066-1071.

Yang H, Knapp J, Koirala P, Rajagopal D, Peer WA, Silbart LK, Murphy A, Gaxiola RA. (2007). Enhanced phosphorous nutrition in monocots and dicots over-expressing a phosphorous-responsive type I H^+-pyrophosphatase. *Plant Biotechnol J,* 5, 735-745.

Yang SJ, Jiang SS, Hsiao YY, Van RC, Pan YJ, Pan RL. (2004). Thermoinactivation analysis of vacuolar H^+-pyrophosphatase. *Biochim Biophys Acta,* 1656, 88-95.

Yang SJ, Jiang SS, Kuo SY, Hung SH, Tam MF, Pan RL. (1999). Localization of a carboxylic residue possibly involved in the inhibition of vacuolar H^+-pyrophosphatase by N, N'-dicyclohexylcarbodi- imide. *Biochem J,* 342 Pt 3, 641-646.

Yang SJ, Jiang SS, Tzeng CM, Kuo SY, Hung SH, Pan RL. (1996). Involvement of tyrosine residue in the inhibition of plant vacuolar H^+-pyrophosphatase by tetranitromethane. *Biochim Biophys Acta,* 1294, 89-97.

Yang SJ, Jiang SS, Van RC, Hsiao YY, Pan RL. (2000). A lysine residue involved in the inhibition of vacuolar H+-pyrophosphatase by fluorescein 5'-isothiocyanate. *Biochim Biophys Acta,* 1460, 375-383.

Yoon HS, Kim SY, Kim IS. (2013). Stress response of plant H^+-PPase-expressing transgenic *Escherichia coli* and *Saccharomyces cerevisiae*: a potentially useful mechanism for the development of stress-tolerant organisms. *J Appl Genet,* 54, 129-133.

Zancani M, Skiera LA, Sanders D. (2007). Roles of basic residues and salt-bridge interaction in a vacuolar H^+-pumping pyrophosphatase (AVP1) from *Arabidopsis thaliana*. *Biochim Biophys Acta,* 1768, 311-316.

Zhang J, Li J, Wang X, Chen J. (2011). OVP1, a vacuolar H^+-translocating inorganic pyrophosphatase (V-PPase), overexpression improved rice cold tolerance. *Plant Physiol Biochem,* 49, 33-38.

Zhao FY, Zhang XJ, Li PH, Zhao YX, Zhang Y. (2006). Co-expression of the *Sueda salsa* SsNHX1 and *Arabidopsis* AVP1 confer greater salt tolerance to transgenic rice than the single SsNHX1. *Mol Breed,* 17, 341-353.

Zhen R-G, Kim EJ, Rea PA. (1997a). The molecular and biochemical basis of pyrophosphate-energized proton translocation at the vacuolar membranes. *Adv Bot Res,* 25, 153-159.

Zhen RG, Kim EJ, Rea PA. (1997b). Acidic residues necessary for pyrophosphate-energized pumping and inhibition of the vacuolar H^+-pyrophosphatase by N,N'-dicyclohexylcarbodiimide. *J Biol Chem,* 272, 22340-22348.

Zhen RG, Baykov AA, Bakuleva NP, Rea PA. (1994). Aminomethylenediphosphonate: A Potent Type-Specific Inhibitor of Both Plant and Phototrophic Bacterial H^+-Pyrophosphatases. *Plant Physiol,* 104, 153-159.